Characterising the heat shock response in African trypanosomes

Hannah Pyle

Lancaster University

Department of Biomedical and Life Sciences

September 2025

This thesis is submitted for the degree of MSc by Research.

1. Abstract

African trypanosomes, the causative agents of sleeping sickness (*Trypanosoma brucei*) and nagana (*Trypanosoma congolense*), experience host-derived increases in temperature, due to the prominent mammalian symptom of fever during infection. In response, these parasites activate a heat shock (HS) response that promotes survival under elevated temperatures. This work aimed to characterise the HS response in *T. brucei*, with preliminary comparative analysis in *T. congolense*.

The results show that *T. brucei* immediately responds to a 1 hour 41 °C HS with a lag in cell growth lasting around 24 hours, influenced by a HS-induced reversible cell cycle arrest observed as an enrichment of G2M cells, which was resolved following around 8 hours of recovery. Immediately after HS in *T. brucei* an increase in DHH1 foci occurred, interpreted as the formation of P-bodies, alongside the collapse in polysomes. The collapse in polysomes reflects the state of global translational arrest, through the decrease in active translational machinery via a decrease in polysomes and an increase in ribosomal subunits. Polysome collapse in *T. brucei* post-HS was viewed as being more severe in procyclic form cells than bloodstream form cells, potentially indicating differences in thermotolerance across the cell cycle. Polysome analysis in *T. congolense* also found a decrease in polysomes post-HS, also presenting an increase in ribosomal instability as observed in *T. brucei*, indicating a level of conservation in the two species' HS response.

Understanding the HS response in trypanosomes is crucial for uncovering parasite survival strategies under host-induced stress and may highlight unique regulatory pathways absent in mammalian hosts. These insights offer potential avenues for future targeted therapeutic development; potential common targets in *T. brucei* and *T. congolense* are of interest due to their ability to co-infect the same hosts and their exposure to similar selective pressures.

Table of Contents

Acknowledgements

Firstly, I would like to express my complete gratitude to my first supervisor Professor Mick Urbaniak for your unwavering support in the project, but also for having a huge role in my academic journey from my first year onwards. Thank you for always pushing me to grow.

To Dr Caroline Dewar, my second supervisor, thank you for supporting me throughout this rollercoaster of a year and helping me with my confidence. Your knowledge and teaching have been instrumental to this project and beyond.

Dr Aro Nugawela, thank you for giving me the tools to complete this project and your patience in training me. Thank you again alongside Lizzie Thwaites for introducing me to the world of research.

A huge thank you to all the people within the Lancaster University Biomedical and Life Sciences research community that brought positivity into each day while I was working in the lab. Notably Lydia Ireland, (soon to be Drs) Chloe Barnes and Megan Dooley, thank you for being the best role models and science friends.

To my best friends, Abbey, Ellie and Soph, thank you for always listening to me talk about parasites and trying to understand. You have all kept me sane and smiling throughout the tough times.

Finally, to my Mum, Dad and James, I simply could not have done this without you all. Thank you for teaching me that hard work pays off and to aim high…even if that is in the world of trypanosome biology!

Declaration

I, Hannah Pyle, confirm that the work presented in this thesis is my own and has not been submitted in substantially the same form for the award of a higher degree elsewhere. Where information has been derived from other sources, I confirm this has been indicated in the thesis.

Signed 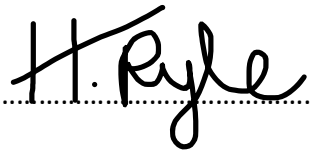

Abbreviations

AAT – Animal African trypanosomiasis

ALPHA1 – AlaH-like phosphatase

BSF – Bloodstream form

CNS – Central nervous system

DHH1 – DEAD box RNA helicase

eIF2a – Eukaryotic initiation factor 2 alpha

HAT – Human African trypanosomiasis

HS – Heat shock

HSG – Heat shock granule

HSP – Heat shock protein

HSF1 – Heat shock factor 1

NECT – Nifurtimox-Eflornithine Combination Therapy

ORF – Open reading frame

PABP – Poly-A binding protein

PCF – Procyclic form

PTU – Polycistronic transcription unit

RBP – RNA binding protein

rSAP – recombinant Shrimp Alkaline Phosphatase

SIF – Stumpy induction factor

SL – Spliced leader

SRF – Serum Response Factor

Tm – Melting temperature

UTR – Untranslated region

VSG – Variant surface glycoprotein

ZC3H11 – Zinc finger CCCH-type 11

2. Introduction

2.1 *Trypanosoma* and disease

Trypanosoma brucei ssp. are obligate extracellular parasitic eukaryotes transmitted by sub-Saharan African tsetse flies, causing human African trypanosomiasis (HAT) (Roditi and Lehane, 2008; Daniels et al., 2010). This disease is also known as 'sleeping sickness,' due to its distinctive symptoms of affected sleep patterns, caused by disturbed circadian rhythms through inflammatory responses in hypothalamic structures within the brain (Lundkvist et al., 2004). Further implications of HAT include hypersensitivity reactions, cardiac arrhythmias, and liver portal infiltration (Dunn, Wang and Adigun, 2018).

HAT has two distinct stages of disease: initially the haemolymphatic stage, in which trypanosomes circulate in the blood or lymphatics. It is characterised by symptoms including intermittent headaches, fevers, malaise, and arthralgia (Ibrahim et al., 2022). The second stage is the meningoencephalitic stage, in which the trypanosomes penetrate the blood-brain barrier and infect the central nervous system (CNS), causing the characteristic neurological symptoms of the disease (World Health Organisation, 2023).

The incidence of HAT peaked in both 1997 and 1998 with records of over 35,000 cases (Franco et al., 2022). Improved preventative measures via vector control, for example the use of insecticides in tsetse traps, have decreased the number of HAT cases (Bauer et al., 2011). Alongside the improvement in detection methods, the use of more sensitive and faster antigen-based tests as well as improved therapeutic agents have reduced the burden of the disease (Geerts et al., 2020). Despite progress, surveys in 2008 estimated the annual burden of HAT to be at 70,000 cases, whilst exceeding a million disability-adjusted life years lost (Fèvre et al., 2008). A reduction in cases has been observed, notably in 2020 there were 663 cases recorded, but issues of records on the field may not account for all patients affected (Franco et al., 2022).

Following the decline in cases, there has been a shift in concern to the disease in animals known as animal African trypanosomiasis (AAT) and is also referred to as

'Nagana.' AAT is a significant concern due to its direct impact upon around 70% of rural poor people in Sub-Saharan Africa that are reliant upon livestock, with around 200 million livestock owners in the region. Infected cattle decrease in value (Erdaw, 2023): the disease results in fever, muscular wasting, anaemia, and oedema, reducing milk production and meat yields (Love and Mair, 2012). This has a profound economic effect upon African agriculture, with annual losses of US $4.75 billion, through the death of 3 million cattle implicating gross domestic production, for example due to the loss of animal power for traction (Food and Agriculture Organization and World Health Organisation, 2001).

Further to the discussed microenvironments of the blood, lymph and CNS that cause the characteristic symptoms of trypanosomiasis, trypanosomes also inhabit extravascular tissues including skin and adipose tissues (Trindade et al., 2016). This has been shown in *in vivo* mouse infections, finding that 28 days post infection 6 depots of fat were found to contain more trypanosomes than in the blood, brain and all other tested organs combined (Trindade et al., 2016). These alternative parasite host niches are important as nearly all existing treatments and diagnostics of trypanosomiasis use the assumption that the parasites are within the bloodstream; therefore, in some cases some patients may be treated incorrectly or misdiagnosed.

2.2 Trypanosome Biology

2.2.1 Species of African *Trypanosoma*

The main species of African trypanosomes are *Trypanosoma brucei, Trypanosoma congolense* and *Trypanosoma vivax* (visualised in Figure 2.1), as the three main species contributing to HAT and AAT in Sub-Saharan Africa as vector-borne parasites (Katabazi et al., 2016). The most detected sub-species in HAT cases is *T. brucei gambiense*, found in 98% of patients (Vourchakbé et al., 2020), with the remainder of patients infected with *T. brucei rhodesiense*, the only other human-infective sub-species. *T. vivax* is the most prevalent trypanosome species found infecting African cattle (Ooi et al., 2016). However, *T. vivax* is a trypanosome that is also found outside of Sub-Saharan Africa, in

Central and South America and the Caribbean, where other biting flies transmit the parasite mechanically (Boes and Durhan, 2017).

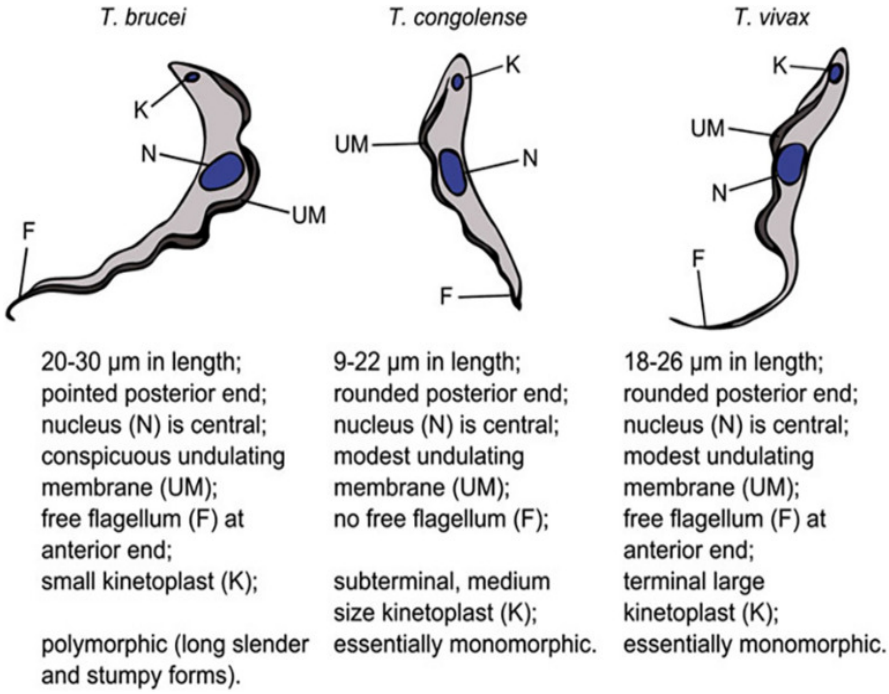

Figure 2.1: Schematic highlighting the morphological differences between the species of *Trypanosoma.* Such differences may be exploited for species identification, however with biological variability PCR techniques are used for accuracy (Kizza et al., 2021). (Figure extracted from Kizza et al., 2021).

T. congolense and *T. vivax* are the major causative agents of Nagana and are unable to infect humans (Gardiner and Mahmoud Musa Mahmoud, 1992; Pereira et al., 2022). Co-infections occur where the host may be infected by multiple species at one time, this is highlighted by Paguem et al (2019) in finding 11.4% of infected cattle to have mixed infections. Co-infections of both *T. brucei spp.* and *T. vivax* were most common at around 70%; 0.68% of animals were found to be infected with all three species (Paguem et al., 2019). The prevalence of the African trypanosome species is location-dependent, *T. vivax* is predominantly in the East, *T. congolense* in the West and *T. brucei spp.* is more sporadic across Sub-Saharan Africa, thus making co-infections with *T. brucei* more common (Katabazi et al., 2021).

The different trypanosome species causing HAT and AAT affects the disease epidemiology, severity, and management; therefore, efficient detection is vital (Adams,

Hamilton and Gibson, 2010). The species are distinguished using their differing genes encoding a small ribosomal subunit for detection in PCR (Desquesnes and Dávila, 2002). However, in Sub-Saharan Africa diagnostic testing is limited, particularly as PCR detection requires specialist equipment and is more expensive than the treatment costs (Gummery et al., 2020).

2.2.2 African Trypanosome Life Cycle

Trypanosomes have a complex lifecycle that occurs in two phases of within the tsetse fly (*Glossina*) vector and within the mammalian host bloodstream, this lifecycle for *T. brucei* is shown in Figure 2.2; this complete cycle occurs over three weeks (Centers for Disease Control and Prevention, 2019). Within the mammalian host *T. brucei* bloodstream form parasites initially have a slender morphology and undergo binary fission, before reaching a density threshold to produce an oligopeptide stumpy induction factor (SIF) (Rojas et al., 2019). SIF is used in cell-to-cell communication via quorum sensing, inducing the differentiation into stumpy form trypanosomes, required for the chronic stage of disease for subsequent transmission (Rojas et al., 2019).

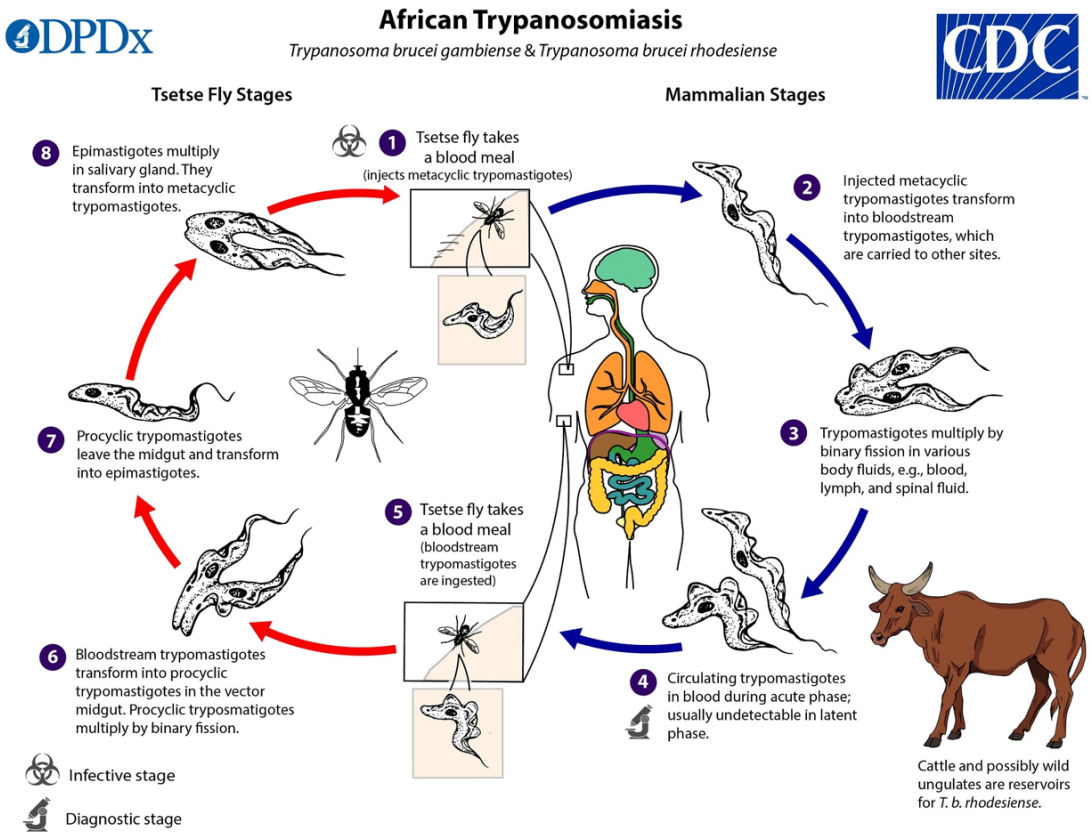

Figure 2.2: Schematic of the extracellular biphasic lifecycle in *Trypanosoma brucei gambiense* and *Trypanosoma brucei rhodesiense*. The life cycle involves an infected tsetse fly injecting metacyclic trypomastigotes into a mammalian host, enabling entrance into the lymphatic system and bloodstream. In which, these parasites differentiate into bloodstream form trypomastigotes, which replicate via binary fission and penetrate further within the host. Within the bloodstream, to maintain infectivity in the host, the trypanosomes differentiate from proliferative slender forms into non-proliferative stumpy forms (Larcombe et al., 2023). A tsetse fly becomes infected upon ingestion of these bloodstream form trypanosomes in the uptake of blood from an infected host. Within the tsetse fly midgut, the trypomastigotes differentiate into procyclic trypomastigotes, that migrate to the fly salivary gland and undergo replication via binary fission, enabling continued transmission (Centers for Disease Control and Prevention, 2019). (Figure extracted from Centers for Disease Control and Prevention, 2019).

To complete the digenetic cycle, trypanosomes have adaptations that enable continued metabolism across different hosts. Transcriptomic data demonstrated that initial expression is of high affinity hexose transporters and glycolytic enzymes that support glycolysis in the glucose-rich mammalian bloodstream (Naguleswaran et al.,

2021). A shift in mitochondrial activity occurs alongside the differentiation of slender to stumpy cells, with increased mitochondrial activity seen in stumpy form cells in preparation for the environment of the tsetse fly midgut (Dewar et al., 2018). Gene expression switches to facilitate proline uptake and catabolism within the midgut of the tsetse fly, thus enabling continued survival in changed extracellular environments of the host and vector (Naguleswaran et al., 2021).

The life cycle for *T. congolense* differs to that of *T. brucei* within the vector, as *T. congolense* undergoes an asymmetric division stage that facilitates the differentiation of proventricular trypomastigotes into epimastigotes (Peacock et al., 2012). Furthermore *T. congolense* is initially established in the fly midgut with differentiation of the parasites into PCF before their migration to the anterior of the fly and invasion of the mouthparts or proboscis in their metacyclic form (Peacock et al., 2012). The insect-form *T. congolense* parasites do not colonise the salivary glands for transmission as observed within the *T. brucei* life cycle (Peacock et al., 2012). In contrast to *T. brucei*, *T. congolense* does not have a morphologically distinct stage of parasites in stumpy form; instead, they transition into cell cycle arrest at peak parasite burden within the mammalian host to control growth (Silvester, Ivens and Matthews, 2018). Bloodstream *T. congolense* adjust their transcriptome at higher densities, decreasing the expression of genes involved in the cell cycle, whilst genes associated with stress responses and immune evasion are upregulated; therefore *T. congolense* do not have a stumpy morphology but their transcriptome is modified to be stumpy-like (Silvester, Ivens and Matthews, 2018).

Trypanosomes complete a life cycle that enables the parasites to sustain proliferative and differentiation stages, to infect both the insect vector and mammalian host (Wheeler, Gull and Sunter, 2019). The cell cycle enables the duplication of the nucleus, kinetoplast and cytoskeletal structures through the progression from quiescence to mitosis, summarised in Figure 2.3 (Benz et al., 2017). However, within the literature there is disagreement that quiescence is not a distinct form due to its association with stumpy form differentiation, potentially acting as a transitional state before cells re-enter the cell cycle for proliferation within a suitable environment (Reuter et al., 2023). Within the cell cycle the flagellum duplicates to form a new flagellum, which assembles alongside the old from the pro-basal body acquiring a transition zone or axoneme prior to cytokinesis (Vaughan and Gull, 2015).

Stage	Characteristics	Nucleus Count	Kinetoplast Count
G0 (Quiescent)	Cells are metabolically active but non-proliferative.	1	1
G1 (Gap 1)	Preparation for DNA replication, growth phase and increase in protein synthesis.	1	1
S (DNA Synthesis)	DNA replication (both nuclear and kinetoplast).	1	1
G2 (Gap 2)	Synthesis of mitotic proteins and DNA checkpoint control.	1	1
M (Mitosis)	Mitosis, chromosome and kinetoplast segregation, followed by cytokinesis.	2	2

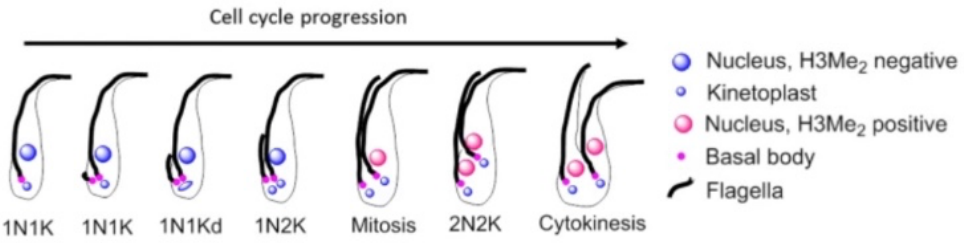

Figure 2.3: A summary of events that occur within the cell cycles of *T. brucei* and *T. congolense*. The 1 and 2 for the nucleus count highlights uninucleate and binucleate cells

respectively. The 1 and 2 for the kinetoplast count highlights monogenomic and bikinetoplastic cells respectively. These nuclear and kinetoplast counts are visually shown in the diagram along with flagellar changes that occur in the *Trypanosoma* cell cycle (Adapted and extracted from Benz et al., 2017).

2.2.2.1 African trypanosome survival of the mammalian host immune response

Virulence refers to the degree of harm or damage a pathogen causes to its host; is a measure of severity of disease caused by the pathogen (Sharma et al., 2016). The degree of virulence has evolutionary significance in maximising 'parasite fitness' and survival for selection (Bose, Kloesener and Schulte, 2016). Virulence factors enable continued pathogen survival and subsequent harm to the infected host, often overcoming the host's defences (Sharma et al., 2016).

Variant surface glycoproteins (VSGs), compose a dense coat to the outer surface of *Trypanosoma* spp. BSF parasites, which subsequently "shields" or limits access of host immune cells to other invariant surface proteins (Mugnier, Stebbins and Papavasiliou, 2016). An example of a virulence factor is antigenic variation through VSG switching; this changes the surface molecules enabling active evasion from the immune system of the mammalian host (Mugnier, Stebbins and Papavasiliou, 2016). The immune system generates a specific response via polyclonal B cell activation initially resulting in the production of IgM antibodies against the VSG to support parasite elimination (Donelson, 1998). Therefore, following change in VSG, the antibodies are no longer able to bind, resulting in increased parasite burden (Figure 2.4) (Oldenburg, 2021).
VSG switching provides trypanosomes protection against the host immune system attack, as specific antigen-antibody binding is required to support parasite elimination. For example, by marking the parasite for phagocytosis or activating the classical complement pathway for subsequent parasite lysis (Forthal, 2014). Therefore, with an absence of antibodies with specificity to a changed VSG coat, subsequent downstream immune system activities are unable to be promoted, supporting parasite survival.

VSG switching occurs through various mechanisms including gene conversion or telomere exchange between polycistronic transcription units, a transcriptional switch in which a new expression site is expressed and gene conversion activating a silent VSG gene via *in situ* recombination events (Li and Zhao, 2021).

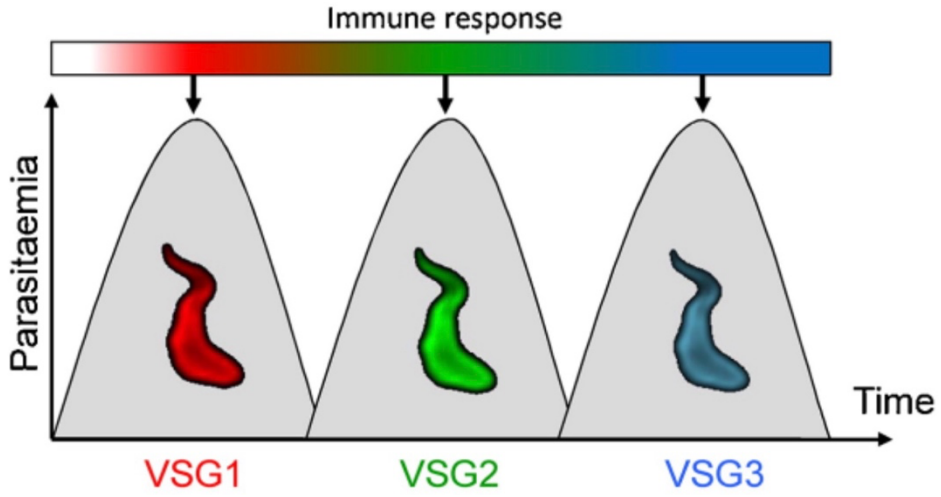

Figure 2.4: Graphical representation of the effect of VSG switching upon the immune response resulting in waves of parasitaemia. The figure demonstrates in initial infection the increase in parasite burden or parasitaemia with parasites with VSG1, once at the peak of parasitaemia the host immune system responds specifically subsequently decreasing parasitaemia. The parasite completes VSG switching to express VSG2, causing an increase in parasitaemia in the absence of specific immunity. This continues until peak parasitaemia at which the immune system specifically responds with anti-VSG2 antibodies, decreasing parasitaemia before repeated events with further VSG switching and resulting waves of parasitaemia (Magez et al., 2002). (Figure extracted from Oldenburg, 2021).

VSG also limits the impact of the mammalian immune response via the removal of bound anti-VSG antibodies. This occurs through movement via hydrodynamic forces to the flagellar pocket for endocytosis and degradation of the antibodies (Mugnier, Stebbins and Papavasiliou, 2016).

Late infections of *T. brucei* subspecies cause severe neurological symptoms to the host, which occur due to the penetration of parasites across the blood brain barrier (W. Masocha et al., 2008). This movement across the cerebral vessels is facilitated by

lymphocyte-derived interferon-gamma (Masocha et al., 2004). Trypanosomes within the CNS results in increased pathology and provides the parasites with protection from the host's immunological response. This is because the CNS vessels provide a barrier to inflammatory cell infiltration through a structure composed of endothelial cells, astrocytes and basement membranes (Masocha et al., 2004). However, this also has the capacity to limit parasite survival as increased pathology is associated with increased mortality of the required mammalian host.

These abilities of the parasites to survive the defence of the immune system increases the difficulty for a patient to eliminate the infection; therefore, drug treatments for trypanosomiasis are essential. This is emphasised by VSG switching preventing vaccine development, as there is no constant antigen present for vaccines to specifically target.

2.2.3 Trypanosome Genome Structure and Protein Expression

2.2.3.1 Trypanosome Genome Structure

Trypanosoma and *Leishmania* are kinetoplastids, which are protozoan flagellates characterised by DNA localising to both the nucleus, and unlike other eukaryotes, mitochondrial DNA is localised to a discrete body (kDNA, or the 'kinetoplast') (Stuart et al., 2008). The genome of *T. brucei* is composed of approximately 9068 predicted genes that are organised as 11 megabase chromosomes, compacted to fit within the 2.5 μm diameter of the nucleus (Berriman, 2005; Daniels, Gull and Wickstead, 2010).

Most eukaryotes use a monocistronic transcription system, with each gene having a specific promoter enabling the production of its own mRNA (Cortazzo da Silva, Aoki and Floeter Winter, 2022). However, kinetoplastid parasites lack specific promoters for each gene; therefore, RNA polymerase II binds to few initiation sites. This generates long clusters of precursor messenger mRNA (pre-mRNA), which are described as a polycistronic transcription units (PTUs), and these contain up to 100 kb of functionally unrelated genes (Kieft et al., 2024) (shown in Figure 2.5). The PTUs in *T. brucei* are arranged in head-to-tail fashion with around 8,131 protein-coding open reading frames

(ORFs) (Subramaniam et al., 2006; Daniels, Gull and Wickstead, 2010). Due to the sequence of continuous ORFs, trypanosomes lack introns (non-coding genes), with 0.00022 introns per gene compared to 10.37 introns per gene in humans; conventional intron splicing is not required in trypanosomes (Sakharkar, Chow and Kangueane, 2004; Kramer et al., 2016). The PTUs are further arranged via histones, which support the regulation of transcription initiation and termination via altering the chromatin structure to being more open or compacted and influencing the access of effector proteins (Saha, 2020; Gauri Deák et al., 2023).

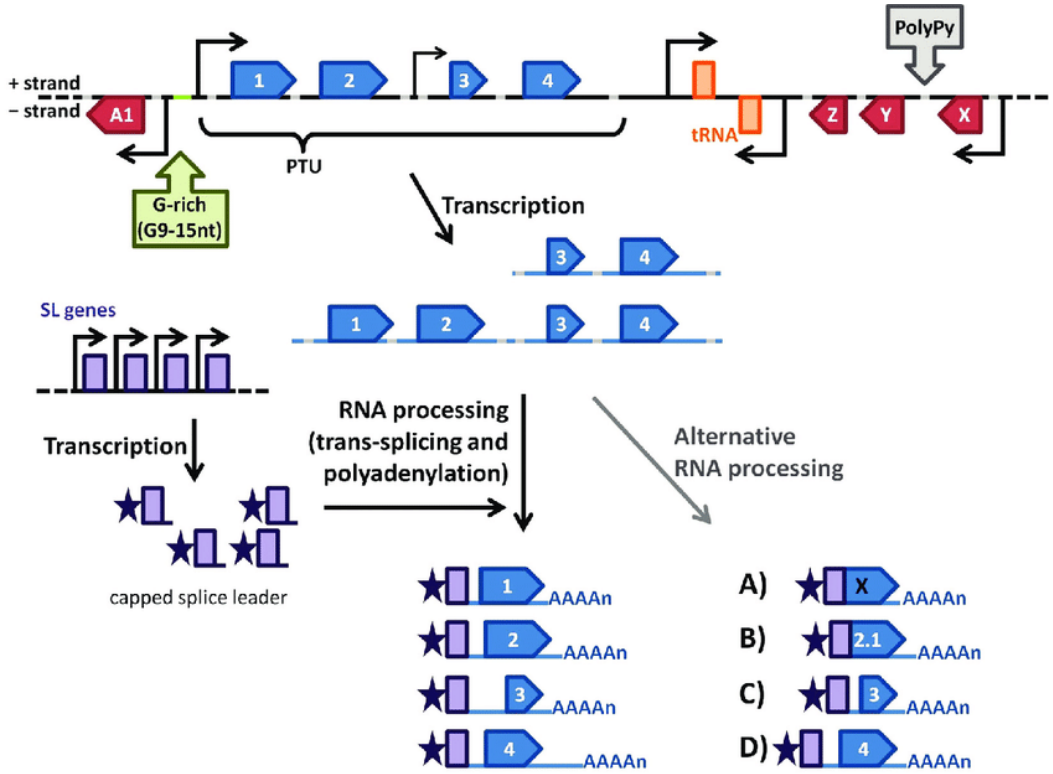

Figure 2.5: Schematic of polycistronic gene expression in trypanosomes. Trypanosome post-transcriptional mRNA modifications are completed following polycistronic RNA synthesis; including trans-splicing of the spliced leader RNA, polyadenylation, and internal splicing (Kieft et al., 2024). The blue numbered arrows represent large clusters of unrelated genes as polycistronic transcription units (PTUs), which are transcribed by RNA pol II from the transcriptional start sites. This results in individual monocistronic mRNAs that have the addition of the capped splice leader (SL) via trans-splicing coupled with polyadenylation. Mature mRNAs are then exported to the cytoplasm for alternative RNA processing or internal trans-splicing and polyadenylation occurs (Teixeira et al.,2018). (Figure extracted from Teixeira et al.,2018).

In *T. brucei* the PTUs of different stabilities and lengths are located at different chromosomal regions. 'Core' chromosomal regions contain long and stable PTUs; are the site of conserved housekeeping genes (Müller et al., 2018). Whilst subtelomeric regions contain shorter and fragmented PTUs with frequent strand switches, these are enriched to support the rapidly evolving gene families, for example those required for VSG switching (Müller et al., 2018).

Ribosomes translate a single coding sequence per mRNA, and as a result trypanosomes require processing to separate unrelated genes within a PTU (shown in Figure 2.5). RNA processing is completed via trans-splicing, in which an identical 39 nucleotide 5' spliced leader (SL) cap sequence is added to the 5' end of 'cut' mRNAs from the PTUs (Liang et al., 2003). This SL sequence is encoded by a separate spliced leader gene; its presence is vital for the stability and translation of the mRNA. Polyadenylation is the 3' addition of a polyA tail and is co-ordinated to occur one transcript downstream of SL addition (Koch et al., 2016). Like trans-splicing, polyadenylation influences the stability and translation initiation of the mRNA; together this processing results in the production of individual, mature, capped and polyadenylated mRNAs for transcription. Alternative splicing may occur in trypanosomes as around 11% of protein-coding transcripts present a unique 3' single SL site (Kolev., 2010). Alternative polyadenylation may also occur in trypanosomes, through recognition of different polyA sites at the 3' end, resulting in altered 3' untranslated region (UTR) lengths, which can influence stability and translation (Koch et al., 2016). The polycistronic genome prevents regulation at transcription initiation, meaning post-transcription provides an essential level of control (2.2.4.2) (Kieft et al., 2024).

2.2.3.2 Trypanosome Post-transcriptional control

Control of gene expression is determined through the fate of mRNA, which is reliant upon their associated RNA-binding proteins (RBPs) that can alter mRNA abundance and translation (Sabalette et al., 2023). This is completed by ApaH-like phosphatase 1 (ALPH1), which binds to the coding regions of mRNA, and as a phosphatase is hypothesised to remove phosphate groups from the 5' of mRNA to prepare for its

degradation by XRNA, their co-localisation at the cellular posterior indicates their connection (Kramer, 2017). The activity of ALPH1 is essential as its RNAi depletion is lethal to trypanosome cells, due to an increase in deadenylated mRNAs that have not yet started decay (Kramer, 2017). Other RBPs can have the opposite effect in stabilising RNAs or enhancing translation, for example DRBD18, which forms essential interactions with DRBD2 in bloodstream form, and ZC3H41 in procyclic form *T. brucei,* shown in its depletion resulting in the decreased translational efficiency in around 40% of transcripts analysed in ribosome profiling (Clayton, 2013; Ciganda et al., 2023).

The importance of RBPs for translation regulation is demonstrated in the trypanosome life cycle, for example ZFP1 and ZFP2 (Hendriks et al., 2001). ZFP1 has a significant role in expression of EP procyclin within procyclic forms of *T. brucei*; knockdown of ZFP2 reduced the EP procyclin expression and as a result inhibited differentiation of cells into PCF (Kolev, Ullu and Tschudi, 2014). The precise mRNA targets of ZFP1 are not yet established, but for ZFP2 it is understood that for its activity it binds to proline-rich regions in other proteins (Hendriks, 2001). ZFP2 RNAi knockdown highlighted its requirement for differentiation into procyclic forms, causing reduced EP procyclin expression, impaired kinetoplast repositioning and inhibited morphological changes (Hendriks et al., 2001; Kolev, Ullu and Tschudi, 2014).

RBP10 in *T. brucei* has an important role in modulation of the BSF stage, as its knockdown resulted in a decrease in expression of typical BSF-specific mRNAs (Kolev, Ullu and Tschudi, 2014). This translational suppression is specifically achieved through RBP10 binding to procyclic-specific mRNAs with a ‘UAUUUUUU’ motif at the 3’ UTR (Mugo and Clayton, 2017). Additionally, RBP10 expression in PCF cells resulted in an increase in these BSF-specific mRNAs, highlighting the control it exhibits within the trypanosome life cycle (Wurst et al., 2009; Kolev, Ullu and Tschudi, 2014).

Finally, within the trypanosome cell cycle RBPs are utilised to control expression within the tsetse fly, for example RBP6 which is increased in expression in parasites within the fly proventriculus, compared to PCF cells within the midgut (Kolev, Ullu and Tschudi, 2014). RBP6 binds the 3’ UTRs of target mRNAs, particularly those encoding transmembrane proteins to regulate mRNA stability (Trenaman et al., 2019).

Therefore, RBP6 is able to support life cycle progression with expression of infective metacyclic-specific surface glycoproteins (Kolev et al., 2012; Kolev, Ullu and Tschudi, 2014). The significance of RBP6 in differentiation is shown *in vitro,* that RBP6 alone may be used in in its inducible expression to trigger the differentiation of cells from procyclic to metacyclic to bloodstream form (Shi, Butler and Tschudi, 2018).

2.2.3.3 Trypanosome Translation

Translation is the process of producing polypeptide chains from mature mRNA, this process in trypanosomes is comparable to mammalian translation, due to evolutionary conservation (Clayton, 2019). Translation is shown within mammalian organisms to be one of the most tightly regulated cellular processes, essential for correct gene expression and protein synthesis (Jia et al., 2024). Therefore, translation in trypanosomes is comparative to the process in other eukaryotes, consisting of stages of initiation, elongation and termination.

However, key differences include the unique six cap binding translation initiation factors, a novel de-capping enzyme and the role of RNA-BPs that recruit a mRNA stabilising factor to regulate translation, to compensate for the lack of transcriptional control (Clayton, 2019). Translation is shown to be crucial in the stage-specific regulation within the parasite life cycle for the shift in protein expression between the forms in mammalian host and tsetse fly vector (Clayton, 2019). The importance of extensive translational complexity in the life cycle has been demonstrated through comparative ribosome profiling of bloodstream and procyclic forms, finding a 100-fold range and life cycle-specific differences in translational efficiency (Vasquez et al., 2014).

2.2.4 Parasite Burden and Host Temperature

Fever or pyrexia occurs within the mammalian host as a response to infection and has been conserved in warm and cold-blooded vertebrates for over 600 million years of evolution (Evans, Repasky and Fisher, 2015). Fever is defined as being an increase in the body's 'set point' temperature beyond the daily variation threshold; in humans the

body temperature is expected to vary by around 0.5 °C, therefore increases greater than this are classified as feverous (Balli, Sharan and Shumway, 2023). This increase is of the body's core temperature, causing the elevation of both intravascular and extravascular tissue temperatures, both of which trypanosomes use as niches during infection (Trindade et al., 2016; Balli, Sharan and Shumway, 2023). Fever is initiated when an infection triggers an increase in the hypothalamic 'set point' temperature, causing vasoconstriction of blood vessels to increase body temperature (Evans, Repasky and Fisher, 2015). The fever response is associated with inflammatory disease as 'calor' or heat via body temperature is recognised as one of the four cardinal signs of inflammation (Evans, Repasky and Fisher, 2015). Fever has an immunological benefit, specifically in adaptive immunity, through promoting the overall activation, function and delivery of immune cells, whilst causing direct damage to the pathogen (Appenheimer and Evans, 2018).

Pyrexia occurs differently in poikilotherms as they are unable to internally raise their body temperature and instead complete behavioural fever which increases their body temperature through movement into warmer environments (Huntingford, Rey and Quaggiotto, 2020). For example, fish move to warmer water as a part of their response to infection, to support the stimulation of a strong immune response to eliminate a pathogen (Huntingford, Rey and Quaggiotto, 2020). This is important within the life cycle of trypanosomes as the tsetse fly vectors are poikilotherms, meaning insect-form parasites may also experience HS due to the fly completing behavioural fever (Lord et al., 2018).

Peaks in trypanosome parasitaemia or parasite burden have been closely associated with fever since 1910; this relationship is defined by the peak in temperature corresponding with the ascending wave of parasitaemia (Figure 2.6) (Ross and Thomson, 1910). An effective immune response decreases the parasite load, therefore, as the load increases, the immune response also increases which signals to the hypothalamus to increase the temperature of the host; thus, causing a continuation of the period of fever or triggering further pyrexia (Evans, Repasky and Fisher, 2015; Macaluso et al., 2023).

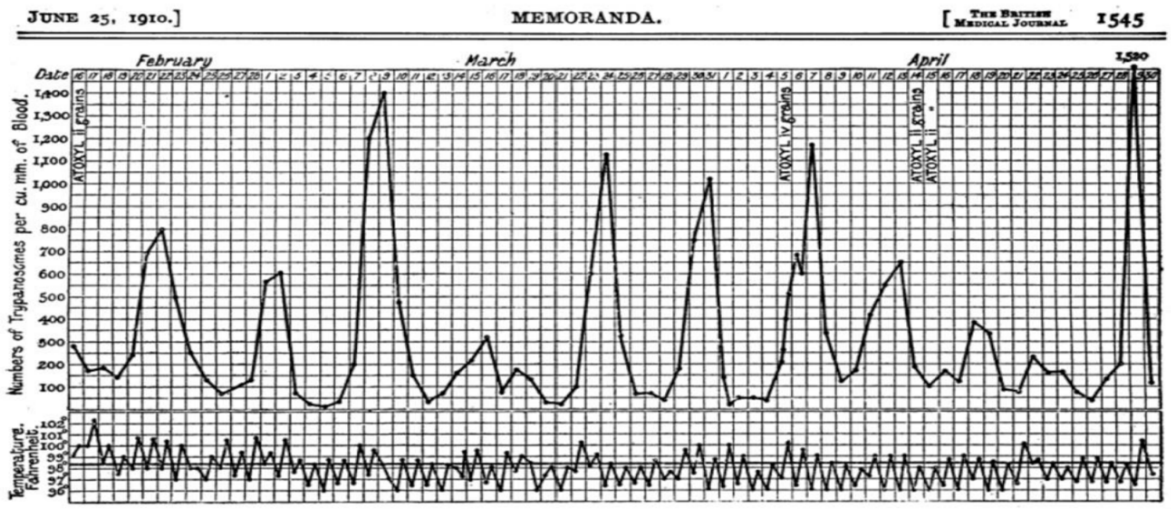

Figure 2.6: Graphical representation of the waves of parasitaemia during infection and the corresponding waves in fever experienced by the host. (Figure extracted from Ross and Thomson, 1910).

Fever in humans results in an increased metabolic demand. This is shown in the increase in body temperature by 1 °C requiring a 10-12.5% increase in metabolism, weakening the host and facilitating a sustained parasitic burden (Balli, Sharan and Shumway, 2023). As a result, parasite load and fever define the stage of infection. As in the acute phase, there is a rapid increase in parasitaemia and fever (Bush and Vazquez-Pertejo, 2024). Whilst in the chronic phase, the host's immune system may act to reduce damage by downregulating the fever response and therefore enabling persistent parasitaemia (Bush and Vazquez-Pertejo, 2024).

Temperatures within humans during a trypanosomiasis infection have been found to exceed 38 °C and reach 41 °C in two patients infected with *T. b gambiesense* in Gabon within a case study in 2019 (Iroungou et al., 2020). Temperatures of cattle infected with AAT can have rectal temperature measurements exceeding 39.4 °C and can have temperatures significantly higher than those recorded in non-infected cattle (Magona et al., 2008).

However, pyrexia is not the only instance that causes an increase in the temperature of the mammalian host beyond its physiological norms. Physical activity is also able to elevate the host's temperature, for example the body temperature of cattle can

increase up to 2 °C in the duration of the day due to movement (Magona et al., 2008). Furthermore, a gazelle which is a natural host of AAT, have body temperatures recorded up to 43 °C upon physical activity (Taylor and Lyman, 1972). Therefore, physical activities of a mammalian host may also result in an increase in the temperature trypanosomes are exposed to during infection without immunological involvement.

Overall, the understanding of the relationship between parasite burden and host temperature is vital for the understanding of trypanosomes, as fever is a prominent symptom observed across mammalian hosts. Despite being insufficient for diagnosis, fever may indicate stage of infection as acute or chronic, which supports the use of drugs that are stage specific. Due to the role of fever within trypanosomiasis infections, treatment using anti-parasitic drugs would also help to reduce fever as a symptom through a decrease in the parasite burden. Therefore, as an established side effect to the infection in both HAT and AAT, understanding of how trypanosomes sense and respond to the elevated temperatures they encounter during periods of host fever to ensure their continued survival is of great interest. In future work this understanding could be extended to support the discovery of new molecular targets to be used in drug development for the combined treatment of *T. brucei* and *T. congolense.*

2.2.5 Treatments for Trypanosomiasis

In the process of understanding potential new molecular targets, it is vital to consider the existing treatments and how they target trypanosomes to reduce the parasite burden. Historically, the disease stage was vital in deciding the methods of treatment, as upon CNS involvement in the meningoencephalitic stage, treatments required more toxic and invasive drugs that penetrate the blood-brain barrier (World Health Organization, 2023).

The early observation in 1904 by Paul Ehrlich of the anti-trypanosomal activity of the dye trypan blue, led to the development of more potent derivatives and ultimately suramin (Wiedemar, Hauser and Mäser, 2020). Therefore, the first stage of disease was

treated with suramin, used for its trypanocidal activity by its interference with trypanosome energy production in respiration and glycolysis, via inhibition of enzymes involved in the oxidation of reduced nicotinamide-adenine dinucleotide (Drug Bank, 2025). Pentamidine was introduced as a treatment of early disease stages, which acts through interfering with *Trypanosoma* DNA biosynthesis and disrupts mitochondrial processes, following active transport of the drug intracellularly, resulting in parasite death (Sands, Kron and Brown, 1985; Babokhov et al., 2013). Both agents cause side effects ranging from nausea to renal issues (Babokhov et al., 2013).

Treatment of the second stage primarily used melarsoprol, which enters the trypanosomes via adenosine transporters, allowing interactions with thiol groups on essential proteins, resulting in the deprivation of the main sulfhydryl antioxidant and trypanothione reductase inhibition (Friedheim, 1949; McCarthy, Wortmann and Kirchhoff, 2015). This activity impairs the ability of trypanosomes to utilise oxygen. Melarsoprol is highly toxic as it may cause the complication of reactive arsenical encephalopathy which itself has a high mortality, killing 5% patients (Lejon, Bentivoglio and Franco, 2013).

The use of both melarsoprol and pentamidine has been limited due to cross-resistance observed over 60 years, due to adaptation of the *T. brucei* adenosine transporter to avoid drug uptake, through the loss of function of aquaglyceroporin 2, which has the role of supporting drug accumulation (Baker et al., 2013).

Infections within the CNS can also be treated by eflornithine, which inhibits ornithine decarboxylase, which catalyses amine-based compound synthesis (Milord et al., 1992; Rogers, 2024). This interferes with replication within the CNS, whilst having side effects of gastrointestinal disturbances, bone marrow toxicity, convulsions and hearing impairment (Burri and Brun, 2003).

Replacing eflornithine monotherapy, Nifurtimox-Eflornithine Combination Therapy (NECT) has been the front-line treatment since the early 2000s, due to its ability to be administered more easily, requiring fewer human and material resources (Yun et al., 2010). The combination uses nifurtimox with its production of toxic reduced products of oxygen and eflornithine with ornithine decarboxylase inhibition (Scholar, 2008;

Rogers, 2024). The use of NECT as a treatment for the second stage of HAT was recognised for its improved safety and efficacy profiles, compared to other existing stage 2 treatments, leading to its addition to the WHO Essential Medicines List in 2009 (Yun et al., 2010).

Recent developments have also enabled the use of fexinidazole to treat both the first and second stage of *T. brucei gambiense* infections as an oral treatment, with further reduced life-threatening adverse effects (Lindner et al., 2024). This is achieved through generating damage to the trypanosome DNA and proteins using active amines, sulfoxide and sulfone as active metabolites (Tarral et al., 2014; Ryan, Gutman and Chancey, 2022). However, identifying both the disease stage and species of infection remains essential for effective treatment of trypanosomiasis (Table 2.1).

Table 2.1: Notable drug treatments for trypanosomiasis, with their specific disease stage for treatment, their target *Trypanosoma* species and year of first use. Table made using Babokhov et al., 2013 and Lindner et al., 2024. The numbers in disease stage are indicative of first (1) or second (2) stage. References for the first year of use in corresponding order: Suramin (Wiedemar, Hauser and Mäser, 2020), Pentamidine (American Chemical Society, 2017), Melarsoprol (Darby, 2017, pp.195–211), Eflornithine (Steverding, 2010), NECT (Drugs for Neglected Diseases initiative, 2003); Fezinidazole (Drugs for Neglected Diseases initiative, 2004).

Drug	**Disease stage**	**Target species**	**Year of first use**
Suramin	Haemolymphatic (1)	*T. brucei gambiense*	1922
Pentamidine	Haemolymphatic (1)	*T. brucei rhodesiense*	1937
Melarsoprol	Both (1+2)	*T. brucei rhodesiense* *T. brucei gambiense*	1949
Eflornithine	Meningoencephalitic (2)	*T. brucei gambiense*	1990

Nifurtimox-Eflornithine Combination Therapy	Meningoencephalitic (2)	*T. brucei gambiense*	2009
Fexinidazole	Both (1+2)	*T. brucei gambiense*	2018

Furthermore, current work has oxaboroles in clinical trials, which are small compounds that contain boron, which have promise in their potency, oral activity and have efficacy after one dose (Jacobs et al., 2011). Specifically, acoziborole has been shown to cross the blood-brain barrier and therefore has success in treating both stages of disease, whilst maintaining a low toxicity (Tarral et al., 2023).

2.3 Heat Shock Response in Eukaryotes

An increase in temperature causes protein unfolding, which acts as a signal of stress inducing the heat shock (HS) response. The HS response is an evolutionary conserved response in eukaryotes, working to protect cells from a proteotoxic environment in increased temperature, maintaining protein homeostasis (Mahat et al., 2016). The response occurs at the transcriptional level enabling the immediate expression of cytoprotective genes that encode molecular chaperones and powerful protein re-modelers (Verghese et al., 2012).

The mechanism is well-established in eukaryotes including the increased expression of heat shock proteins (HSPs) that limit damage to cellular proteins upon increased temperatures, reducing the effects of heat-induced protein denaturation and mis-folding (Zheng et al., 2024). The extent of heat-induced protein damage is dependent upon the protein, as each has its own melting temperature (Tm). Upon increasing the temperature of exposure by a few degrees towards a protein's Tm, there is an increase in the proportion of proteins that are aggregated and partially unfolded; complete denaturation occurs beyond a protein's specific Tm value (Day et al., 2002).

In this state of stress with heat-induced damage to proteins, general housekeeping genes, including those involved in growth and metabolism, are downregulated to 'prioritise' the expression of the HS response-specific genes to support survival. This is shown in the upregulation of 1,500 genes and the downregulation of 8,000 genes (Mahat et al., 2016). Examples of genes upregulated include heat shock factor 1 (HSF1) and serum response factor (SFR), which are translation factors altering the promoters of specific genes and increasing transcription by RNA polymerase II (Mahat et al., 2016).

Within the mammalian response, heat shock transcription factors trimerize and translocate to the nucleus where they bind to heat shock elements within the promoter regions of heat shock genes, activating transcription and selectively upregulating HSP expression (Alagar Boopathy et al., 2022). Essential HSPs upregulated in this process include HSP70, HSP90 and small HSPs (Hu et al., 2022).

Due to the polycistronic genome in trypanosomes, specific gene regulation via promoters, HSF1 and SFR are absent within their HSR. As a result, distinct differences in the response may be used as a novel target for therapeutic development to treat trypanosomiasis. However, further research is required in understanding the response in pathogenic protists prior to exploring drug opportunities.

2.3.1 Translational arrest and phosphorylation of eIF2a

In mammalian models, the HSR is triggered through intracellular sensing of stress through damaged proteins, this stress triggers the phosphorylation of eukaryotic initiation factor 2 alpha (eIF2a) (Jagadeesh Kumar Uppala et al., 2018). Phosphorylation occurs specifically at serine 51, resulting in the inhibition of the eIF2-GTP-$tRNA^{Met}$ ternary complex, which has vital activity in initiating protein translation (Kedersha et al., 2005). Therefore, when its activity is inhibited, it results in translational arrest and reduced protein synthesis. This phosphorylation is also vital for the formation of stress granules (Kedersha et al., 2005).

2.3.2 The role of P-bodies and stress granules in the HSR

Polysomes, or polyribosomes are groups of ribosomes that translate a single mRNA, in the conditions of heat-induced stress polysomes collapse to monosomes and release mRNAs into the cytoplasm (Timur Baymukhametov et al., 2022). The increase in free mRNA in the cytosol results in the formation of stress granules and increase in processing bodies (P-bodies). Stress granules are used to store, stabilise and protect untranslated mRNAs, which following a decrease in the heat stimulus may be released from the granules and move to the P-bodies to re-initiate translation or to be degraded (Marcelo et al., 2021).

The origin of the mRNAs in stress granules has been demonstrated using inhibitors of translation elongation that stabilise polysomes and result in the dissociation of stress granules, whereas inhibitors that destabilise polysomes increase the formation of stress granules (Kedersha et al., 2000; Kramer et al., 2008). This is suggestive of a dynamic exchange of mRNAs between the polysomes and stress granules that may occur during and after a stress stimulus (Kedersha et al., 2000; Kramer et al., 2008).

During the stress response, P-bodies are formed and expanded. These are cytoplasmic granules that have a regulatory role in translational repression through the decay of mRNAs (Luo, Na and Slavoff, 2018). Therefore, P-bodies have a vital role in preventing the production of damaged proteins and in favouring the expression of essential proteins during the HSR. The maintenance of P-bodies is reliant upon the presence of resident proteins. In humans this is specifically the RGG domain of Lsm4 and DDX6, with depletion causing a decrease in the number of P-bodies (Luo, Na and Slavoff, 2018). Like with stress granules, the dynamic association between polysomes and P-bodies has also been shown through the involvement of polysome-associated RNA binding proteins, including SCP160 which regulates the formation of P-bodies in yeast (Weidner et al., 2014).

Both stress granules and P-bodies are membrane-less ribonucleoprotein-based granules that have been suggested to form via liquid-liquid phase separation in stress, stimulated by the increased concentrations of protein and mRNAs (Riggs et al., 2020). Fluorescence-activated particle sorting was completed for P-bodies, enabling the

identification of 125 stable protein components, of which 28 were identified as being present within the core proteome of stress granules (Kearly et al., 2024). This presents a level of similarity that supports the exchange that occurs between stress granules and P-bodies.

Furthermore, the similar compositions of both stress granules and P-bodies are shown through their common proteins including translational repressors, for example CPEB1, RAP55, YB-1, and the RNA helicase DHH1, but their roles may differ dependent on the granule (Stoecklin and Kedersha, 2013). However, differences in stress granules include the presence of translation factors, such as eIF3b, eIF4A and eIF4G, as well as RBPs (PABP and G3BP) (Stoecklin and Kedersha, 2013), whilst within P-bodies there are distinct components that support their role in mRNA degradation including de-capping enzymes Dcp1 and Dcp2 (Stoecklin and Kedersha, 2013).

Within the HS response, there is also the formation of heat shock granules (HSGs) which specifically occur only in the presence of a heat stimulus. These are composed of HSPs, which may also be present in some stress granules. There are also HSG-specific proteins including HSP27 which has been found to be exclusive to HSGs over other stress-induced stress granules (Reineke and Lloyd, 2013). The role of HSGs utilises the HSPs in their sequestration of damaged proteins in the HSR.

Overall, in the HS response, the collapse of polysomes results in the movement of mRNAs to stress granules for storage or to P-bodies for degradation. This supports the selective upregulation of the HS-essential proteins that facilitate survival including HSPs, through preventing non-essential mRNAs from accessing translational machinery.

2.3.3 HS response regulation: The HSP70-HSF1 titration model

The receiving of a HS signal is vital to initiate the protective HS response; this is supported through the activation of HSF1, a vital component of the eukaryotic heat shock pathway. HSF1 is a transcription factor, in non-stressed conditions it is bound to HSP70 and therefore inactive. In the stress of a heat shock stimulus, causing damage

to intracellular proteins, HSP70 is recruited in its protective role as a molecular chaperone; therefore, is unbound from HSF1 (Masser, Ciccarelli and Andréasson, 2020). The unbound status of HSF1 results in its activation via its trimerization and causes it to translocate into the nucleus for downstream activation of HS response genes via RNA polymerase II (Sarge, Murphy and Morimoto, 1993; Masser, Ciccarelli and Andréasson, 2020). Following the production of sufficient HSP70 to respond to the stimulus, HSP70 binds HSF1 resulting in its inactivation, thus creating a negative feedback loop called the HSP70-HSF1 titration model (Figure 2.7) (Masser, Ciccarelli and Andréasson, 2020).

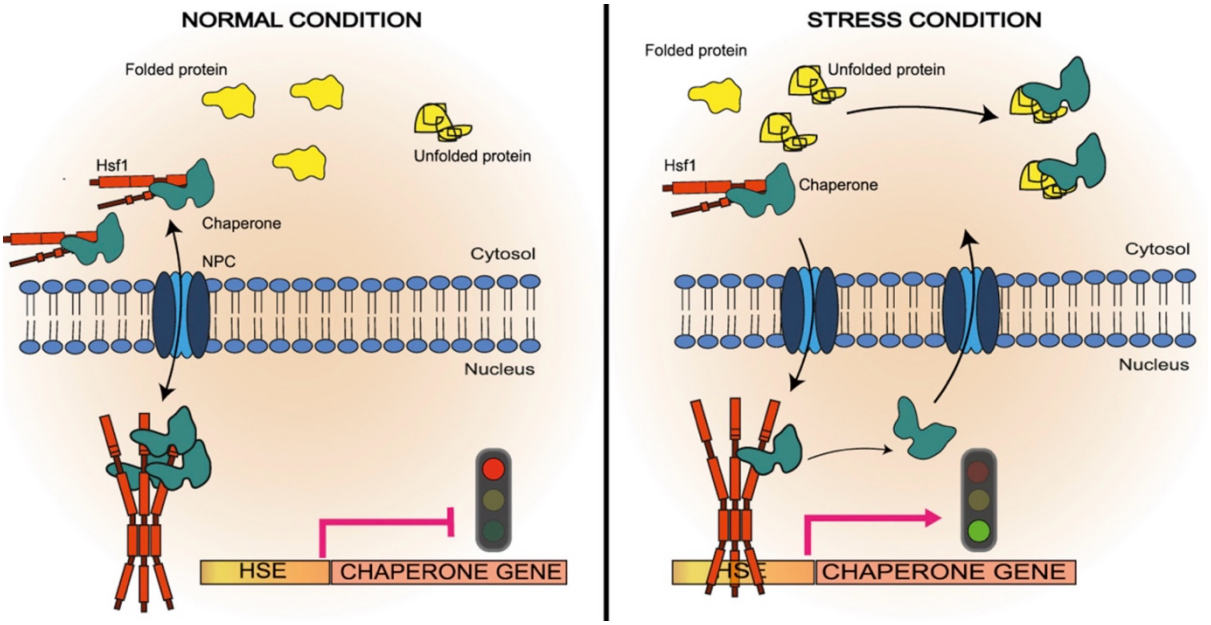

Figure 2.7: Schematic image demonstrating the change that occurs during the HS response controlled by the HSP70-HSF1 titration model. Under normal conditions there is a lack of damage for HSP70 (blue) to respond to; therefore, is bound to HSF1 (red) in an inactive conformation, preventing the expression of HS genes. In stress induced by heat there is demand for HSP70 to act as a chaperone in the increased levels of damaged protein. This causes HSP70 to unbind HSF1 resulting in its active conformation, enabling it to activate the expression of heat shock genes. This increases the expression of HSP70 until the levels exceed the demand for damage at which HSP70 binds HSF1, causing inactivation and the return to normal conditions. (Figure extracted from Masser, Ciccarelli and Andréasson, 2020).

2.4 Heat shock in Trypanosomes

Unlike the equivalent heat shock response in eukaryotes, the response is less well-defined in trypanosomes. However, there are known differences due to the polycistronic genome of trypanosomes, lacking the ability to complete the specific upregulation of individual genes. Therefore, one key difference in the response between trypanosomes and other eukaryotes is the control mechanism of changed expression, as trypanosomes lack the classical HSF1 pathway, highlighted in Figure 2.7 (Schwede, Kramer and Carrington, 2011). Instead, trypanosomes use the zinc finger CCCH-type 11 (ZC3H11) RNA-binding protein, and an as-yet-unclarified mechanism of SL cap addition. However, the HS response is thought to have its similarities across kinetoplastids and eukaryotes through the conserved outcome of increased expression of select genes required for survival, whilst decreasing the expression of most other genes uninvolved in the response (Schwede, Kramer and Carrington, 2011).

The HS response in trypanosomes may be summarised as being initiated by exposure to an increased temperature, causing cellular damage including protein denaturation, triggering stress signalling pathways. This signalling enables the activation of HS transcription factors, the collapse of polysomes with global translational arrest and the formation of stress granules. These changes to the cells enable the preferential expression of HS-essential proteins (including HSPs), whilst non-essential mRNAs uninvolved in the response are decreased in expression by being sequestered or degraded. Due to the change in expression of all mRNAs to be upregulated or downregulated to prioritise survival, there is a lack of a comparative control that remains constant both pre- and post- HS in studies of the response. The overall change in expression levels enables HSPs to act as molecular chaperones to support protein refolding and limit aggregation, having a protective effect until the HS stimulus subsides and HS recovery is able to occur for the cells to return to their pre-HS growth rate (Schwede, Kramer and Carrington, 2011). This process in *T. brucei* is outlined alongside the HS response pathway in mammalian systems for comparison in Figure 2.8.

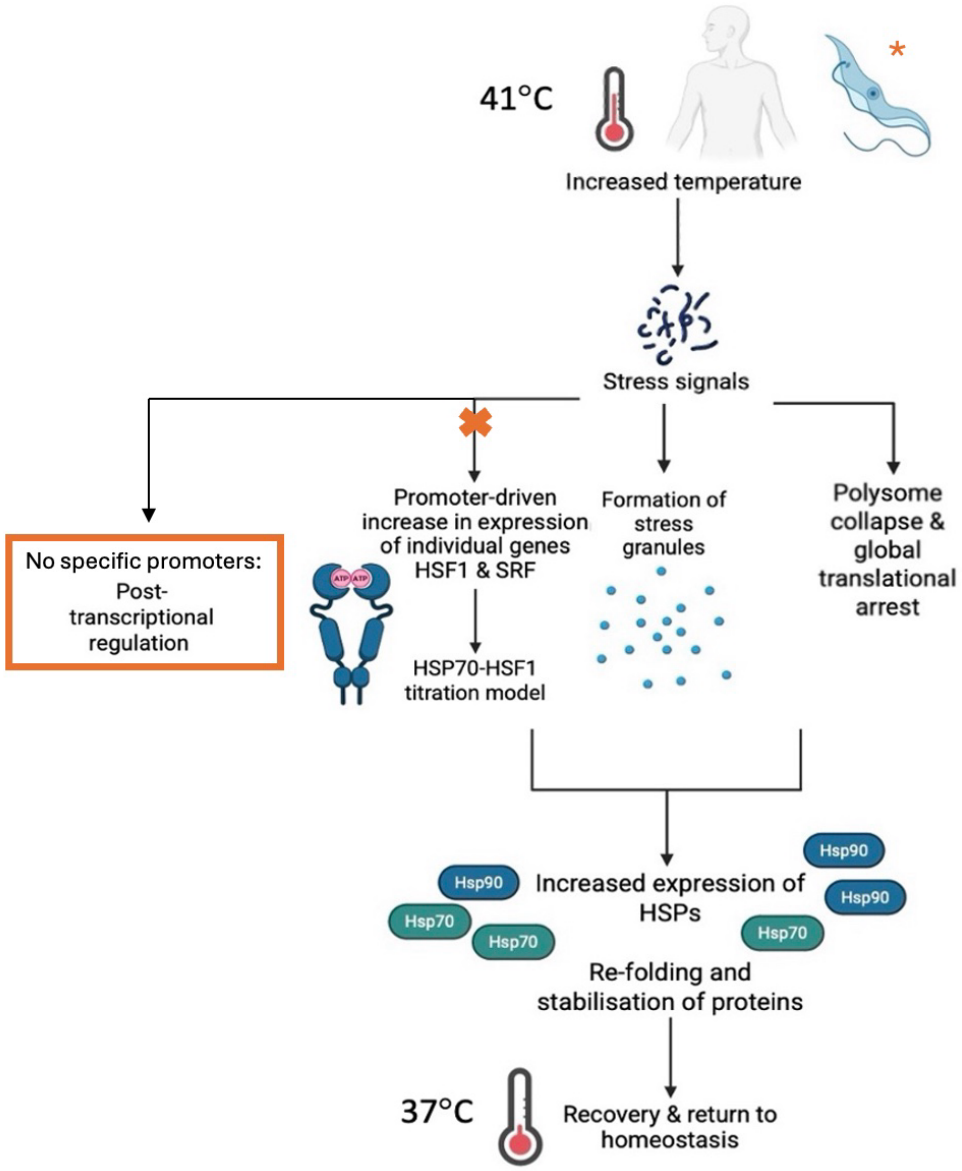

Figure 2.8: Schematic summary representing the timeline of events that occurs in the heat shock response at 41 °C in mammalian systems and *T. brucei.** The differences in the trypanosome HS response are highlighted in orange. Across both systems the HS response is initiated through stress signals, for example heat-induced protein denaturation. In mammals this activates specific gene upregulation using promoters, enabling the activity of HSF1 in the titration model with HSP70. Whilst, in trypanosomes there is no specific gene promoters due to the polycistronic nature of the genome; therefore, the parasites use post-transcriptional regulation. These mechanisms of expression alongside the formation of stress granules and collapse of the polysomes, enables the selective upregulation of HSPs which act as molecular chaperones to enable the re-folding and stabilisation of heat-damaged proteins. This response is maintained in both organisms until the heat stimulus subsides, enabling the return of homeostasis: via the dissolution of stress granules, the reformation of polysomes (end of

global translational arrest) and the return to the normal levels of expression for housekeeping genes and HS-specific genes. This figure was made using BioRender.

Due to the differences between the parasite and host HS response, understanding the trypanosome HS response may enable the discovery of novel drug targets that have limited effects upon the mammalian host.

2.4.1 The heat shock response in *Trypanosoma brucei* mammalian and insect forms

Kinetoplastid parasites demonstrate a conserved HS response involving heat shock proteins acting as molecular chaperones, for example HSP90, HSP60 and small HSPs), which are upregulated in thermal stress (Prasanna and Upadhyay, 2021). *Leishmania* parasites use this mechanism for intracellular survival and to support their differentiation from promastigotes to amastigotes. The HS response is used within *Leishmania* life cycle progression as promastigotes experience an increase in environmental temperature from the sandfly vector (around 25 °C) into the mammalian host (around 37 °C), enabling a remodelling of HSP expression and activity required for survival and proliferation (Prasanna and Upadhyay, 2021).

The HS response in *T. brucei* can occur in both the bloodstream and procyclic morphological forms, with no established comparable role in the life cycle like in *Leishmania;* notably the response in PCF trypanosomes demonstrates a more pronounced rapid increase in heat shock protein expression. This is because PCF reside at cooler temperatures (around 27 °C). Therefore, they have a lower basal expression of HSPs than BSF parasites, which reside at a higher temperature (around 37 °C) and as a result require a higher baseline expression level of HSPs to ensure stability within their environment (Igor Minia et al., 2016).

Thermotolerance is defined as a transient adaptation to thermal stress that enables cells to be more resistant to higher temperature (Dewhirst et al., 2003). PCF *T. brucei* may be interpreted as being more thermotolerant than BSF, as PCF parasites are required to withstand a greater range of temperatures experienced within the tsetse

fly between 20 and 37 °C (Droll et al., 2013). This large range in temperature exists as the fly's internal temperature is regulated by its movements between light and shade (Pagabeleguem et al., 2016). This is emphasised within the laboratory setting as PCF cells are cultured at 27 °C, however they can be cultured for up to 4 days at 37 °C, surviving an increase of 10 °C from the standard culture conditions (Droll et al., 2013). Whilst BSF are cultured at 37 °C and are unable to survive 2 hours of heat shock at 41 °C (Ooi, Benz and Urbaniak, 2020), this is suggestive of a smaller range of temperatures BSF parasites are able to tolerate compared to that of PCF parasites. However, there is similarity between the responses in *T. brucei* PCF and BSF, including the induction of the HS response at around 41 °C, but the response in procyclic forms has been studied considerably more due to the presence of a clearer and more significant response.

The heat shock response in *T. brucei* (BSF) has been shown experimentally to occur after incubation at 41 °C, with 1 hour being optimal to measure the response (Kramer et al., 2008; Ooi, Benz and Urbaniak, 2020). This was demonstrated as 30 minutes at 41 °C showed no difference in the growth rate of cells compared to cells without HS treatment, whilst, 1 hour at 41 °C caused an insignificant 22% decrease in motile cells, with viable cells but a reduced rate of growth (Ooi, Benz and Urbaniak, 2020). Further exposure showed greater decreased capacity to recover, as 2 hours lead to a significant 74% decrease in motile cells, with a loss in viability up to 48 hours following exposure; and 4 hours incubation caused cell death following treatment (Ooi, Benz and Urbaniak, 2020). The correlation of the increased exposure time at 41 °C with decreasing viability of the BSF cells is shown in Figure 2.9A and agrees with the work of Kramer et al (2008) in PCF cells and since supported by the unpublished Masters work by Aelmans (2022) and Taylor (2024); therefore, demonstrating an effect upon growth across both life cycle stages of *T. brucei* and indicating similar levels of thermotolerance.

Furthermore, Ooi, Benz and Urbaniak (2020) confirmed that the remaining viable cells after exposure to the heat stimulus were able to survive due to the HS response. This was demonstrated via RT-PCR, to observe the fold-change in mRNAs corresponding to heat shock proteins to confirm the HS response had occurred via the conclusion that HS proteins are being expressed in response to HS (Figure 2.9B).

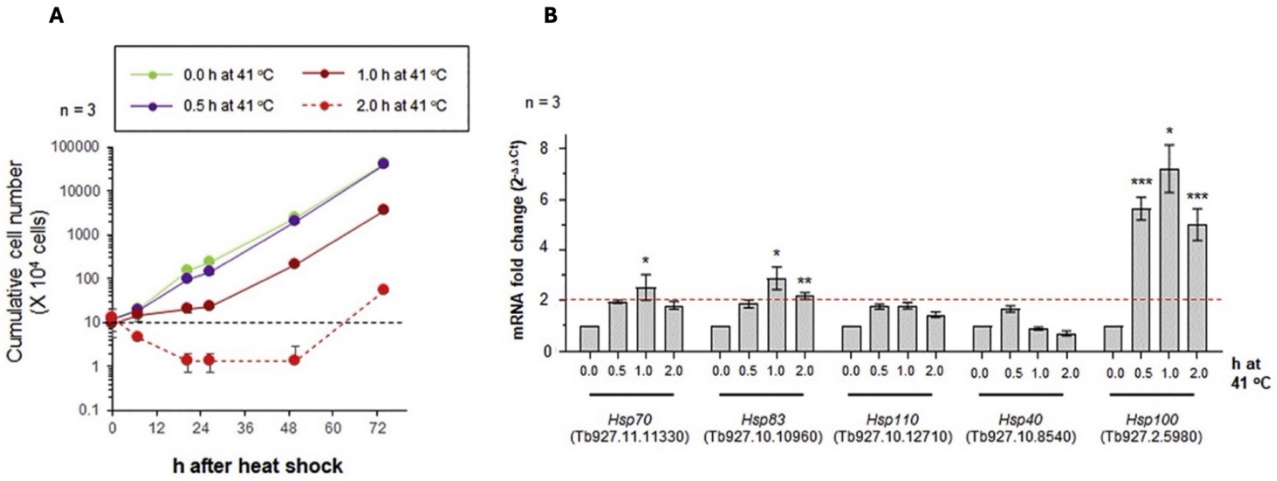

Figure 2.9: (A) A graphical representation of the impaired growth of BSF *T. brucei* for different times of treatment at 41 °C. (B) The fold change in HSP mRNA observed via qPCR for the change in treatment time at 41°C. (A) The increase in exposure to the stimulus of 41 °C is shown to have a more detrimental effect on growth and recovery, with 1 hour being optimal to observe the HSR. (B) Furthermore, 1 hour at 41 °C is shown as the ideal condition to measure the HSR, as it is the condition at which the greatest fold change in mRNA is observed across the selected HSPs. (Figures extracted from Ooi, Benz and Urbaniak, 2020).

2.4.1.1 Motility in trypanosomes

A read-out this study uses, with the intention to represent the HS-induced lag in growth displayed in Figure 2.9A, is the analysis of trypanosome motility as an additional quantification of cell health. The name *Trypanosoma* or 'auger cell' refers to the parasite's motility driven by a single flagellum (Shimogawa et al., 2018). The movement is considered 'auger-like' because the flagellum wraps around the cell body in a left-handed helix from the posterior to the anterior ends of the cell; its beating results in a spiral waveform causing the cell to rotate (Hill, 2003).

Motility of trypanosomes is dependent upon the single flagellum, which emerges from the basal body at the posterior end of the cell, in proximity to the flagellar pocket invagination in the plasma membrane (Hill, 2003). The flagellum is attached to the cell body via an ordered array of transmembrane cross-links, forming the flagellum attachment zone, a unique cytoskeleton-membrane domain (Hill, 2003). The flagellum generates movement through ATP-dependent conformational changes in the axonemal dynein motors attached to incomplete microtubule structures (Langousis and Hill, 2014).

Within serum, *T. brucei* has been recorded to move as fast as 20 μm/second (Engstler et al., 2007). This level of movement is beneficial for the parasite's transmission and pathogenesis, through allowing their migration to the tsetse fly salivary gland and supporting the crossing of the blood brain barrier for the invasion of the CNS (Langousis and Hill, 2014). Motility has value in highlighting the viability of trypanosomes, as Broadhead et al (2006) demonstrated that RNAi knockdown of various proteins identified within the trypanosome flagellar proteome in *T. brucei* inhibited motility and subsequently resulted in non-viable phenotypes. This is explained as in the absence of flagellar motility, cytokinesis is unable to occur, with the formation of new flagella and pockets formed in incorrect locations, causing an increase in endocytosis that is toxic to the cell (Broadhead et al., 2006). As a result, this study tests the hypothesis that because a reduction in cell growth occurs post-HS (Ooi, Benz and Urbaniak, 2020) a reduction in cytokinesis also occurs which is driven by a reduction in cell motility.

2.4.1.2 Justification of 41 °C as the standard HS experimental temperature

This study uses 41 °C for 1 hour as the stimulus for HS as both studies by Kramer et al (2008) and Ooi, Benz and Urbaniak (2020) provide evidence that 1 hour at 41 °C are experimentally tractable conditions to measure the HS response in both PCF and BSF *T. brucei* respectively. However, this results in questions of physiological relevance particularly as in humans 41 °C is considered as the threshold for hyperpyrexia, which

is rare and can be fatal, causing ischemic brain injury and permanent hepatocellular damage (Balli, Sharan and Shumway, 2023). Therefore, experiments ran in these conditions may be questioned as to whether the response measured is representative of the one that occurs *in vivo*. However, with the observed experimental survival of *T. brucei* cells after HS, this mimics the same survival that occurs *in vivo* in fever just over a shorter induction with a higher temperature. As a result, the use of 41 °C for 1 hour as a HS appears to stimulate the same response that occurs within the host, whilst being experimentally tractable with the previous work of Kramer et al (2008) and Ooi, Benz and Urbaniak (2020) and producing comparative data.

2.4.1.3 Polysome collapse and global translational arrest

Polysomes are RNA-protein complexes, potentially associated with the cytoskeletal network; they each contain a single mRNA with a bound ribosome around every 100 nucleotides, or a bound ribosomal subunit in the absence of mRNA (Reithmeier, 1996; Heyer and Moore, 2016). It takes approximately 30 seconds for a polysome in a eukaryotic cell to synthesise a protein of 400 amino acids, demonstrating their essential activity in protein expression (Reithmeier, 1996). Global translational arrest is the halt of protein synthesis and polysomes collapse into monosomes: this occurs during the HS response to conserve cellular resources towards survival. The precise trigger of this arrest is not yet fully known if it is due to an unknown eIF2A phosphorylation mechanism or an eIF2A-independent mechanism (Ooi, Benz and Urbaniak 2020). However, Kramer et al (2008) found after HS a decrease in polysomes is associated with a global translational arrest and occurs independent of phosphorylation of eIF2A at its Thr169 site. The early events of phosphorylation in the trypanosome HS response are later discussed in more detail (2.4.1.6).

Kramer et al (2008) characterised heat shock in PCF *T. brucei* as causing a reduction in polysomes and mRNA levels, alongside an increase in cytoplasmic stress granules and P-bodies. This reduction in polysomes was shown to occur after 15 minutes of HS at 41 °C by measurement of the absorbance profiles of sucrose density gradients after centrifugation (Figure 2.10). Sucrose density gradients are used as an indication of

translational status, as mRNA found in more sucrose-dense fractions have a higher ribosome content bound and are longer in length providing more space for ribosomes to bind to, indicating these mRNAs as being actively translated by the polysomes (Chassé et al., 2017).

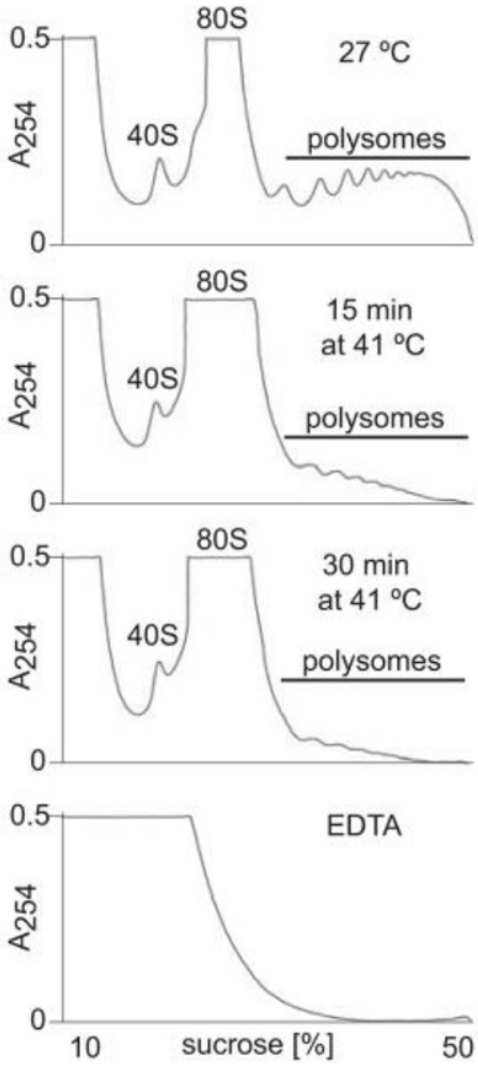

Figure 2.10: Polysome gradient fractionation profiles of *T. brucei* with HS treatment. The profiles were generated using absorbance at 254 nm and a sucrose gradient. HS at 41 °C shows polysome collapse into monosomes via the loss of peaks, which is shown to increase with severity upon an increased exposure time to the stimulus of 41 °C. This effect is comparative to the known positive control of 50 mM EDTA treatment which dissociates polysomes. (Figure extracted from Kramer et al., 2008).

This method of using sucrose gradients for polysome gradient fractionation to observe the collapse of polysomes was also used with PCF *T. brucei* at a lower HS temperature (37 °C) and additionally with bloodstream form *T. brucei* by Minia and Clayton (2016) (Figure 2.11). The HS of PCF cells at a lower temperature (37 °C), is shown to induce a weaker response than the one observed at 41 °C, indicated by less of a shift in the polysome peaks. Taken together, this work presents evidence for the collapse in

polysomes with global translational arrest within the *T. brucei* HS response in both procyclic and bloodstream forms, with its severity dependent upon the temperature and time. However, evidence for the re-formation of polysomes within HS recovery and the precise timing alongside the dissolution of stress granules is unclear and requires more research (discussed further in 2.4.1.4).

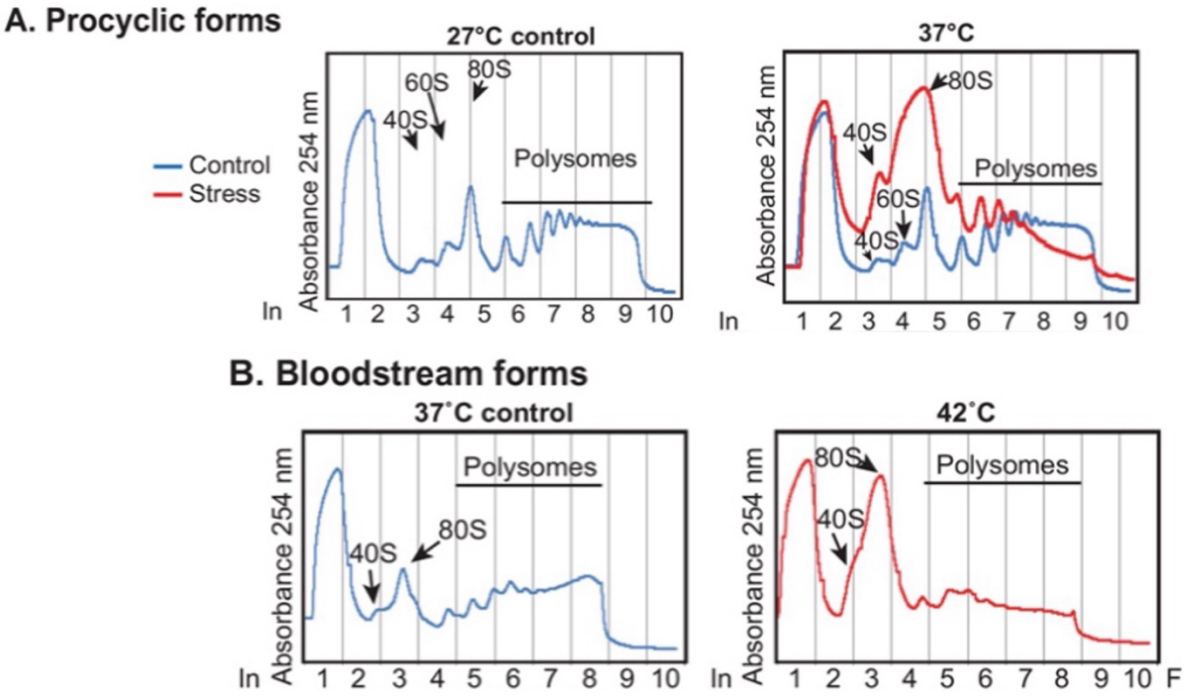

Figure 2.11: Polysome gradient fractionation profiles of *T. brucei* with HS treatment. The profiles were produced using absorbance at 254 nm, with the peaks representing the small (40S), large (60S) ribosomal subunits, monosomes (80S) and polysomes. Heat shock, with increased temperature in both procyclic (A) and bloodstream (B) forms show a decrease in the polysome peak, highlighting the collapse in polysomes within the *T. brucei* HS response. (Figure extracted from Minia and Clayton 2016).

2.4.1.4 The formation of HS stress granules

In trypanosomes, the formation of stress granules (SGs) is a key aspect of the HS response due to their potential function as a reservoir to sequester non-essential mRNAs from the cytosol, shown in a decreased level of protein expression achieved by reduced access to active polysomes (Aye, Li and He, 2024). There is debate within the

literature as to whether these sequestered non-essential mRNAs are stored within SGs to be released and re-used following HS or if all mRNAs are degraded within SGs and new mRNAs are synthesised for expression after HS.

The continued use of the mRNAs released by stress granules after cellular stress has been demonstrated in mammalian cells using RNA sequencing (Das et al 2022). However, another study also in mammalian cells found that a key role of SGs was in mRNA degradation, rather than storage (Namkoong et al.,2018). These observations of SGs post-stress have primarily been conducted in mammalian cells with other stress stimuli and therefore further research is required to understand this aspect of HS recovery within trypanosomes. However, in trypanosomes it is established that SGs form in stress to support the expression of prioritised mRNAs, however evidence of this specifically within the HS response is lacking. The storage of mRNAs for future use after HS is supported by SGs containing translation initiation complexes, including poly-A binding protein (PABP), eIF4E and eIF4G, as components of the eIF4F complex (Aye, Li and He, 2024). The presence of these complexes indicates them supporting mRNAs re-entering an active translation cycle upon their release post-HS, facilitating the return of pre-HS mRNA expression levels (Kramer et al., 2008).

However, the role of SGs as being degradative is highlighted by them containing essential components for mRNA decay for example AlaH-like phosphatase (ALPHA1), DEAD box RNA helicase (DHH1) and SCD6 (Aye, Li and He, 2024). ALPHA1 is a major mRNA decapping enzyme essential for 5’ mRNA decay that is enriched in SG punctates post-stress (Aye, Li and He, 2024). Whilst DHH1 functions as an ATPase in mRNA decay and translation repression (Sweet, Kovalak and Coller, 2012). Thus, DHH1 requires ATP binding for its localisation within the granules; the requirement of ATP is demonstrated in the SG composition differing in ATP depleted conditions correlating with the change in SG dynamics (Mugler et al., 2016). SCD6 has a downstream effect of mRNA decay and storage, as it induces ribonucleoprotein granule formation and in the resolution of HS, the SGs release SCD6 which supports the formation of polysomes (Krüger, Hofweber and Kramer, 2013). As a result, the role of stress granules and the factors involved in determining the fate of mRNAs within the trypanosome HS response are areas requiring more work.

The formation of SGs is dependent upon the collapse of polysomes, which is a conserved mechanism also observed within mammalian cells (Kedersha et al., 1999; Kramer et al., 2008). The collapse in polysomes results in an increase in non-polysome associated free mRNAs within the cytoplasm to be incorporated into SGs (Kramer., 2008). The requirement for polysome collapse to enable the formation of SGs is highlighted in *T. brucei* cells treated with cycloheximide, which stabilises polysomes to maintain their mRNA content, resulting in inhibited SG formation due to an absence of free mRNA (Kramer et a., 2008). This was observed by Kramer et al (2008) as maintained polysomes in polysome analysis after HS and no increase in SG-like localisations observed by immunofluorescence microscopy. Further work of Aye, Li and He (2024) treated *T. brucei* cells with puromycin, which induces a premature termination of translation and releases mRNA from active polysomes. Puromycin was shown to induce a collapse in polysomes but not increase the number of SGs, showing that the collapse of polysomes is not sufficient alone to promote SG formation (Aye, Li and He, 2024). Therefore, future work is required to develop our understanding of this dynamic relationship between polysomes and SGs, as well as to observe this relationship as the SGs dissolve and polysomes reform in recovery.

One issue within this area of research includes the fact that the difference between P-bodies and SGs is not well-defined within the trypanosome HS response. P-bodies are often recognised due to the presence of degradation markers, including XRNA; further differences are presented within Table 2.2 (Kramer et al., 2012). However, their composition overlaps as RBPs colocalise with each other; this level of similarity is represented in both having DHH1 and SCD6 as components (Kramer et al., 2008). DHH1 has a crucial role in translational repression; DHH1 is seen to localise to P-bodies with mRNA as an alternative to translation, but in early stress it is seen to relocate to the SGs (Kramer et al., 2010). SCD6 is present in both P-bodies and SGs, indicative of their roles in both translational control and mRNA decay pathways, with SCD6 interacting with translation initiation factors and proteins required for de-capping (Krüger, Hofweber and Kramer, 2013). However, the composition of these foci may differ depending upon the stress that induced their formation.

Table 2.2: The protein components of stress granules and P-bodies in *T. brucei.* The sources for the information presented within the table is highlighted for each component.

Component	Stress granules	P-bodies	Role	Sources
PABP2	Present	Not detected	mRNA polyadenylation and polyA length	Benoit et al., 2005; Aye, Li and He, 2024
XRNA	Not detected	Present	mRNA degradation	Cassola, 2011; Kramer et al., 2012
ALPH1	Present	Not detected	mRNA decapping	Aye, Li and He, 2024
eIF4E/4G	Present	Not detected	Translation initiation	Kramer et al., 2012; Aye, Li and He, 2024
Alba3/4	Present	Not detected	Stress translational control	Subota et al., 2011
UBP1	Present	Not detected	Translational regulation	Kramer and Carrington, 2011

Evidence for the formation of stress granules specific to the HS response or HSGs is limited to being observed in PCF *T. brucei,* following a heat shock at 41 °C. This was observed following polysome collapse by Kramer et al., 2008, using fluorescent microscopy to visualise stress granules, using stress granule markers expressed as eYFP fusion proteins. Comparing the cells at 27 °C and 41 °C, the fluorescence in heat shocked cells is more localised into punctate granules in the cytoplasm, suggestive of the formation of stress granules (Figure 2.12) (Kramer et al., 2008). This SG formation is comparative to the SG visualised in other stress responses in PCF *T. brucei*, including

PBS starvation, showing their formation as a key event within the trypanosome stress response that is common across different stress stimuli (Aye, Li and He 2024).

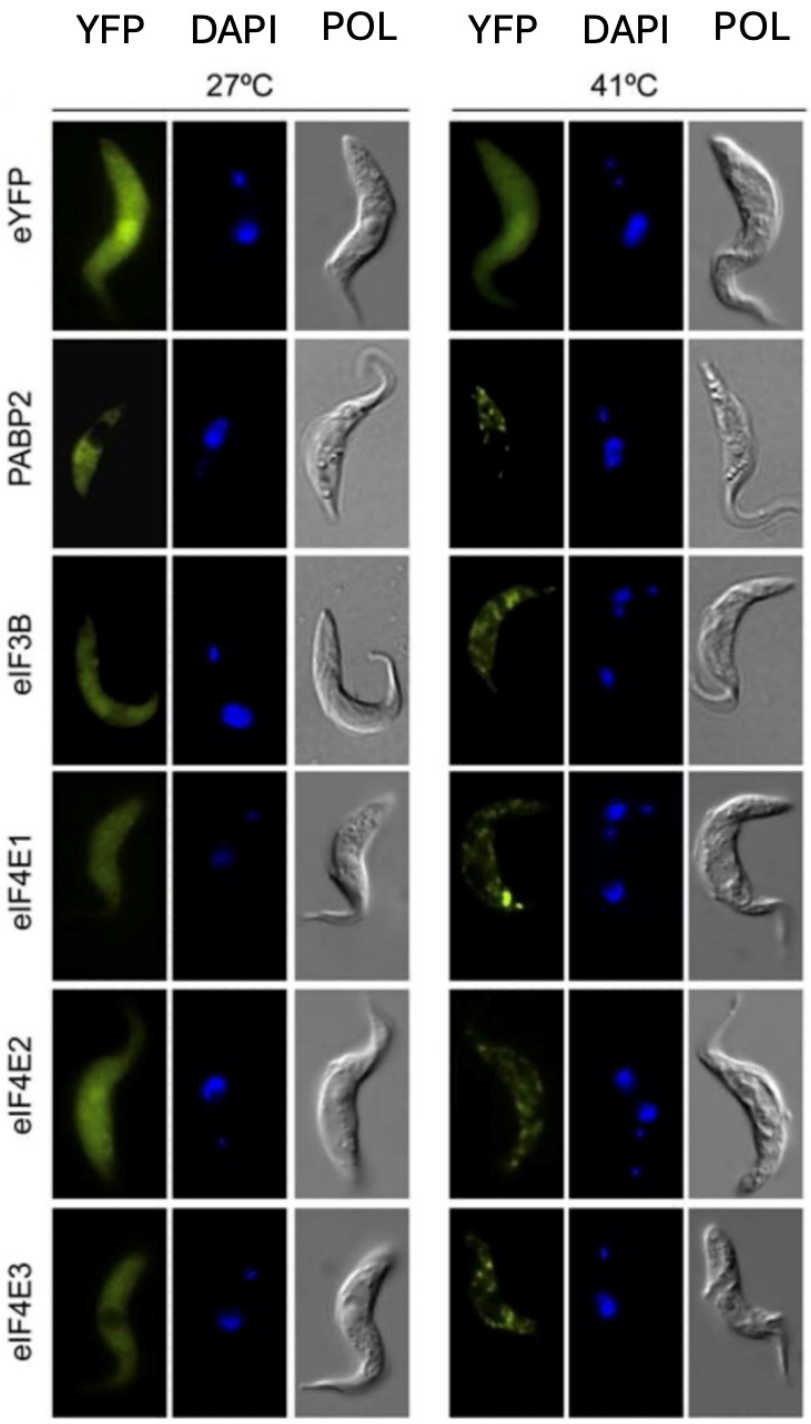

Figure 2.12: Immunofluorescence images of homologues of stress granule markers expressed as eYFP fusion proteins. Images of unstressed (27 °C) and heat shocked (41 °C for 1 hour) in PCF *T. brucei* are shown. Compared to the unstressed cells, the heat shocked cells show an increased granular appearance across the cytoplasm presenting the formation of stress granules within the HS response. (Figure extracted from Kramer et al., 2008).

2.4.1.5 The role of ZC3H11 in the HS response of African Trypanosomes

The ZC3H11 RNA-binding protein is conserved across kinetoplastids and has a crucial role in the HS response acting as a 'master regulator' of the response (Droll et al., 2013). An essential function of ZC3H11 is to post-transcriptionally regulate the mRNA of chaperone proteins or HSPs (Droll et al., 2013). To prioritise an increased translation of HSPs within the HS response, in HS conditions there is an increase in ZC3H11 at the protein level (Droll et al., 2013).

The same increase is not observed at the mRNA level of ZC3H11, remaining constant in HS and therefore, ZC3H11 increases in expression via post-transcriptional regulation, with the movement of ZC3H11 mRNAs to active polysomes to increase their translation (Droll et al., 2013). Sucrose density centrifugation and polysome profiling following heat stress show that ZC3H11 mRNA is recruited to the polysomes, with 71 nucleotides within the ZC3H11 3'UTR governing its regulation (Minia and Clayton, 2016). Due to a lack of evidence, the stability of ZC3H11 mRNA is speculated to be supported by phosphorylation events enabling the binding of an RBP, driven by an unknown translocation (Ooi, Benz and Urbaniak, 2020). Furthermore, Minia and Clayton (2016) also highlight that translation initiation has a role in controlling ZC3H11 protein levels in *T. brucei* as both protein stability and translation efficiency facilitate ZC3H11 accumulation (Minia and Clayton, 2016). ZC3H11 is an *in vitro* substrate for casein kinase 1 isoforms 2 (CK 1.2) and *in vivo* CK 1.2 RNAi reduces phosphorylation of ZC3H11 and reduces its stability (Minia and Clayton, 2016).

ZC3H11 is rapidly degraded under normal culture conditions for PCF *T. brucei* but at 37 °C ZC3H11 is degraded at a slower rate, supporting the increased abundance of ZC3H11 in HS. This change in the rate of degradation of ZC3H11 in HS of PCF *T. brucei* is shown by an increase in the protein half-life from 20±8 to 123±55 hours after a 41 °C HS, presenting increased stability post-HS (Minia and Clayton, 2018). Therefore, Minia and Clayton (2016) demonstrate that both translation initiation and protein degradation have a regulatory role in determining the expression of ZC3H11, but the control of both mechanisms is not understood.

This increase observed in ZC3H11 at the protein level upon HS has been shown by western blotting of ZC3H11 N-terminal V5-epitope tagged procyclic and bloodstream form *T. brucei,* visualising a band at 60 kDa (Droll et al., 2013). This band intensifies following HS of the cell lines, demonstrating an increased expression of ZC3H11 (Figure 2.13) (Droll et al., 2013).

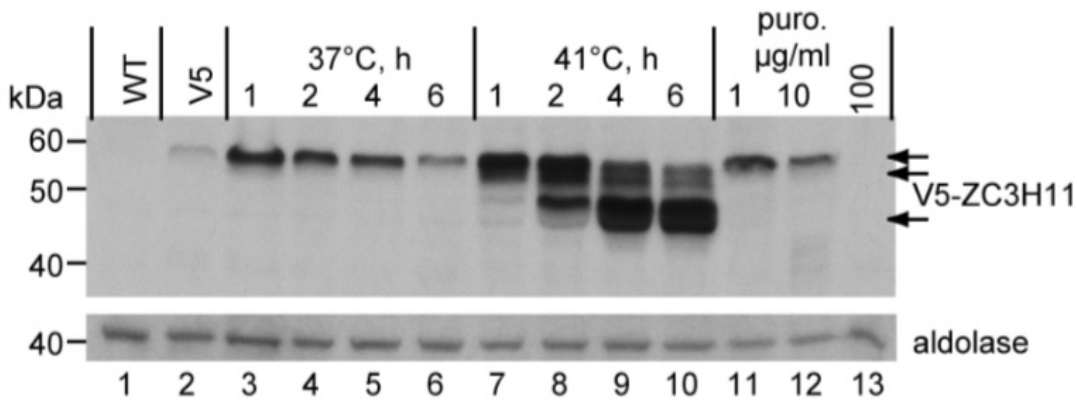

Figure 2.13: Western blot result for V5-ZC3H11 procyclic *T. brucei* in HS. The bands highlighted with arrows show the *in situ* expression of V5-ZC3H11 in PCF cells across the different conditions of treatment. At an increased temperature from the procyclic culture temperature of 27 °C to 37 °C a transient induction of ZC3H11 was observed, which is shown to be intensified at 41 °C with a stronger banding pattern on the blot. Puromycin treatment at low concentrations also shows an increased expression of ZC3H11 in response to mild translational stress. The aldolase lanes are present to demonstrate an even load of cells as a loading control. (Figure extracted from Droll et al 2013).

ZC3H11 is shown to have a direct role in the upregulated expression of HSPs in HS, shown by upon RNAi depletion of ZC3H11 there is a decrease in HSP70 at the mRNA level (Droll et al., 2013). This is emphasised in microarray analysis of mRNAs, comparing ZC3H11 RNAi cells with non-RNAi cells, revealing that, after HS, 27% of all mRNAs required ZC3H11 for their upregulation (Droll et al., 2013). This demonstrates the crucial role of ZC3H11 in stabilising mRNAs for their preferential upregulation within the HS response. But this conclusion is limited by the limitations of RNAi experiments, including that upon RNAi the ZC3H11 protein is not immediately depleted; the inability to distinguish between primary or secondary effects and

therefore it is unknown if the observed results are a direct consequence of ZC3H11 knockdown.

Increased expression of HSPs occurs via increased ZC3H11 protein abundance binding HSP mRNAs and increasing their stability. ZC3H11 binds specific 3' UTR sequences of target mRNAs via the contribution of AUU repeat motifs (Droll et al., 2013). The binding of ZC3H11 to mRNAs within the stress response was shown in over half of those sequenced by RNASeq, notably including 13 cytosolic HSPs that support protein refolding as chaperones in the HS response (Droll et al., 2013). However, ZC3H11 also binds to the mRNA that encodes proteins unrelated to the stress response including GPEET (Droll et al., 2013).

A proposed model for mRNA stabilisation involves ZC3H11 being bound to AUU repeat elements on a target mRNA, enabling the recruitment of PBP1 binding protein 1 (PBP1) via MKT1 and PABP1 (Figure 2.14) (Singh et al., 2014). MKT1 binding with mRNAs promotes the subsequent binding of mRNAs to PABP2 for translation using eIF4E1 (Zinoviev et al., 2011; Singh et al., 2014). This model differs from that in other eukaryotic organisms, in which the AU-rich sequence at the 3' UTR of target mRNA has an opposite role in destabilising mRNA (Singh et al., 2014).

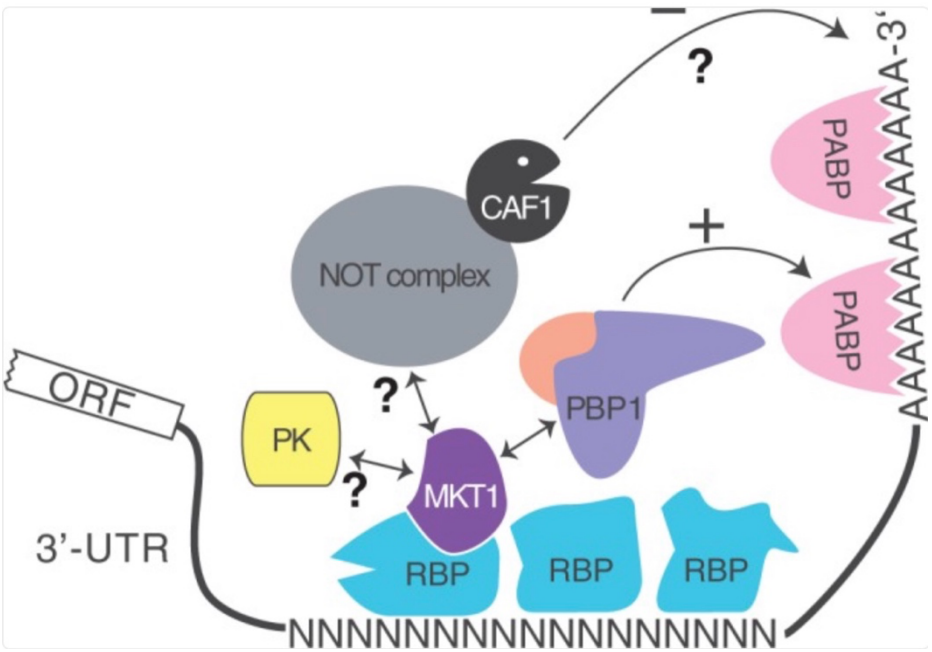

Figure 2.14: A diagram of the potential mechanism for the activity of ZC3H11 in stabilising mRNAs to increase their expression in the HS response. ZC3H11 N-terminal region is proposed to bind RNA, whilst the C-terminal region interacts with PBP1 and MKT1 which recruits PABP (1+2) and LSM12; these proteins can interact with the polyA tail as well as eIF4G; resulting in downstream interactions with chromatin assembly factor 1 and protein kinases, influencing mRNA stability. (Figure extracted from Singh et al 2014).

For the activity of ZC3H11 to increase HSP expression it requires an interaction with MKT1 which acts as a stabilising scaffold (Singh et al., 2014). The ZC3H11-MKT1 complex occurs as a key integration node within the HS response via the binding of a conserved HNPY interaction motif (Singh et al., 2014; Ooi, Benz and Urbaniak, 2020). The stabilisation effect induced by MKT1 is enhanced by the binding of further proteins including PBP1 and SM like 12 (LSM12), thus creating a complex of proteins for the increased HSP expression during HS (Singh et al., 2014). The importance of MKT1, PBP1 and LSM12 as interaction proteins with ZC3H11 in *T. brucei* is demonstrated in their high percentage coverages within a ZC3H11-TAP purification as 48%, 47% and 20% respectively (Singh et al., 2014). These higher percentages indicate a more stable and stronger association with ZC3H11 than other proteins, demonstrating that these proteins associate within a complex to support ZC3H11 as the master regulator of the HS response (Singh et al., 2014). Interestingly, in *T. brucei* MKT1 and PBP1 relocate to stress granules in response to starvation, but these remain dispersed in the cytosol alongside ZC3H11 in HS, suggesting a stress stimuli-specific response which is not yet fully understood (Singh et al., 2014).

2.4.1.6 Phosphorylation in the early events of the HS response

Droll et al (2013) demonstrated that phosphorylation of ZC3H11 is a key event in the HS response of *T. brucei.* Following a HS at 41 °C a shift in the molecular weight band of ZC3H11 is observed in western blotting (Figure 2.13). This shift was comparable to the shift observed in the molecular weight of ZC3H11 upon phosphatase inhibitor treatment (Figure 2.15). Therefore, this presents that HS induces phosphorylation events of ZC3H11 that are responsible for the observed shift in molecular weight (Droll et al., 2013). This phosphorylation of ZC3H11 occurs for its stabilisation to support its

accumulation and its role of increasing the expression of HSPs (Droll et al., 2013). This observation of ZC3H11 phosphorylation post-HS was confirmed by Ooi, Benz and Urbaniak (2020), finding that ZC3H11 experienced a 16-fold change at a single phosphorylation site (S279) after heat shock.

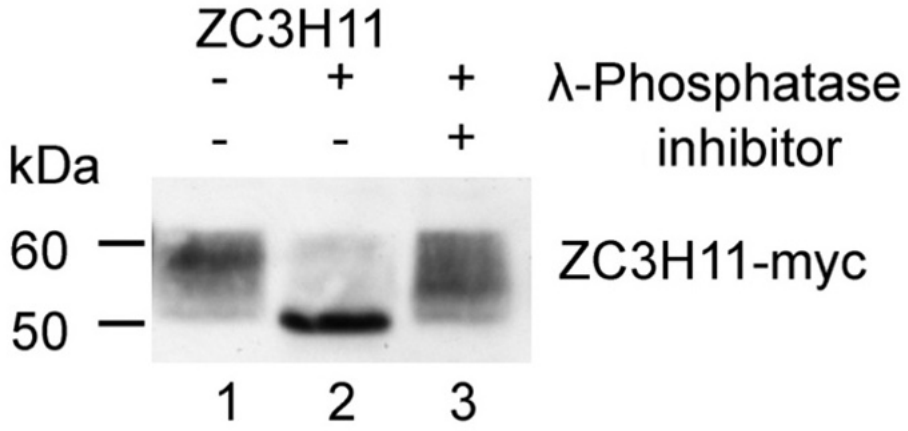

Figure 2.15: The phosphorylation shift of ZC3H11 shown via western blotting. The *T. brucei* cell samples were incubated with lambda phosphatase in the presence or absence of inhibitors. The single band at around 60 kDa observed in lane 1, its formation was prevented in the samples treated with inhibitors. Instead, the cells treated with the inhibitors showed a band migration of around 10 kDa to ~50 kDa, which is a similar migration observed in cells heat shocked at 41 °C, shown in lanes 8-10 in Figure 2.13 (Droll et al., 2013). Suggesting that in HS ZC3H11 is shown to be phosphorylated. (Figure extracted from Droll et al 2013).

The phosphorylation events upon HS have been investigated by Ooi, Benz and Urbaniak, (2020) using SILAC-based quantitative phosphoproteomic analysis. Bloodstream form *T. brucei* cells were heat shocked for 1 hour at 41 °C. 193 phosphorylation sites on 148 proteins were found to respond to HS significantly, with 138 sites increasing by an average of 6-fold and 55 sites decreased in abundance by an average of 4-fold (Ooi, Benz and Urbaniak, 2020). However immediately after HS the proteomic analysis of the change in abundance of 2581 proteins found that only 20 proteins that showed a significant change. Therefore, this presents that phosphorylation is part of the immediate HS response, whilst changes in protein expression, for example the increased expression of HSPs, occurs during later stages within the response to support recovery (Ooi, Benz and Urbaniak, 2020; Muhich, Hsu

and Boothroyd, 1989). As a result, phosphorylation may be used within a signalling mechanism to induce the subsequent changes in protein expression.

In response to HS a significant difference in phosphorylation is observed on RNA binding proteins, stress granule and P-body associated proteins, the translation initiation 4F complex and the ZC3H11-MKT1 complex (Ooi, Benz and Urbaniak, 2020). Using the interaction data from Singh et al (2014) alongside this phosphorylation data, a model was developed to highlight the ZC3H11-MKT1 complex as being a key signal integration node within the HS response (Figure 2.16) (Ooi, Benz and Urbaniak, 2020).

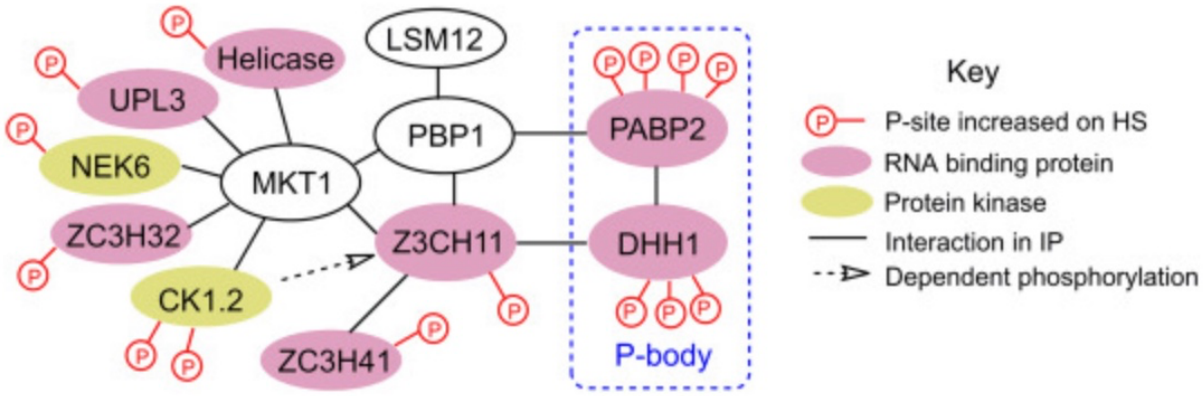

Figure 2.16: Schematic showing the phosphorylation sites in relation to the complexes associated with the ZC3H11-MKT1 complex. The phosphorylation sites shown are those that significantly increased after heat shock of the *T. brucei* cells. This visually demonstrates the key proteins, and their phosphorylation observed within the HS response. (Figure extracted from Ooi, Benz and Urbaniak 2020).

Proteins known to be involved in the HS response were shown to be phosphorylated after HS, for example DHH1 with a 140-fold increase at two of its phosphorylation sites and PABP2 with an 8-16-fold increase across all its phosphorylation sites. Further changes were observed in translational machinery proteins shown in Table 2.3. This dataset is valuable in providing a read-out immediately after HS, allowing comparison with experimental data detailed in the literature and in highlighting the key phosphorylation events that occur in the early events of the HS response.

Table 2.3: Selected translational machinery proteins and their phosphorylation sites in *T. brucei* that showed an increase following heat shock at 41 °C for 1 hour. Data from Ooi, Benz and Urbaniak (2020).

Name	Phosphorylation site	Fold-change
eIF4A-1	S51 S101 S147 T155 S237 T325	24-fold up 17-fold up 3.5-fold up 3.0-fold up 13-fold up 7.7-fold up
eIF4E-3	S424	3.5-fold up
eIF4G-4	S23 S68	3.9-fold up 6.3-fold up
Translation associated element 2	S502	26.2-fold up
PABP2	S93 T167 S212 S259	16-fold up 8.2-fold up 8.8-fold up 8.1-fold up

There was no significant change observed in the phosphorylation state of the HS-essential proteins PABP1, HSPs 110, 84 and 83 (Ooi, Benz and Urbaniak, 2020). This may be explained that such phosphorylation of these proteins may occur at a later time point within HS recovery that was not captured within this experiment or that their phosphorylation is not required within the response. Therefore, to confirm their phosphorylation status upon HS, an extended time course for analysis would thus be required. This would enhance our understanding of the signalling pathways that occur within the HS stress response.

2.4.1.7 The expression of heat shock proteins and heat shock resolution

In general, HSPs increase in expression upon HS, and their transcripts continue to be trans-spliced, despite other trans-splicing events being halted by HS (Muhich, Hsu and Boothroyd, 1989). An example of a HSP that is upregulated at the mRNA level during

HS is HSP70, which is protective against the cytotoxic effects of denatured and aggregated proteins that appear upon heat-induced stress (Hartl, 1996; Ooi, Benz and Urbaniak, 2020). RNAi knockdown of HSP70 highlights its requirement for survival across the life cycle, suggesting a role for HSP70 in the cellular response against the range of environmental temperatures experienced across the life cycle (Bentley, Jamabo and Boshoff, 2018).

However, the requirement of HSP70 in *T. brucei* may be for its roles outside of the HS response, for example HSP70 is shown to play an important role in mitochondrial DNA replication and maintenance (Týč, Klingbeil and Lukeš, 2015). Cytosolic HSP70 interacts with mitochondrial proteins encoded by the nucleus, preventing the proteins from adopting its folded structure; enabling their passage across the mitochondrial membranes (Larburu et al., 2020).

For its role in HS, HSP70 is supported by HSP40 as a co-chaperone, required to stimulate HSP70 ATPase activity (Burger, Ludewig and Boshoff, 2014). The upregulated activity of HSP40 in the HS response enables HSP70 to re-fold damaged polypeptides into their native states, supporting cell recovery (Bentley and Boshoff, 2019). The upregulated HSP90 also acts as a chaperone to stabilise proteins maintaining proteostasis, however, less is known on its specific interactions in trypanosomes (Meyer and Shapiro, 2013).

Upon the HS stimulus subsiding, homeostasis is restored with the polymerisation of monosomes re-forming polysomes, a resolution of global translational arrest and the dissolution of stress granules (Kramer et al., 2008; Fritz et al., 2015). As conserved in mammalian cells, HSPs prevent toxic aggregation of proteins and support the degradation of misfolded proteins, enabling the cells to return to an undamaged state (Hu et al., 2022). Once the cells are in this state, as a reversible change the mRNA expression of general housekeeping genes increases again, and HS-specific genes decrease back to their baseline expression levels; this is observed after around 3 hours of recovery in PCF *T. brucei* (Kramer et al., 2008). Dependant on the extent of damage by the heat and the success of this recovery, some trypanosomes are able to complete repair and continue to proliferate (Kramer et al., 2008; Ooi, Benz and Urbaniak, 2020).

2.4.2 The heat shock response in *Trypanosoma congolense*

2.4.2.1 Comparing *Trypanosoma brucei* and *Trypanosoma congolense*

As both *T. brucei* and *T. congolense* are within the same phylum (Figure 2.17), they have similarities as flagellated kinetoplastid parasites. Both species complete cyclic transmission, interacting with the same tsetse fly vector to infect the same animal hosts and cause a form of trypanosomiasis disease (Eyford et al., 2011). The most recent common ancestor of both species is predicted to have lived 100 million years ago (Kay, Williams and Gibson, 2020). With this evolutionary difference, the species have different gene content and their expression resulting in phenotypic differences.

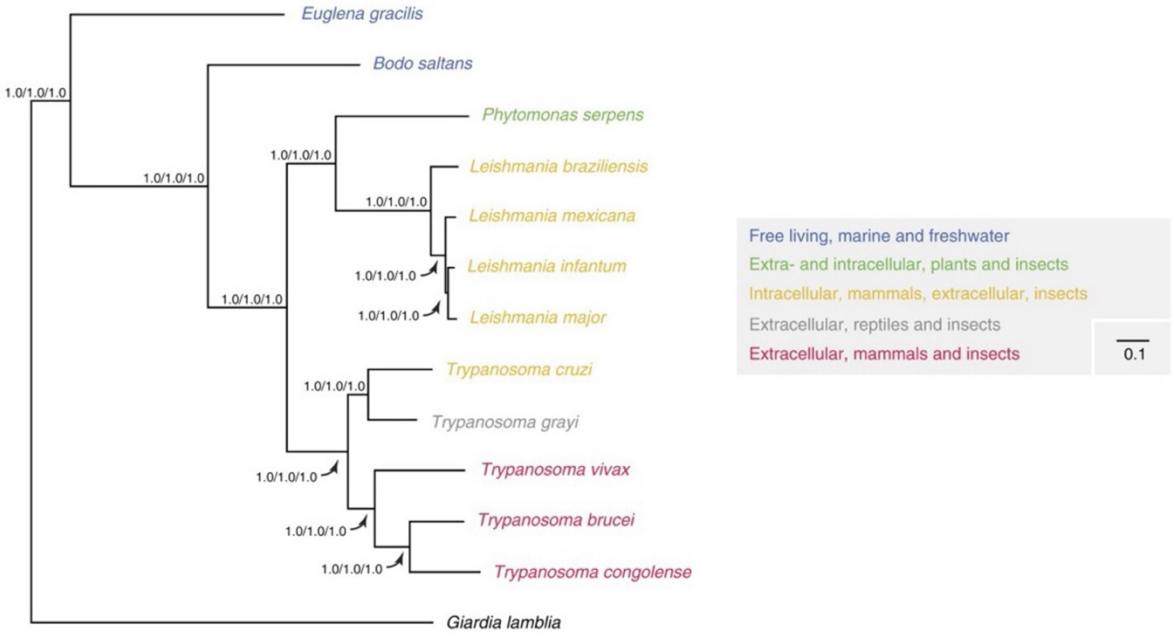

Figure 2.17: A phylogenetic tree of the *Trypanosoma* species within the Euglenozoa clade. The phylogeny was generated using 119,006 aligned amino acid positions (1,546,078 amino acids) from 959 nuclear genes (Kelly et al., 2014). *T. brucei* and *T. congolense* are on neighbouring branches of the tree, showing their evolutionary proximity and genetic similarities. (Figure extracted from Kelly et al., 2014).

Their genetic differences result in distinct properties, *T. congolense* is an intravascular parasite with adherence, whilst *T. brucei* is able to migrate from blood vessels for invasion of further tissues, having virulence implications (Coustou et al., 2010). Divergent metabolic pathways have also been elucidated between *T. congolense* and

T. brucei. For example, unlike *T. brucei* BSF which uses glucose metabolism leading to high pyruvate excretion, *T. congolense* BSF metabolises glucose to other end products including succinate, malate and acetate (Steketee et al., 2021). Furthermore, unlike *T. brucei* which synthesises lipids and fatty acids *de novo*, *T. congolense* scavenges these from their environment; therefore, they are less sensitive to inhibitors of fatty acid synthesis (Steketee et al., 2021).

Further differences between *T. brucei* and *T. congolense* are exhibited in their cell structure and morphology (Table 2.4). Such differences implicate the movement of the cells, as the shorter flagellum of *T. congolense* follows a straight path of movement, whilst the path in *T. brucei* is more asymmetric and flexible completing 180° half turns (Bargul et al., 2016). As a result, *T. brucei* cells swim faster than *T. congolense* (Bargul et al., 2016).

Table 2.4: Differences in morphological or cell structure components in *T. brucei* and *T. congolense*. This table was synthesised using the following references Bargul et al., 2016; Bertiaux et al., 2020.

Component	***T. brucei***	***T. congolense***
Size (cell volume)	Larger (76 μm^3)	Smaller (27 μm^3)
Shape	Rounder, S-shaped cell body	Thinner, slender-like
Flagellum	Long, free (up to 30 μm)	Lack of free anterior flagellum
Undulating membrane	Distinct	Poorly defined or not present
Kinetoplast position	Posterior	Perinuclear

There are multiple different cell lines of *T. brucei* that are extensively worked with, but for *T. congolense* only the IL3000 cell line is extensively used; therefore, most

understanding of *T. congolense* is developed using a single cell line (Awuah-Mensah et al., 2021). These *T. brucei* and *T. congolense* cell lines are cultured differently *in vitro.* This includes temperature as *T. brucei* is grown at 37 °C, whilst *T. congolense* is cultured at 34 °C; however, both require 100% humidity and 5% CO_2 (Awuah-Mensah et al., 2021). Additionally, the species require different media, *T. congolense* media notably containing 15% goat serum, and media containing fetal bovine serum for *T. brucei* (Awuah-Mensah et al., 2021).

However, these culture differences may not reflect *in vivo* differences between the species, instead these differences may have occurred due to an artefact of adaption through exposure of different conditions via different culture histories (Chantal, Minet and Berthier, 2021). The processes of adapting the cells for culture will have differed, for example the number of passages completed in laboratory rodents; the number of which is shown to induce changes in gene copy numbers in *T. brucei* and this could further phenotypic differences between *T. congolense* and *T. brucei* (Mulindwa et al., 2021).

Overall, *T. brucei* and *T. congolense* are closely related in their phylogeny, therefore both infect the same mammalian hosts and cause disease with common mechanisms. However, differences include their genetic content, metabolism, cell structure and their conditions in culture. Further differences are exhibited within the trypanosome life and cell cycles (2.2.2).

2.4.2.2 Existing understanding of the *Trypanosoma congolense* HS response

There has been little experimental work directly carried out on *T. congolense,* and to date nothing is published concerning their HS response. *T. congolense* is considered a close relative of *T. brucei,* both having the ability to infect the same hosts and being exposed to the same selection pressures (Silvester, Ivens and Matthews, 2018). Therefore, it leads to the assumption that they have similar responses to HS, but this is unconfirmed as it is unknown whether conserved HSPs and proteins with increased

phosphorylation increase alongside a global translational arrest during the HS response in *T. congolense* as observed in *T. brucei.*

This assumption is supported through there being homology in the key components of the response. Bioinformatic analysis of six proteins with known involvement within the HS response in PCF *T. brucei* were compared to homologues in *T. congolense;* this found a 98% protein conservation and 85% phosphorylation site conservation (Aelmans, 2022). Despite the clear homology, these proteins may have a different role within *T. congolense*.

The difference in the response to temperature change between the sub-species is emphasised by their culture conditions. *T. congolense* is cultured at 34 °C and is unable to survive the *T. brucei* culture temperature of 37 °C, with a reduced growth rate after 4 days and complete culture death occurring by 7 days (Awuah-Mensah et al., 2021). This is supported by Aelmans (2020) finding for 4 days of *T. congolense* culture at 37 °C cell growth occurs at a normal rate, by day 5 a severe growth lag is observed before complete cell population death by day 7.

As a result, instead of reliance upon its homology to *T. brucei* to understand the HS response of *T. congolense,* more research is required to experimentally confirm its similarity to *T. brucei* or to potentially elucidate a distinct response mechanism.

2.5 Project Aims and Objectives

The aims of this project together aim to characterise how *T. brucei* responds to increased temperature as a stress stimulus, with initial work to compare the same HS-induced response in *T. congolense.* The specific objectives of the project are to:

1. Observe any disturbances to normal cell growth upon HS, producing growth analysis of BSF *T. brucei* comparable of that published by Ooi, Benz and Urbaniak (2020).
2. Observe if HS causes deviation from the normal cell cycle events of BSF *T. brucei,* reproducing the unpublished work of Aelmans (2020) and Taylor (2024).

3. Visualise whether DHH1 localisation changes from before and after HS, to further corroborate the findings of Kramer et al (2008).
4. To observe if change of intensity of a HS stimulus influences trypanosome motility and if motility may be used as a read-out for the fate of cells after HS.
5. To observe whether the abundance of ZC3H11 changes at the protein level after HS, comparative to the observation by Droll et al (2013).
6. To produce cell lines in *T. brucei* with a tagged MKT1 and a mutated HNPY interaction motif in ZC3H11 to support future work in observing the significance of the ZC3H11-MKT1 complex within the HS response.
7. To use polysome profiling analysis to view if any changes occur to polysomes after HS, producing initial reproducibility with Minia and Clayton (2016) in PCF and BSF *T. brucei*, before making comparisons to that in *T. congolense.*

Some of these objectives include the reproduction of figures discussed within the literature (for example Figures 2.9A, 2.10, 2.11, 2.12, 2.13; 2.15). This is important because upon repeatability, it may establish that standard HS conditions are being used. Therefore, any further data generated may contribute to the understanding of the HS response in African trypanosomes, that may be used alongside the existent knowledge from the literature.

3. Materials and Methods

3.1 Materials

3.1.1 Cell Lines

The *T. brucei* 2T1 BSF (Alsford et al., 2005), *T. brucei* Lister 427 wild-type PCF and *T. congolense* IL3000 TcoSM (Awuah-Mensah et al., 2021) cell lines were used across all experiments. The Ty-tagged DHH1 *T. brucei* 427 J1339 BSF cell line was kindly provided by Dr Caroline Dewar.

3.2 Methods

3.2.1 *T. brucei* BSF cell culture

All *T. brucei* BSF cells were cultured in an incubator set at 37 °C, with 5% CO_2, and 100% humidity. Cells were cultured in 25 cm^2 sterile filter cap flasks, with 5 ml HMI-11 media (Hirumi & Hirumi, 1989). HMI-11 media was made up to 5 L; contained 1 pack of HMI-9 powder (Invitrogen), 10 g of sodium bicarbonate (Sigma S5761, RT) and 500 ml of Fetal Bovine Serum (Labtech), made to a 5L volume with molecular grade water (Sigma).

The pH was adjusted accordingly with NaOH to reach pH 7.3, prior to the addition of 50 ml of L-glutamine (100×, Labtech), and 50 ml of Penicillin-Streptomycin (100×, Labtech). This was filtered using a vacuum pump and a 0.2 μm filter under sterile conditions into 500 ml aliquots in sterile bottles, to then be stored at 4°C.

The cells were split into new pre-warmed media to be maintained in a logarithmic growth phase (<2 × 10^6 cells/ml), with cell counts determined using a DeNovix cell counter.

3.2.2 *T. brucei* PCF cell culture

Procyclic form *T. brucei* were maintained at a higher density between 1 × 10^6 and 1 × 10^7 cells/ml determined prior to splitting using a DeNovix cell counter. The cells were cultured in SDM-79 media (Table 3.1) in 25 cm^2 sterile filter capped flasks which were placed into a 27 °C incubator. A notable difference of the *T. brucei* PCF media to the BSF includes the use of heat-inactivated serum, which is significant as the heat disrupts and inhibits complement proteins present within the serum that would otherwise lyse the parasites in culture.

Table 3.1: *T. brucei* PCF SDM-79 media composition. The media was made in a 5 L batch, making 10 × 500 ml bottles, which were stored at 4 °C until use prior to the fresh addition of the * components.

Ingredient	Product	Amount in 5 L	Amount in 500 ml
SDM-79 powder	Invitrogen 07490916	1 pack	
Heamin stock, 10 mg/ml in 0.1M NaOH	Sigma H9039, 4 °C	3.75 ml	
Sodium bicarbonate	Sigma S5761, RT	10 g	
Water	MilliQ	Up to 450 ml	
Foetal bovine serum, heat inactivated *	Sigma F4135, -80 °C	-	75 ml
Adjust to pH 7.3 with NaOH, sterile filter			
Glutamax 1, 100x *	Gibco 35050038, -20 °C	-	5 ml

3.2.3 *T. congolense* cell culture

T. congolense cells were cultured in an incubator set at 34 °C, with 5% CO_2 and 100% humidity. Cells were grown in TcBSF-1 (Coustou et al., 2010), made using the components of Table 3.2, made to a total volume of 850 ml using molecular grade water (Sigma). Prior to storage at 4 °C, the media was filtered using a vacuum through a 0.2 μm filter in sterile conditions and stored as 425 ml aliquots across two sterile 500ml bottles. Before use, 425 ml of media had the addition of 75 ml of Goat serum (Gibco), and NaOH was used to adjust the pH to 7.3, before further filtration through a 0.2 μm filter for complete media.

The cells were split into new media accordingly into 25 cm^2 sterile filter cap flasks, to be maintained in a logarithmic growth phase, requiring agitation prior to splitting, due to cell-to-flask adherence.

Table 3.2: *T. congolense* media components for 2 × 425 ml bottles.

Ingredient	Product	Amount in 850 ml	Amount in 425 ml
MEM powder	Sigma, MO643	9.6 g	4.8 g
Sodium bicarbonate	Sigma, S576, RT	2.2 g	1.1 g

HEPES	Melford, Mw 238.3	5.96 g	2.98
Glucose	Duschefa, Mw 198.2	1.1 g	0.55 g
Sodium Pyruvate	Sigma, Mw 110.0	110 mg	55 mg
Adenosine	Sigma, Mw 267.2	5.3 mg	2.65 mg
Hypoxanthine stock solution*	0.1 M, Mw 136.1	1 ml	0.5 ml
Thymidine	Sigma, Mw 242.2	4.84 mg	2.42 mg
Bathocuproinedisuplonic acid	Sigma, Mw 564.5	11.3 mg	5.65 mg
2-mercaptoethanol	Labtech, Mw 78.13, di 114	14 μl	7 μl
L-glutamine	Labtech, 100×	10 ml	5 ml
Penicillin	Labtech	5 ml	2.5 ml

* The Hypoxanthine stock was prepared using 1.36 g in 100 ml of 0.1M NaOH, warmed to dissolve, before storage of aliquots (0.5 ml) at -20°C.

3.2.4 Heat Shock Protocol

All the cell types were heat shocked at a mid-log density in a 10 ml volume, this was determined using triplicate counts generated by a DeNovix automated cell counter. The temperature of the water bath was validated using a calibrated digital thermometer (RS) to ensure consistency.

There were two groups: the control (not subjected to heat shock, kept at 37 °C) and the experimental group. Both 10 ml culture groups were placed into 50 ml Falcon tubes with loose lids and were placed into a 37 °C incubator for 1 h to recover from the change from the flask conditions. The experimental population Falcons were placed into a pre-heated recirculating water bath (Clifton) for the specified time (0-2 hours), the time starting from the first reading of the required temperature in a blank sample (with equivalent volume to the experimental tubes), measured using a digital thermometer (RS). During the assay the temperatures of both the blank and the water bath were monitored and recorded.

After the required HS time, the experimental tubes were removed from the water bath for subsequent analysis (including flow cytometry, growth and motility analysis), compared to the control population.

3.2.4.1 Heat Shock Recovery

Following HS, an increased mortality is observed but of the remaining viable cells, recovery was measured by transferring the culture from the experimental Falcon tubes into sterile Grenier 25 cm^3 filtered culture flasks and were placed back into incubators for their standard culture conditions (37 °C for *T. brucei* and 34 °C for *T. congolense*). Following timepoints of 1-8 hours, samples were taken from these flasks hourly as a measure of immediate heat shock recovery.

For the analysis of recovery via growth, cumulative growth curves were constructed using triplicate cell counts using a DeNovix automated cell counter, for the average counts in cells/ml to be plotted against the time in hours post-HS. BSF *T. brucei* cultures were split upon a cell count exceeding around 1×10^6 cells/ml to exactly 1×10^5 cells/ml, recording the dilution factor. The dilution factors were used in the cumulative growth curve as a multiplier for subsequent average counts, thus producing a growth curve of continuous growth and increasing the sensitivity to observe any HS-induced defects in growth. For plotting the growth curves using Excel, average counts were calculated and for culture flasks that were split, subsequent average counts were multiplied by the dilution factors to produce cumulative cell counts. The data was plotted on Excel with the time (up to 4 days) on the x-axis and cumulative count on the y-axis; standard deviation error bars were applied to each point to account for the variation in counts.

3.2.5 Flow Cytometry

Flow cytometry sample preparation was completed for BSF *T. brucei* by isolating the cells (at around 1×10^6 cells/ml) by centrifugation of 1.5 ml of a sample at 5,500 ×g for 3 minutes, then removing the media (supernatant). The remaining pellet of cells was

resuspended in 300 µl of Phosphate Buffered Saline (PBS), then mixed with 700 µl of methanol and stored at 4 °C for overnight fixation.

Following fixation, the samples were centrifuged at 5,500 ×g for 3 minutes to isolate the pellet for resuspension in 1 ml of PBS, with staining using 10 µg/ml of propidium iodide (Invitrogen) and 10 µg/ml of RNaseA (Sigma). These samples were incubated in the dark at 37 °C for 45 minutes-1 hour.

Flow samples were run on a Beckman Coulter flow cytometer, using CytExpert Cytoflex software, on which 50,000 events were recorded. Subsequent analysis used graphical gates on a plot of forward scatter against side scatter, distinguishing the size of cells. The population of selected cells (P1) were then gated using the Phycoerythrin (PE) signal channel which corresponds to emission from PI, by plotting signal area against PE signal height, to allow doublets discrimination creating a P2 population. Across a single experiment of flow cytometry samples for HS recovery, the doublet discrimination range used in following analysis was 47.47% to 93.93% with an average of 62.75% across all samples; variation in doublets gated out was dependent upon cell health or recovery. The P2 population were plotted as histograms of PE intensity, with gates to identify the number of cells within the cell cycle phases of G1, S, and G2/M, Additional gates were used to identify outliers to the normal cell cycle phases, labelled as <G1 and >G2M, which indicate abnormal DNA content. The gating process to get to this final data of the P2 population with cell cycle gates is outlined in Figure 3.1.

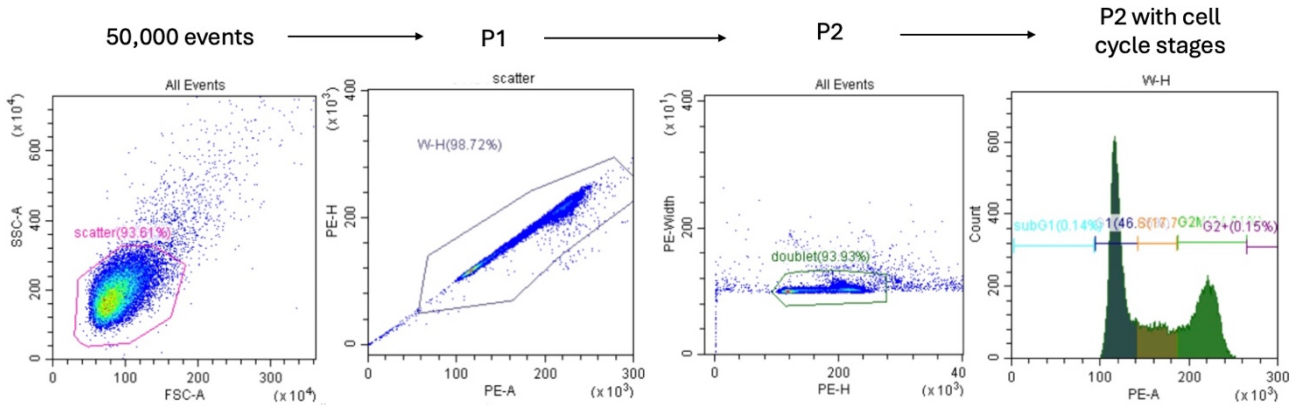

Figure 3.1: Flow chart summarising the progression of gating within CytExpert Software, completed for all flow cytometry analysis. Starting with all 50,000 events,

size filtering got the P1 population which was filtered using PE area and height to collect the P2 population. The P2 population was then gated for doublet discrimination, prior to peaks in PE intensity being identified as stages within the cell cycle (blue for G1, orange for S and green for G2M). This gating was kept constant throughout an experiment.

3.2.6 Motility analysis

3.2.6.1 Video acquisition

A DroiX 4K colour camera system was set up on an Oxion Inverso inverted light microscope, set at its lowest magnification with a 10× objective lens. At the relevant timepoints within the HS assay 500 μl of culture was taken from the experimental Falcon (> 5×10^5 cells/ml exposed to a given temperature) and pipetted into a well of a sterile 24-well plate in triplicate. The plate was agitated to reduce the effects of cellular drift via meniscus formation prior to imaging. Three widescreen 30 second AVI videos were recorded across the three wells per timepoint. These videos were then analysed visually by making comparison to non-HS cells, as well as through using Icy bioimaging Software analysis (de Chaumont et al., 2012).

3.2.6.2 Motility bioimaging analysis using Icy

In the Icy software, the contrast of the videos was altered accordingly to enhance the visibility of the cells to improve the tracking efficiency. A further parameter adjusted was of that to include movement on the Z axis in the analysis, to account for the cells that moved the depth of the well rather than the length.

A spot detector plugin within the Icy software was used to detect motile cells, these were distinguished from motile debris that was excluded from the data through using a size range of 100-20,000 pixels. This plugin was also used to produce ‘tracks’ of the movement of an individual cell, examples of these tracks are shown in Figure 3.2.

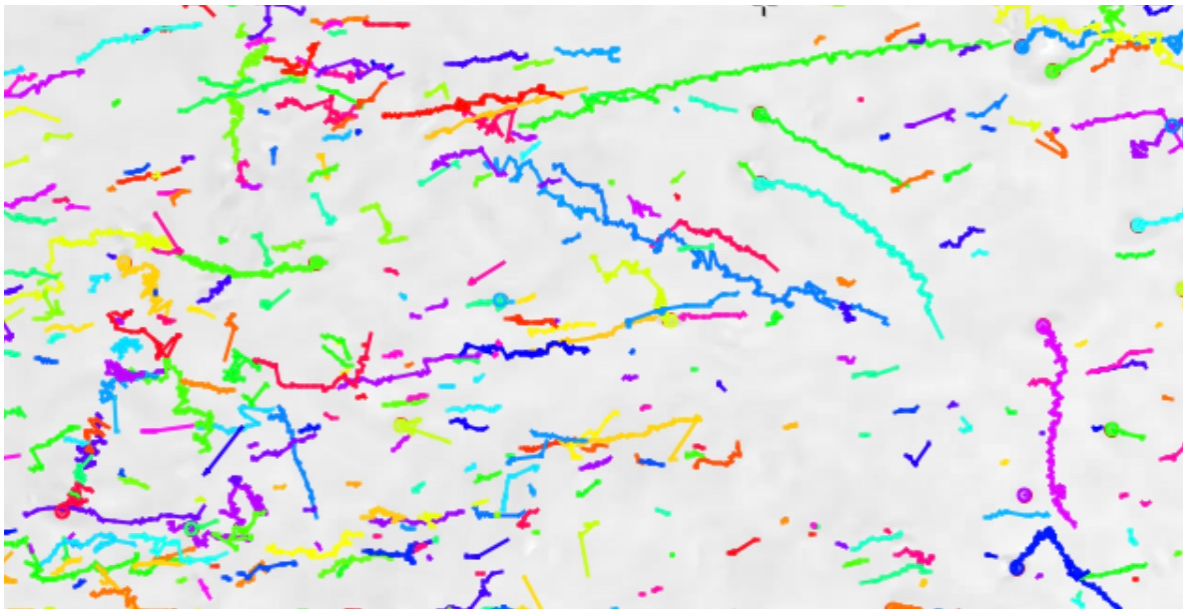

Figure 3.2: Example of the tracks made by cells detected using the spot detector plugin on the Icy software (de Chaumont et al., 2012).

A motion profiling processor within the software (de Chaumont et al., 2012) was used to convert this data collected into a speed of microns per second. The average speed and maximum speed the cells reached was recorded and subsequently analysed using a single ANOVA with Tukeys ad hoc post-tests via the Real Statistics plugin (Zaiontz, 2023) on Excel software; data was deemed statistically significant when $p<0.05$. The tracks produced (shown in Figure 3.2) indicated displacement of cells in multiple directions, suggesting that the flow of the culture was not an issue in implicating the motility data.

3.2.7 Immunofluorescence Assays

Immunofluorescence assays (IFAs) were completed for the visualisation of P-bodies, via an antibody against TY-tagged DHH1. P-body visualisation used DHH1 due to its localisation in P-bodies in HS (Kramer et al., 2008).

Coverslips were prepared firstly by cell centrifugation (of cells at a 5×10^5 cells/ml density) at 550 ×g for 4 minutes to remove the media; remaining cells were pipetted onto a coverslip within a 24-well plate. The cells were incubated on the coverslips for approximately 5 minutes, before a 5-minute incubation with 4% paraformaldehyde

(PFA), which was then removed, and PBS was added for overnight incubation at 4 °C, and wells were sealed with parafilm to prevent evaporation.

The PBS was removed, and cells were permeabilised in 0.05% Tween-20 in 1× PBS (PBS-Tween) for 15 minutes. This was followed by the addition of 100 μl of 1 % BSA in PBS-tween, which was incubated at room temperature for 1 hour in darkness on a rocking platform. This block was then removed, enabling addition of > 100 μl of the primary antibody (sufficient to enable coverage), prior to incubation for an hour at room temperature in darkness on a rocking platform. The primary Ig used was anti-Ty Ig (GenScript) raised in a rabbit, in the dilution of 1/300 in 1% BSA in 0.05% Tween in 1× PBS solution (block).

The primary antibody was then removed, before completing a 5-minute wash in PBS-Tween in triplicate, removing unbound antibody. Following washes, the goat anti-rabbit IgG (Sigma) conjugated to FITC secondary antibody was added, in a 1/200 dilution in the block. A final 1 hour incubation was completed, prior to the removal of antibody and repeated triplicate wash steps in PBS-Tween.

The coverslips were mounted onto slides and fixed in Fluoroshield with DAPI (Sigma) avoiding air bubble formation. These slides were stored in the dark at 4 °C until visualisation using a DeltaVision Elite deconvolution microscope with a 60× oil objective lens; all following analysis was completed using ImageJ Software.

3.2.8 Western blot

3.2.8.1 Western blot sample preparation

5×10^6 cells/sample were collected from 10 ml cultures at a density of 5×10^5 cells/ml. Cells were harvested by centrifugation at 200 ×g for 10 minutes at room temperature. The resultant pellet was washed in 500 μl of 1× PBS and centrifuged at 5,500 ×g for 5 minutes at room temperature. The supernatant was carefully removed before resuspension of the pellet in 15 μl 2× sodium dodecyl sulphate (SDS) buffer (Table 3.3). This was denatured at 95 °C for 5 minutes prior to storage at room temperature until

use. The experimental cell samples that were prepared for western blotting are outlined in Table 3.4.

Table 3.3: Composition of 2 × SDS buffer (10 ml).

Component	**Amount**
Tris-HCl (pH 6.8)	1.25 ml
SDS	0.4 g
Glycerol	2 ml
2-mercaptoethanol	1 ml
Bromophenol blue	2 mg
Water	Up to 10 ml

Table 3.4: Sample conditions of the cells used in western blotting. MG132 (Sigma Aldrich) is a proteosome inhibitor and the + HS conditions follow that of the heat shock protocol (3.2.3).

Sample	**Experimental conditions**
-HS	Sample kept at 37°C for 2 h
+HS	Sample at 37°C for 1 h and 1 h at 41°C
+MG132	Sample at 37°C for 1 h, addition of MG132 (10 μg/ml) and 1 h at 37°C

3.2.8.2 SDS PAGE and Semi-Dry Transfer

15 μl samples were carefully pipetted into the wells of a pre-cast Mini PROTEAN TXG gel alongside a ProteinTech protein ladder, in the presence of 1× SDS running buffer at 150 volts for 45 minutes.

The Semi-dry transfer method was used, with proteins transferred onto a PVDF membrane using the Transblot Turbo kit (Biorad), according to manufacturer's instructions, using the mixed MW programme (7 minutes). The membrane was then blocked in a solution of 5% skimmed milk in 1× PBS with 0.1 % Tween for 20 minutes whilst being agitated at room temperature. The gel was incubated in Coomassie Blue

stain to visualise the efficiency of the transfer from the gel to the membrane, enabling the visualisation of remaining protein within the gel.

The membrane was then stained using primary antibodies 1/2,000 rabbit anti-Ty (Genscript) and 1/20,000 mouse anti-EF1 (Santa Cruz Biotechnology) in 2.5% milk solution in 1× PBS with 0.1% Tween in a cold room (4 °C) overnight. The membrane was washed for 5 minutes in 1× PBS with 0.1% Tween, and probed with the secondary antibodies, 1/5,000 anti-rabbit HRP (Sigma) and 1/20,000 anti-mouse (LI-COR) with peak excitation at 680 nm (via IRDye 680D) were added in 2.5% milk solution in 1×PBS with 0.1% Tween. These were incubated in the dark at room temperature for 1 hour, before washing. This membrane was then imaged using a ChemiDoc MP imaging system (Biorad) for brightfield images or 'chemi' for visualisation of antibody staining. For the detection of fluorophores, a Thermo Fisher iBright was used with the selection of IRDye680 fluorescence and an exposure of 4 seconds.

3.2.9 Generating cell lines

The pPOTv6-3×Myc-MScarlet plasmid (Paterou et al., 2025) was used in the generation of an MKT1 tagged cell line with the G418 resistance cassette.

The primers were designed accordingly using sequences from TriTrypDB (Aslett et al., 2009), and their annealing temperatures were calculated using New England Biolabs Tm calculator (New England Biolabs, n.d.) using OneTaq polymerase. To find the location of the HNPY interaction motif within the ZC3H11 sequence the Kazusa trypanosome codon usage database (Kazusa Database, n.d.) and the Quikchange II primer design program were used to design site-directed mutagenesis primers (Agilent, n.d.). The primers designed are detailed in Table 3.5 and were ordered from Sigma Aldrich.

Table 3.5: Primers and their corresponding details, used in generating cell lines. Restriction enzyme (RE) sites and areas of mismatch to the genomic sequence are highlighted within the primer sequence by being underlined. The annealing temperatures are those experimentally used (after optimisation).

Name	Used in	Directionality	Length (nt)	Sequence	RE site	Mismatch	Annealing temperature (°C)
ZC-F	ZC3H11	Forward	30	TGGCAGTAGGCATTA TGTCGGACACGGCCA		CCC into GCC	55
ZC-R	ZC3H11	Reverse	30	TGGCCGTGTCCGACATA ATGCCTACTGCCA		CCC into GCC	55
G4-F	G418	Forward	34	ACATTAGCTAGCATGATTGA ACAAGATGGATTGC	*Xho*I		46
G4-R	G418	Reverse	32	CGTATTCTCGAGTCAGAAGAA CTCGTCAAGAA	*Nhe*I		46
MK-F	MKT1	Forward	18	ACATTAAAGCTTATGTACCC CCGACACGAT	*Hind*III		58.8
MK-R	MKT1	Reverse	24	CGTATTGGATCCATAATATGTTT CTCGCACTCCC	*BamHI*		58.8

3.2.9.1 Agar plates and bacterial media

All *Escherichia coli* was cultured on LB agar plates. These were made by autoclaving 8 capsules of LB with agar (Thermo Scientific) in 1 L of water. Carbenicillin was added to a final concentration of 100 μg/ml, and the mixture was poured into petri dishes which were set and stored at 4 °C prior to use. For blue-white selection, X-Gal (Thermo Scientific) (20 mg/ml) and IPTG (0.1M) were added and spread on the plates before the addition of the bacteria.

The colonies picked from the agar plates were then cultured in LB media made with 25 g of LB (Thermo Scientific) in 1 L of water, its pH was adjusted accordingly to pH 7.2, before being autoclaved. Carbenicillin was added to a 100 μg/ml final concentration and this complete media was stored at room temperature.

3.2.9.2 Transformation

E. coli DH5 alpha cells (50 μl, NEB) were incubated with 1 μl DNA plasmid on ice for 10 minutes. These cells were heated to 42 °C for 45 seconds before being returned to ice for 2 minutes. 200 μl SOC growth medium (NEB) was added to the cells and incubated at 37 °C for 10-30 minutes in a rocking incubator. This was then plated out onto agar plates containing 100 μg/ml carbenicillin (3.2.8.1) and incubated overnight at 37 °C.

The following day colonies were selected and individually resuspended in 3 ml of LB broth in 50 ml Falcon tubes and were cultured overnight in a shaking incubator at 37 °C.

3.2.9.3 DNA mini prep

Following overnight culture, plasmid DNA was extracted from *E. coli* using the GeneJet Miniprep kit (Thermo Scientific) according to the manufacturer's instructions (Thermo Scientific, n.d.). The concentration of the miniprep products were measured using a NanoDrop One with a ratio of 260 nm/ 280 nm to verify purity.

3.2.9.4 Restriction enzyme digest

For each digest completed (either 100 U for a diagnostic digest or 200 U for gel extractions), the restriction enzymes (New England Biolabs) comprised 1/20 of the total reaction volume, and 10× Cutsmart buffer (New England Biolabs) was 1/10 of the reaction mix. Mini prep and was added up to the total reaction volume and the mix was incubated for at least 1 hour at 37 °C. Recombinant Shrimp Alkaline Phosphatase (rSAP) treatment was completed to remove the 5'-phosphate groups generated by REs, by incubating the digest with 1 μl of rSAP for 30 minutes at 37 °C.

3.2.9.5 Agarose gel electrophoresis

Agarose gel electrophoresis was completed using 1% agarose gel plus SYBR safe DNA red gel stain (Invitrogen). The agarose gel was run in 1× TAE running buffer, with samples run alongside 5 μl 100 bp or 1kb ladder (Promega). A 6× purple loading dye (2 μl) was added to stain colourless samples. Gels were run for approximately 30 minutes at 115 V, before imaging using a BioRad Gel Doc EZ imager.

3.2.9.5.1 Gel extraction

The band of interest produced by gel electrophoresis was cut out, visualised using a UV transilluminator (Syngene). The DNA was extracted from this band using a ThermoScientific GeneJet Gel Extraction kit, following the method provided by the manufacturer.

3.2.9.6 DNA Sequencing

Sanger sequencing was performed at the University of Dundee using standard or custom primers (Table 3.6). Comparisons were made to genomic sequences available on TriTrypDB (Aslett et al., 2009) using ApE software (Davis and Jorgensen, 2022).

Table 3.6: Complete list of primers used for sequencing, their direction and sequence. The * primers were custom primers. F corresponds to forward and R corresponds to reverse directions.

Name of primer	Direction	Sequence
SP6	F	ATTTAGGTGACACTATAG
T7	F + R	TAATACGACTCACTATAGGG
pSiS PFR2 IGS *	F	TTTCCTCCTTTGGGTGCACC
pPOTv6 GS linker 1F *	R	GGTTCTGGTAGTGGTTCCGG

3.2.9.7 Ligation reactions

Backbones (pGEM-T or the final backbone) and inserts were ligated together using 1 μl of T4 DNA ligase (Promega), 1 μl of 10× rapid ligation buffer (Promega), 1 μl of vector and 7 μl of insert. The 10 μl reaction mixtures were incubated overnight at room temperature.

3.2.9.8 PCR Reactions

PCR reactions were used to amplify DNA of interest from genomic DNA. The reaction mix was prepared as outlined in Table 3.7, using reagents from New England Biolabs.

Table 3.7: Volumes of reaction components used within the 50 μl PCR reaction mixture. *The primer mix contained both forward and reverse primers diluted to a respective 10 μM concentration.

Component name	**Volume used (μl)**
2 × OneTaq Master mix	25
*Primer Mix (10 μM)	2
DNA template	1
Water	22

PCR reactions were performed in a BIO-RAD T100 Thermal Cycler (Figure 3.3). The only variations in the cycling conditions were the annealing temperature, which was adjusted to accommodate the temperatures required for both the forward and reverse primers, and the extension time, which was adjusted based on the size of the amplicon as one minute/kb (Table 3.8). Following complete cycle run, the PCR reactions were assessed using gel electrophoresis (3.2.9.5).

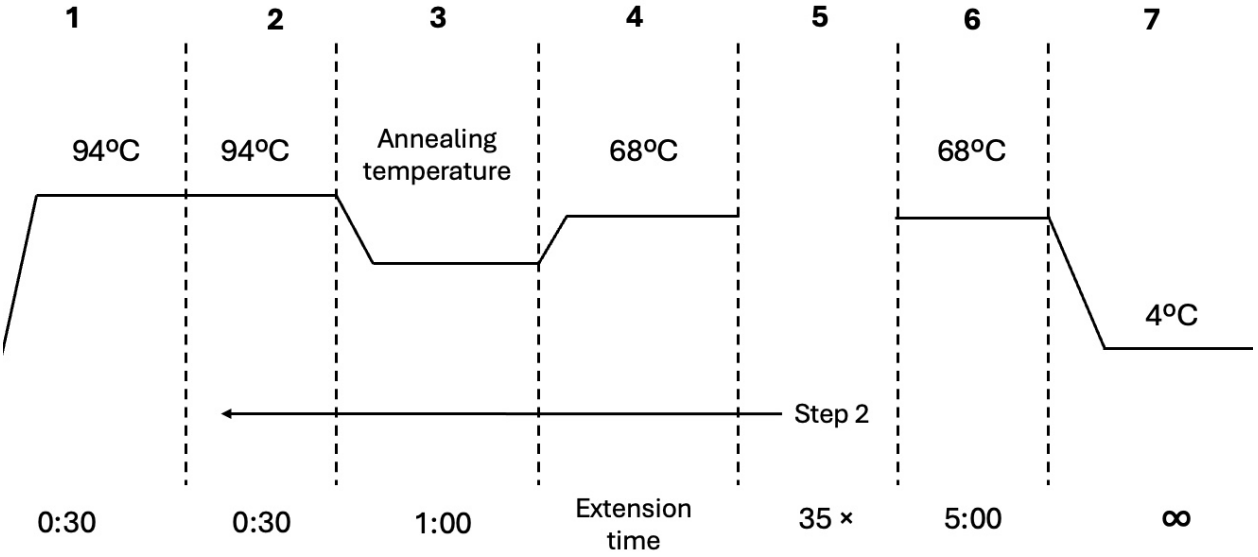

Figure 3.3: The general run cycle used for all PCR reactions using OneTaq or Superfied pol in the BIO-RAD T100 Thermal Cycler. Changes were made in the annealing temperatures and extension times for individual reactions.

Table 3.8: The final annealing temperatures and extension times used for each named amplicon. Optimisation meant that these values were altered, the final values indicated are those used to produce the final PCR product.

Amplicon	**Annealing temperature (°C)**	**Extension time (minutes)**
MKT1	58.8	4.0
G418	46.0	1.5

3.2.9.9 Site-directed Mutagenesis

Site-directed mutagenesis (SDM) was used to mutate the HNPY interaction motif in the ZC3H11 gene (Tb927.5.810) using the Agilent SDM QuikChange II Kit according to manufacturer's instructions, the reaction components are shown in Table 3.9.

Table 3.9: Volumes of reaction components used within the 50 µl SDM reaction mixture. *The primer mix contained both forward and reverse primers diluted to a respective 10 µM concentration.

Component name	**Volume used (µl)**
10 × Reaction buffer	5
*Primer Mix (10 µM)	2.5
dNTP mix	1
Water	39.5
Plasmid DNA template (50 ng/µl)	1
Polymerase (2.5 U/ µl)	1

After PCR cycle completion (Figure 3.4), the tubes were placed onto ice for 2 minutes prior to the addition of 1 µl *Dpn*I and incubation at 37 °C for 1 hour. 10 µl of PCR reaction was then transformed (as 3.2.9.2) using 50 µl of supercompetent *E. coli* cells (provided with the kit).

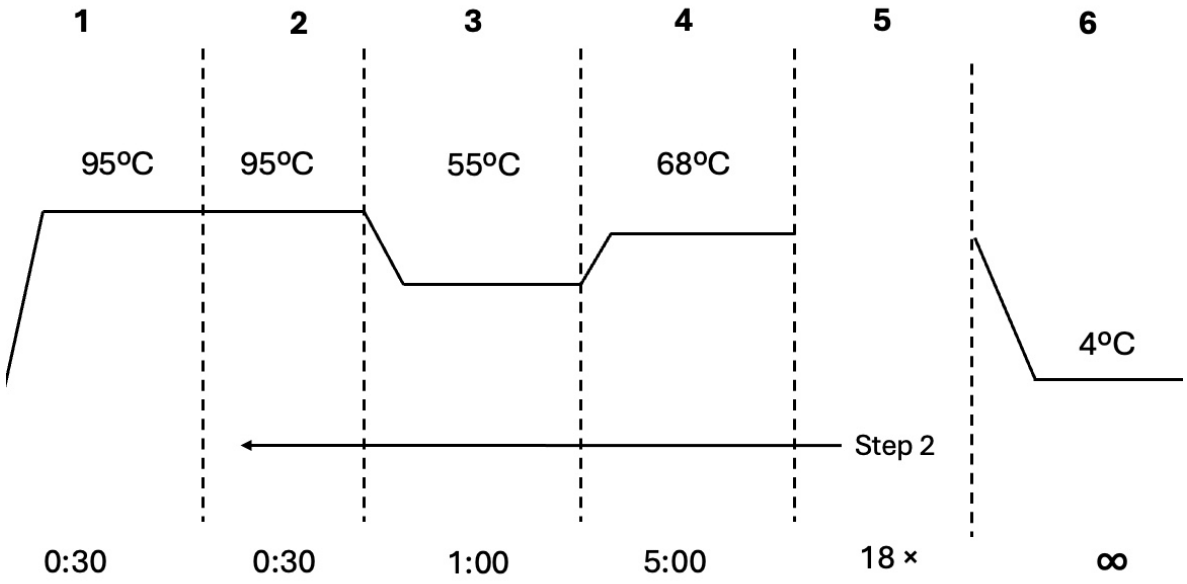

Figure 3.4: The run cycle used for the SDM reaction using the BIO-RAD T100 Thermal Cycler.

3.2.9.10 Transfection into BSF *T. brucei*

3.2.9.10.1 PCR for transfection

The DNA used in the following ethanol precipitation (3.2.8.10.2) required two PCR reactions, one to amplify sgRNAs and another to amplify the segment of DNA containing the blasticidin resistance cassette and mutated ORF; their reaction components are respectively shown in Tables 3.10 and 3.11.

Table 3.10: 50 μl CRISPR PCR reaction mix. *The primer mix contained both forward and reverse primers diluted accordingly to a 10 μM concentration.

Reaction component	**Volume (μl)**
Template plasmid (30 ng/μl)	4.5
5× SuperFi II buffer (ThermoScientific)	18
dNTPs	1.8
*Primer mix (10 μM)	9
SuperFi Pol (ThermoScientific) (2 U/μl)	1.8
Water	54.9

Table 3.11: 90 μl reaction mix for PCR 2 used in ethanol precipitation prior to transfection. *The primer mix contained both forward and reverse primers diluted accordingly to a 10 μM concentration.

Reaction component	**Volume (μl)**
*Primer mix (10 μM)	5
5× SuperFi II buffer (ThermoScientific)	10
dNTPs	1
SuperFi Pol (ThermoScientific) (2 U/μl)	1
Water	33

Following, completion of the PCR reaction mixtures, the tubes were placed into a BIO-RAD T100 Thermal Cycler for the cycles in Figure 3.5 to be completed.

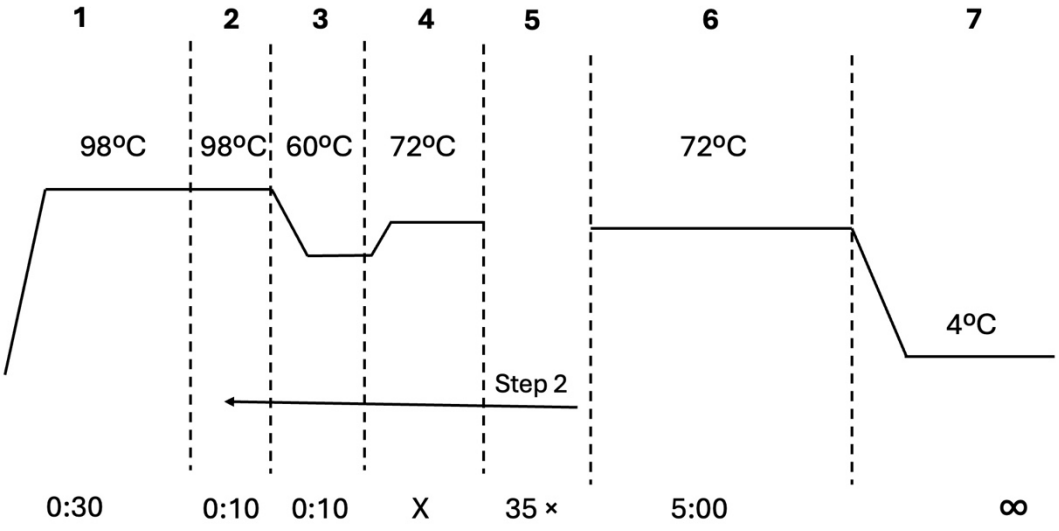

Figure 3.5: The run cycles used for the transfection PCR reactions using the BIO-RAD T100 Thermal Cycler. The PCR reactions used the same cycles, only differing in extension times (step 4), for the CRISPR PCR this was 15 seconds and in PCR 2 this was 1 minute.

3.2.9.10.2 Ethanol precipitation

1/10 volume of sodium acetate (3M pH 5.5) was added to the PCR products, alongside a 2× volume of 100% ethanol. The mixture was vortexed and was incubated overnight at -20 °C. This was then centrifuged at ~ 15,000 ×g for 30 minutes at 4 °C. The remaining pellet was resuspended in 2× volume of 70% ethanol and centrifuged in the same conditions for 15 minutes. The pellet was then air dried to evaporate any remaining ethanol. The pellet was resuspended in 10 μl of distilled water and stored at -20 °C.

3.2.9.10.3 Transfection

2×10^7 BSF *T. brucei* cells pelleted in a centrifuge at 200 ×g for 10 minutes. The cell pellet was resuspended in filter-sterilised 1× PBS (1 ml) and were transferred to a

sterile Eppendorf. The cell pellet was resuspended in 100 μl room temperature Roditi buffer (Table 3.12). This resuspension was added to 10 μl ethanol precipitated DNA and transferred into a transfection cuvette. A DN100 program was used on Lonza Nucleofector machine. Transfected cells were removed from the cuvette and placed into non-drugged HMI-11 media with no additional drugs added and left at 37 °C.

Table 3.12: The composition of Roditi transfection buffer (100 ml) used for BSF *T. brucei* electroporation. This buffer was filter-sterilised and stored at 4°C prior to use.

Component	Amount in 100 ml buffer
KCl (120 mM)	0.894 g
$CaCl_2$ (0.15 mM)	2.2 mg
K_2HPO_4 (10 mM)	To adjust to pH 7.6
HEPES (25 mM)	5.96 g
EGTA (2mM)	0.76 g
$MgCl_2$ (5 mM)	0.102 g

6 hours following the transfection, 4 μg/ml blasticidin was added to the cells. Dilutions were made as in Table 3.13, which were plated out alongside the remaining undiluted cells across separate 24-well plates with 1 ml/well. These plates were monitored for their growth after 5 days and 6 wells with viable cells were picked to be cultured in the presence of 4 μg/ml blasticidin.

Table 3.13: The dilutions used in plating up BSF *T. brucei* with blasticidin resistance following transfection.

Dilution	Cell volume	Media volume	Blasticidin volume
1/10	2.4 ml	21.6 ml	8.6 μl
1/100	240 μl	23.8 ml	9.5 μl
1/1000	2,400 μl	24.0 ml	9.6 μl

3.2.9.10.4 Genomic DNA (gDNA) extraction from transfected *T. brucei*

gDNA was prepared for following PCR amplification of an insert, for the confirmation of insert success via gel electrophoresis, gel extraction and following Sanger sequencing. A 10 ml culture of 1-5 × 10^6 transfected cells were centrifuged at 3,900 ×g for 1 minute at 4 °C. The resultant pellet was resuspended in 100 μl of nucleofector solution (Lonza) and 1 μl of 10% SDS; the resuspension was incubated at 55 °C for 10 minutes and 50 μl of 3M $NaOA_c$ was added. The Lonza nucleofector solution was used to rapidly lyse the cell membrane and break down the nuclear envelope without shearing DNA aggressively, acting as a gentle and effective lysis buffer for improved DNA integrity compared to standard lysis buffers. An incubation was then completed on ice for 5 minutes before centrifugation at 20,000 ×g for 5 minutes at 4 °C. The produced supernatant was transferred into a sterile Eppendorf and 200 μl of 100% ethanol was added; the mixture was centrifuged in the same conditions as previously. This produced a pellet of gDNA that was air dried at room temperature and was resuspended in 100 μl of ddH_2O.

3.2.9.10.5 gDNA insert PCR amplification

The insert of interest (ZC3H11) was amplified by PCR using the reaction mix shown in Table 3.14, which was placed in a BIO-RAD T100 Thermal Cycler to complete the cycle shown in Figure 3.3, with an extension time of 90 seconds and an annealing temperature of 55 °C. This reaction was used in gel extraction and final sequencing using specific primers (Table 3.15) to confirm the success of a transfection.

Table 3.14: Volumes of reaction components used within the 50 μl PCR reaction mixture.

Reaction component	**Volume (μl)**
5× Q5 reaction buffer (NEB)	10
dNTPs (10 mM)	1
Forward primer (10 μM)	2.5

Reverse primer (10 μM)	2.5
DNA template	2
Q5 Polymerase (NEB) (2,000 U/μl)	0.5
Water	31.5

Table 3.15: The sequences of primers used in the PCR of the ZC3H11 gene from gDNA. The location where the primers anneal to the ZC3H11 gene are highlighted within the primer sequence by being underlined.

Primer direction	**Sequence**
Forward	ACATTAAAGCTTATGAGCACTGCAACATCTG
Reverse	CGTATTAGATCTTCACAAGGAAAGAAACATATCC

3.2.10 Polysome Gradient Fractionation

3.2.10.1 Production of sucrose gradients

For initial validation of the gradient fractionation system, 10% and 60% sucrose solutions (w/v) were made with sucrose (Melford) and water, the 60% solution also had the addition of bromophenol blue (Sigma-Aldrich) at a 100 μg/ml concentration.

For the experimental sucrose solutions, 10% and 50% sucrose (w/v) were made using gradient buffer (Table 3.16) and sucrose (Melford). To produce the gradients the light sucrose solution (10%) was transferred to half-fill 13.2 ml ultracentrifuge tubes (Beckman Coulter) using a needle and 20 ml syringe; then the heavy sucrose solution (50 or 60%) was layered at the bottom to fill the remainder of the tube also using a needle and 20 ml syringe. Long caps were then used to seal the tubes (Biocomp) before they were placed onto the Biocomp gradient master, and all gradients were made on a 15-50% sucrose function. These produced gradients were stored at 4 °C for less than 24 hours. Prior to use, the gradients were weighed to ensure balancing within the

ultracentrifuge, ensuring there was no more than 0.1g difference in weight between tubes.

Table 3.16: Composition of 65 ml of gradient buffer. The * components were added upon use fresh.

Component	Volume
1M Tris-HCl	1.3 ml
1M KCl	7.8 ml
1M MgCl2	130 μl
1M DTT	65 μl
10mg/ml Leupeptin*	65 μl
100 mg/ml cycloheximide*	65 μl
Water (MilliQ)	55.6 ml

3.2.10.2 Polysome sample preparation

Samples for gradient fractionation were prepared requiring > 1×10^8 cells total; the number of cells were observed using a DeNovix cell counter. The cells (+/- HS) were transferred into Falcons and had cycloheximide added in a final concentration of 100 μg/ml to preserve polysomes in subsequent lysate preparation. The culture with cycloheximide was then placed into a 37 °C incubator for 10 minutes and then were chilled at 4 °C for a further 10 minutes. The cells were then pelleted in a centrifuge at 700 ×g for 5 minutes at 4 °C, the media was removed, and the pellet was resuspended in 1 ml 1× PBS with cycloheximide (100 μg/ml) and was transferred into an Eppendorf. The resuspension was pelleted by centrifugation (as previously) and the PBS was carefully removed; this wash step with PBS was repeated. The isolated pellet was then flash frozen in a -80 °C freezer until use.

The pellets were placed on ice and were each resuspended in 250 μl of completed lysis buffer (Table 3.17), and the cell suspension was passed through a 21-gauge needle 15 times and then a 27-guage needle 15 times using a 1 ml syringe. The cells in lysis buffer were then incubated at ~4 °C for 10 minutes, before being placed in a centrifuge at ~15,000 ×g for 10 minutes at 4 °C. The supernatant was carefully removed and was slowly loaded on top of the sucrose gradients, by carefully pipetting against the wall of the ultracentrifuge tube.

Table 3.17: The composition of 10ml lysis buffer. The * components were added fresh to complete the buffer on ice prior to use.

Component	Volume (µl)
1M Tris-HCl	200
1M KCl	200
1M MgCl2	20
1M DTT	20
RNasin*	125
10mg/ml Leupeptin*	10
10% IGEPAL	200
1M Sucrose	2000
100 mg/ml cycloheximide*	10
Water (MilliQ)	Make up to 10 ml total volume

3.2.10.3 Ultracentrifugation

Gradients with layered cell lysates were placed accordingly within a pre-chilled SW 41 Ti swinging-bucket rotor (Beckman Coulter). This rotor was placed into an Optima L-100 XP ultracentrifuge (Beckman Coulter) that had been pre-cooled to 4 °C. The ultracentrifuge was run at ~ 207,000 ×g (maximum speed) at 4 °C for 1 hour, with a maximum acceleration and deceleration set at 4.

3.2.10.4 Gradient fractionation

Prior to running samples, the fractionator was turned on and was zeroed using water. Gradients were then assembled in the fractionator, the piston was then lowered to the top of the tube and 14 fractions with a volume of ~250 µl were collected, whilst measuring absorbance at 254 nm across the positions, which was graphically displayed on the Biocomp TRIAX software.

Following analysis was completed using Excel, enabling the change in scale to observe polysome peaks with an improved resolution and peaks were titled 40S, 60S, 80S and polysomes according to comparison with the literature (Kramer et al., 2008).

4. Temporal profiling of the formation and dissolution of P-bodies and heat shock granules

4.1 Validating conditions that induce the HSR

All heat shock experiments were induced by transferring the trypanosome cell culture into 50 ml conical centrifuge tubes and placing them into a stabilised water bath. To ensure that the HS response in African trypanosomes was being characterised, rather than a cell death phenotype, growth, cell cycle analysis via flow cytometry and motility were measured as read-outs of cell viability. It was crucial to observe that the cells were able to survive a controlled heat shock by being placed in a water bath, equivalent to how they would survive within a mammalian host experiencing fever. Therefore, validating the temperature and time the cells were placed in the water bath for, enables the understanding of the HS response in experimental conditions within the lab to be developed that are physiologically relevant.

4.1.1 Heat shock at 41 °C for 1 hour induces a heat shock response in T. brucei

Initially, the effect of the length of HS exposure at 41 °C upon growth of BSF *T. brucei* was measured to ensure previous data was reproducible. The cells were placed into a water bath stable at 41 °C for 0.5, 1 and 2 hours then returned to 37 °C for growth analysis up to 100 hours, alongside control cells that remained at 37 °C (0 h HS). This was completed for the two background cell lines that were used in subsequent experiments pleiomorphic 2T1 (Figure 4.1) and monomorphic J1339 (Figure 4.2).

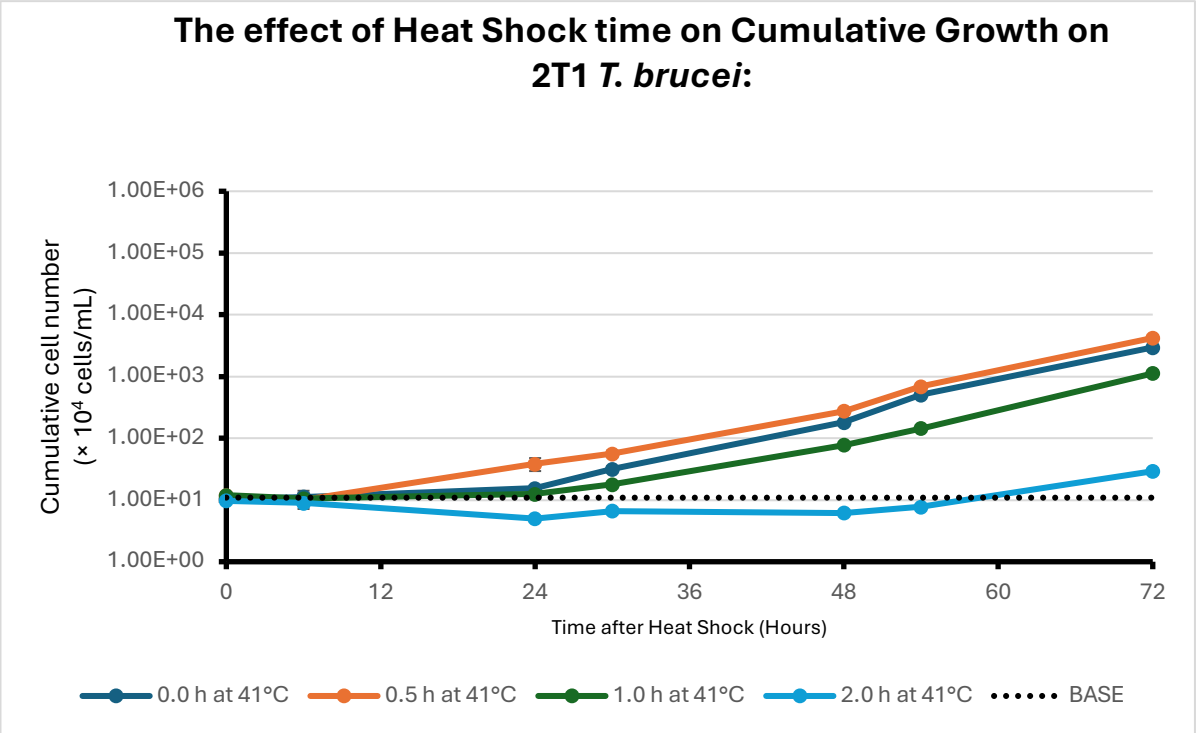

Figure 4.1: Growth of 2T1 *T. brucei* cells exposed to a HS at 41 °C for differing times. Cell growth was recorded using counts in triplicate measured by a DeNovix cell counter up to 100 hours following the heat shock. The error bars plotted represent the standard deviation. The HS was completed for 0, 0.5, 1 and 2h; the base represents the starting cell count average from all cultures.

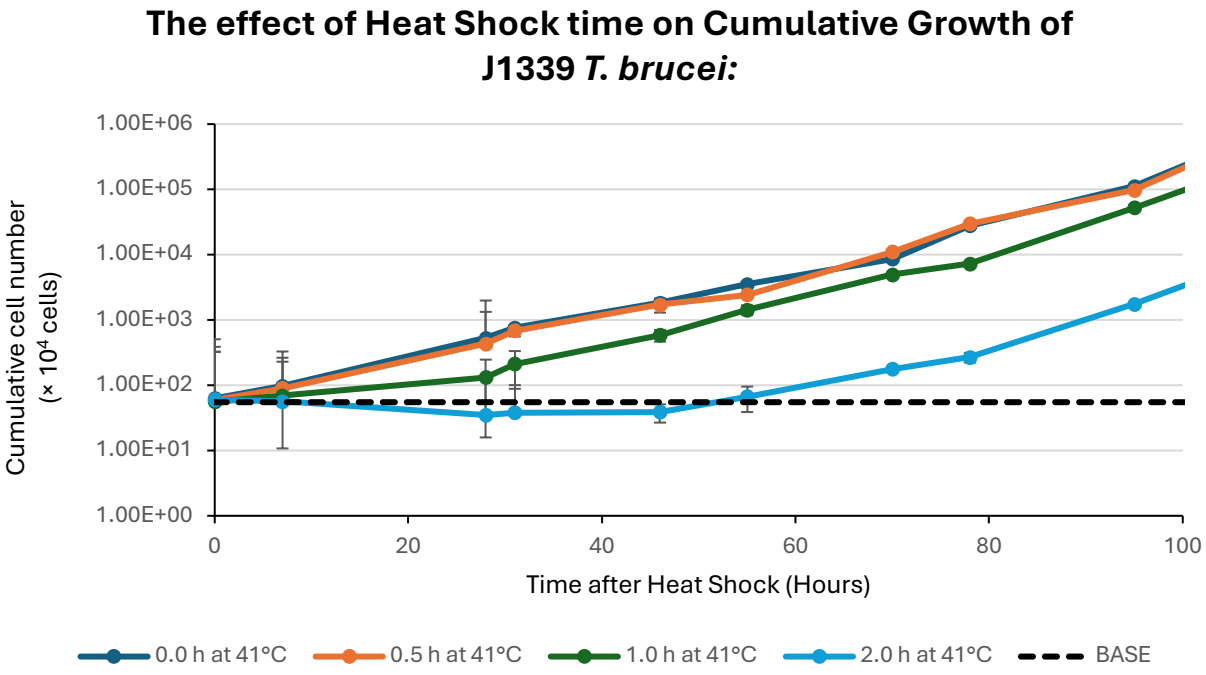

Figure 4.2: Growth of J1339 *T. brucei* cells exposed to a HS at 41 °C for differing times. Cell growth was recorded in triplicate up to 100 hours following the heat shock. The error bars

represent the standard deviation. The HS base represents the starting cell count average from all cultures.

HS at 41 °C for 0.5 hours caused cells to continue to grow at a rate comparable to the control no HS culture. In the 2T1 cells at 0.5 hours there was a slight lag before reaching growth parallel to the non-HS cells; in the J1339 cells 0.5 hours had near equivalent growth to the control throughout the time course of growth. Whilst, 1 hour of 41 °C in both 2T1 and J1339 caused a lag in growth until around 24 hours before returning to a non-HS cell growth rate. Finally, 2 hours at 41 °C caused cell death, observed by a decrease in cell number, shown to have occurred as a significant difference via a two-tailed t-test producing a p-value of 0.023 in comparing the cell number before HS and 24 hours post-HS in 2T1 *T. brucei* cells and a further p-value of 0.0017 via the same analysis in comparing the cell number before and 28 hours post-HS in J1339 *T. brucei* cells (significance when $p < 0.05$). Therefore, after a 2 hour HS an increased recovery time is viewed as a longer lag in growth prior to an increased growth rate; in 2T1 cells this lag lasted over 70 hours and in J1339 this was just less than 60 hours following the HS.

These results suggest 1 hour at 41 °C is suitable to measure the HS response, as both BSF *T. brucei* cell lines survived a lag in growth that was not detrimental to cell growth for an extended period of time, suggesting completion of the HS response. This is comparable to the data published by Kramer et al (2008) in PCF *T. brucei* and further data produced by Ooi, Benz and Urbaniak (2020) in BSF *T. brucei,* showing that the conditions used in following experiments were reproducible.

To understand what occurs to the cells within this period of lagged growth following 1 hour at 41 °C and to ensure the conditions being used were comparable to those previously used (by Aelmans, 2022; Taylor, 2024) analysis of the cell cycle was completed by flow cytometry. Samples were taken and fixed hourly before and for 8 hours after a heat shock, for following DNA staining using propidium iodide (PI). This was completed for both *T. brucei* BSF 2T1 and J1339 cell lines, enabling identification of cell cycle phase distribution across the cell population for each hour of recovery after HS (Figure 4.4 and 4.5).

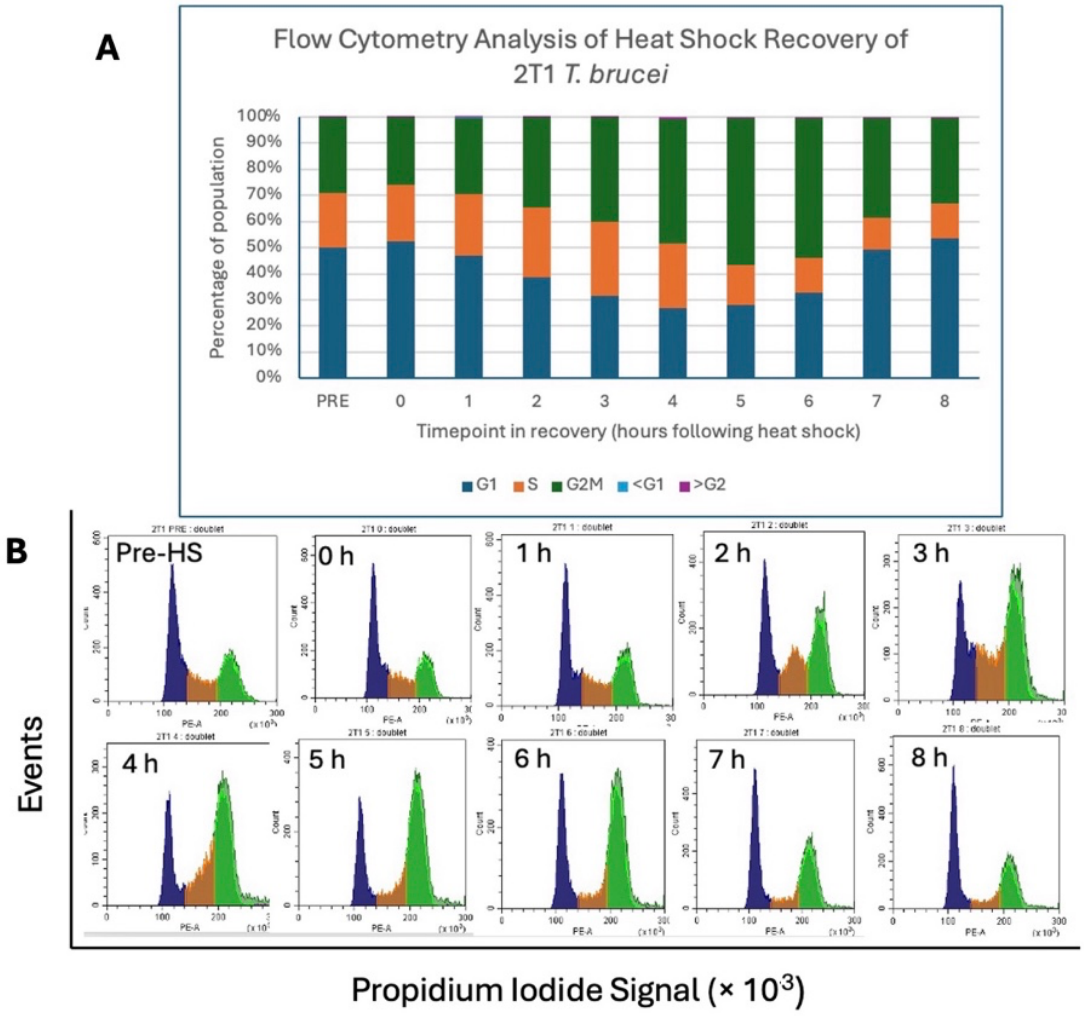

Figure 4.4: *T. brucei* BSF 2T1 cell cycle arrest following a HS at 41 °C for 1 hour. A sample was taken prior to HS (Pre-HS) and following hours after HS 0-8 h. For each sample 50,000 events were recorded and gated on a Cytoflex flow cytometer, the following PI signal was used to distinguish the cell cycle phases. The cell cycle gates were adjusted accordingly to fit the cell cycle phase peaks using CytExpert software, these are shown in panel B of the figure. The proportion of cells in each cell cycle phase as a percentage were plotted as a histogram, panel A of the figure which corresponds with the PI traces below in panel B.

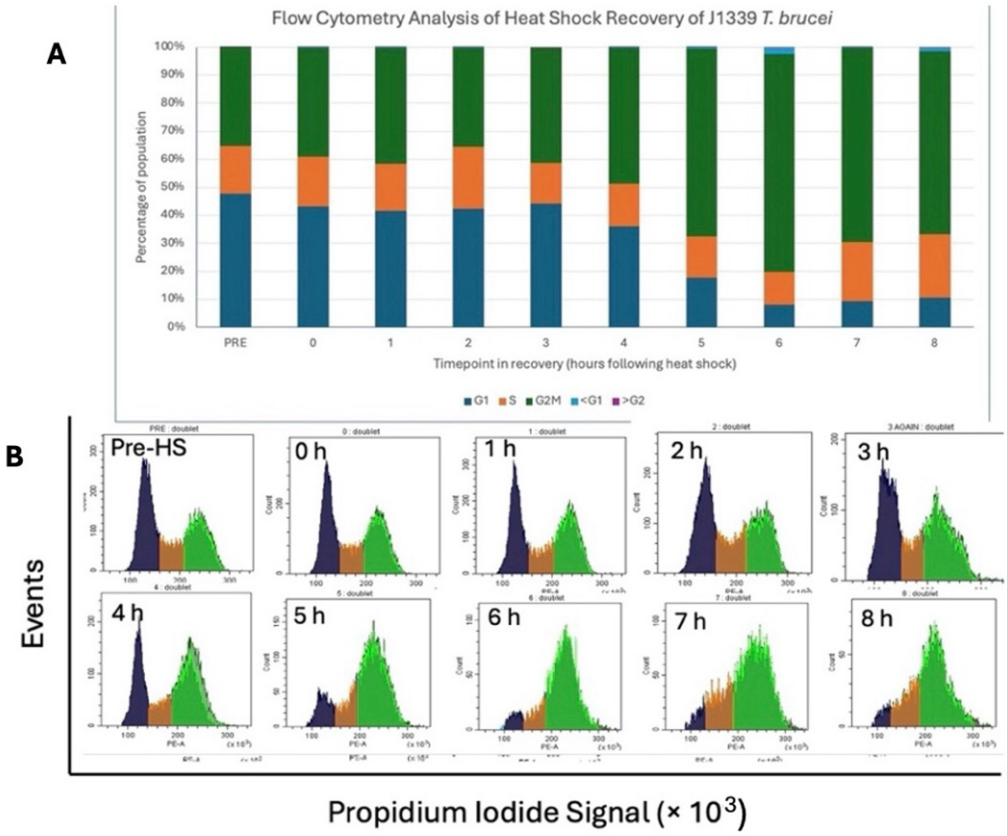

Figure 4.5: *T. brucei* BSF J1339 cell cycle arrest following a HS at 41 °C for 1 hour. A sample was taken prior to HS (Pre-HS) and following hours after HS 0-8 h. For each sample 50,000 events were recorded and gated on a Cytoflex flow cytometer, the following PI signal was used to distinguish the cell cycle phases. The cell cycle gates were adjusted accordingly to fit the cell cycle phase peaks using CytExpert software, these are shown in panel B of the figure. The proportion of cells in each cell cycle phase as a percentage were plotted as a histogram, panel A of the figure which corresponds with the PI traces below in panel B.

After a HS at 41 °C for 1 hour, BSF *T. brucei* underwent a reversible cell cycle arrest, shown in 2T1 cells by an initial enrichment in S phase cells peaking at the third hour of recovery, starting from a pre-HS proportion of 20.89% and reaching 28.6% 3 h after HS. These S phase cells progress into a G2M phase arrest, where cells accumulated in G2M peak at the 5th hour of recovery, suggestive of replicated DNA without cell division. This peak enrichment was observed as a proportion of 56.9% of the cell population being G2M cells 5 hours after HS. This arrest ended with the decrease in G2M cells back to 32.29% at the 8th hour of recovery near to the pre-HS value of 29.44%; the other phases

of the cell cycle also returning to similar proportions that were present before HS, suggesting that the arrest is reversible.

This same G2M phase arrest is shown in J1339 BSF *T. brucei,* however with a less prominent S phase shift into the peak in G2M cells. The peak in S phase cells occurs at the second hour of recovery reaching 22.19% from an initial 16.98%. The following G2M arrest occurs later and greater than that in 2T1 cells at the 6th hour of recovery peaking from an initial 34.8% proportion to 76.56%. As this arrest occurred later within the time course, the full resolution of the arrest was not observed within the time period analysed, but a decrease in G2M phase back towards the pre-HS levels at 8th hour of recovery (64.86%) suggests the return of proportions of phases beyond the timepoints. This experiment was repeated for both cell lines, finding similar trends with the peak G2M arrest occurring between the 4th and 6th hours of recovery but with a varied extent of arrest, with a range of 54.3-76.5 % of G2M cells. The differences between the cell lines in their response to HS may be explained as 2T1 is monomorphic and J1339 cells are pleiomorphic. As the J1339 cells are able to differentiate *in vitro,* this may alter their response to a heat stimulus and may be more representative of how BSF *T. brucei* responds *in vivo.*

To further understand the importance of 41°C as a HS condition, flow cytometry analysis was completed to observe the effect of an increased HS temperature of 42 °C; to examine the extremity of an effect as little as 1 °C difference of a HS temperature has upon the viability of the cells. Therefore, 2T1 BSF *T. brucei* cells were heat shocked for 0.5, 1 and 2 hours at 42 °C, samples for flow cytometry were fixed immediately following HS. The cells were stained with PI and were gated to remove doublets for following gating to identify stages of the cell cycle (shown in Figure 4.6).

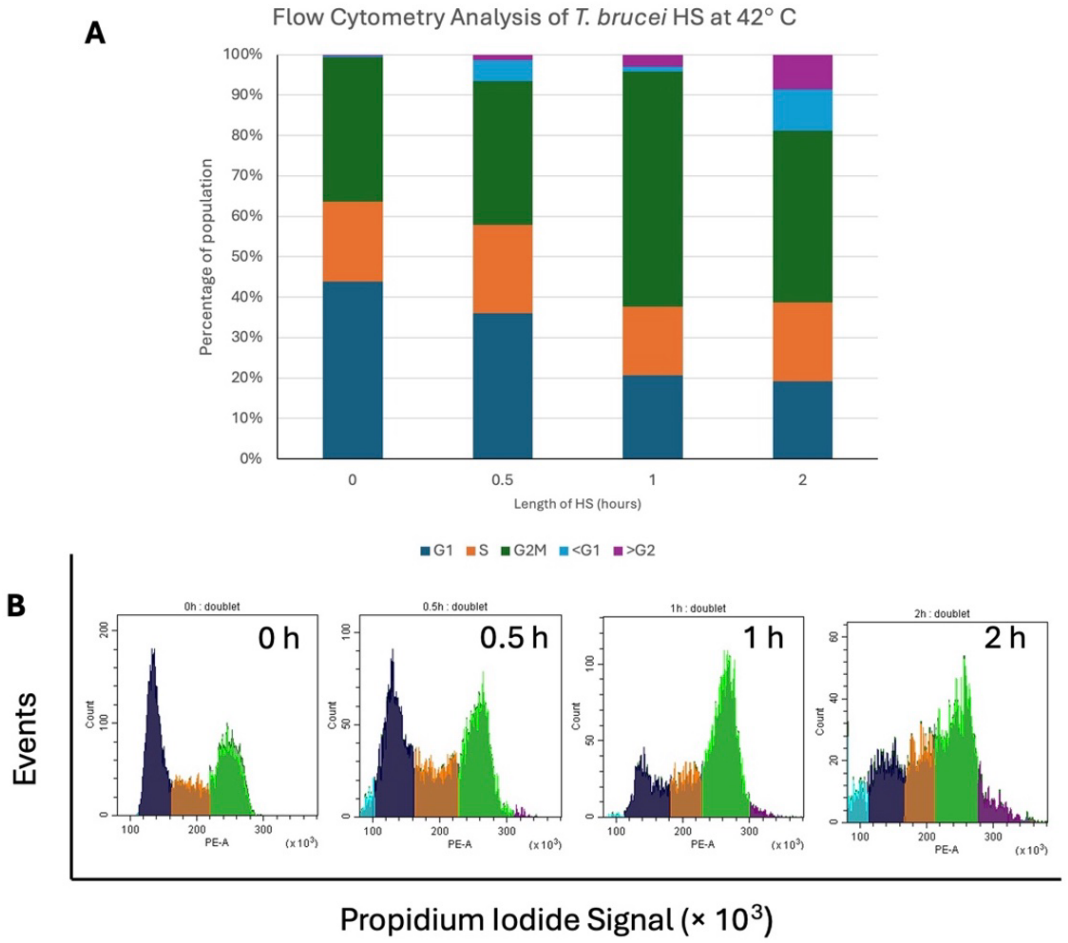

Figure 4.6: *T. brucei* BSF 2T1 effect of 42 °C HS on cell cycle proportions. A sample was taken prior to HS (Pre-HS) and following HS at 42 °C for 0.5, 1 and 2 h. For each sample 10,000 events were recorded and gated on a Cytoflex flow cytometer, the following PI signal was used to distinguish the cell cycle phases (panel B). The cell cycle gates were adjusted accordingly to fit the cell cycle phase peaks using CytExpert software. The proportion of cells in each cell cycle phase as a percentage were plotted as a histogram which corresponds with the PI traces (panel A).

After exposure to 42 °C for 0.5h an increase occurs in <G1 phase cells which are categorised as being fragmented or apoptotic cells, suggestive of a high extent of damage induced to the population of cells. A further cell-cycle phase that increased uniquely at 42 °C includes the >G2 phase and the rapid increase of the G2M stage immediately following 1 hour of HS, reaching 57.1% which took up to around 5 hours of recovery to get to a comparable proportion after a 1 h 41 °C HS. This demonstrates the severity of the effect of a 42 °C HS and as a result that 41 °C is a more favourable

temperature to induce the HS response in BSF *T. brucei,* due to the assumption that both <G1 and >G2M cells will die as typically non-viable phenotypes with irregular DNA staining beyond the cell cycle stages.

4.2 Monitoring heat shock induced P-body formation

Within the literature it is established that P-bodies form within the HS response in *T. brucei* (Kramer et al., 2008; Minia et al., 2016), these P-bodies containing DDH1 which mark non-essential mRNAs for degradation via exonucleases. It has been demonstrated by Kramer et al (2008) within PCF *T. brucei* that DHH1 relocates from being dispersed across the cell to be localised within P-bodies after HS.

4.2.1 Formation of P-bodies in BSF *T. brucei*

The formation of P-bodies is a crucial aspect of the HS response in supporting the expression of 'essential' mRNAs and was therefore investigated further in BSF *T. brucei* via the response of DHH1. To observe the effect of a 1 hour 41 °C HS on BSF, slides were fixed before and after HS for immunofluorescence staining. The cell line expressed endogenously Ty-tagged DHH1; therefore, with anti-Ty staining it could be observed if a HS-induced change in DHH1 localisation occurs in BSF *T. brucei.* Six representative images of the cells prior to HS are shown in Figure 4.7 and post-HS in Figure 4.8.

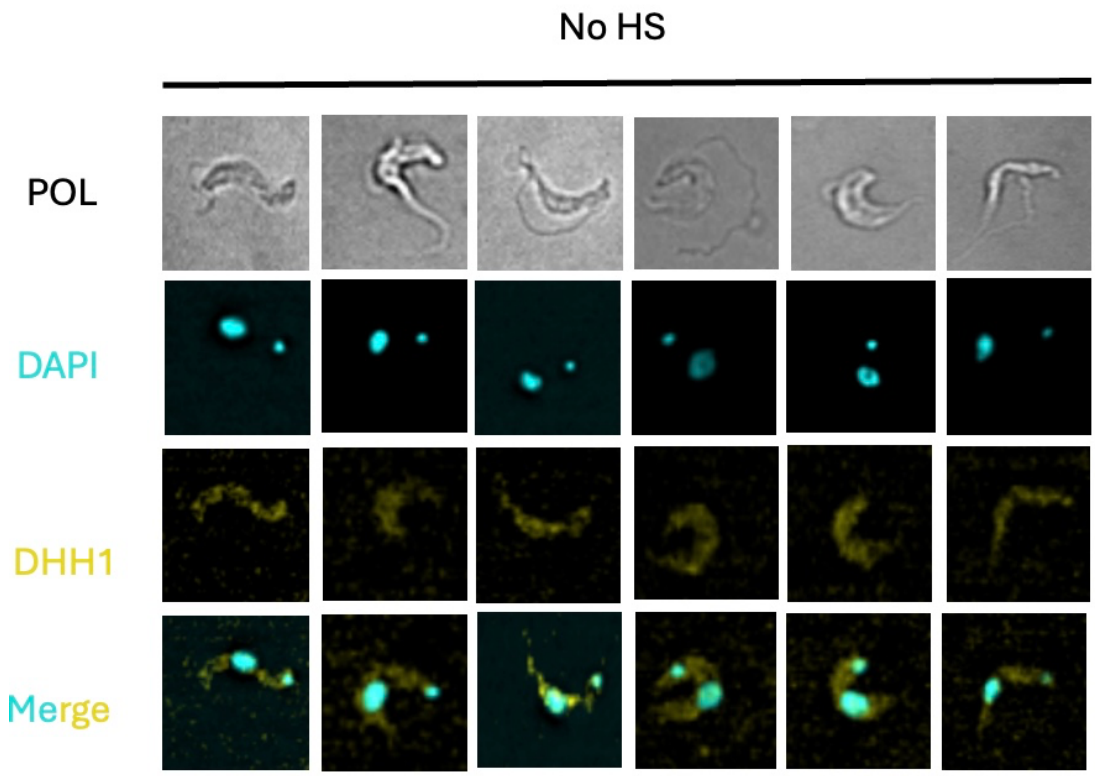

Figure 4.7: BSF *T. brucei* expressing DHH1-Ty before HS. Cells at a density of ~ 7 × 10^5 cells/ml were fixed using 4% PFA; were stained with anti-Ty rabbit antibody (anti-rabbit FITC secondary) and DAPI via fluoroshield mounting medium. Images were taken using the 60× objective lens on a DeltaVision elite deconvolution microscope and normalised using ImageJ software.

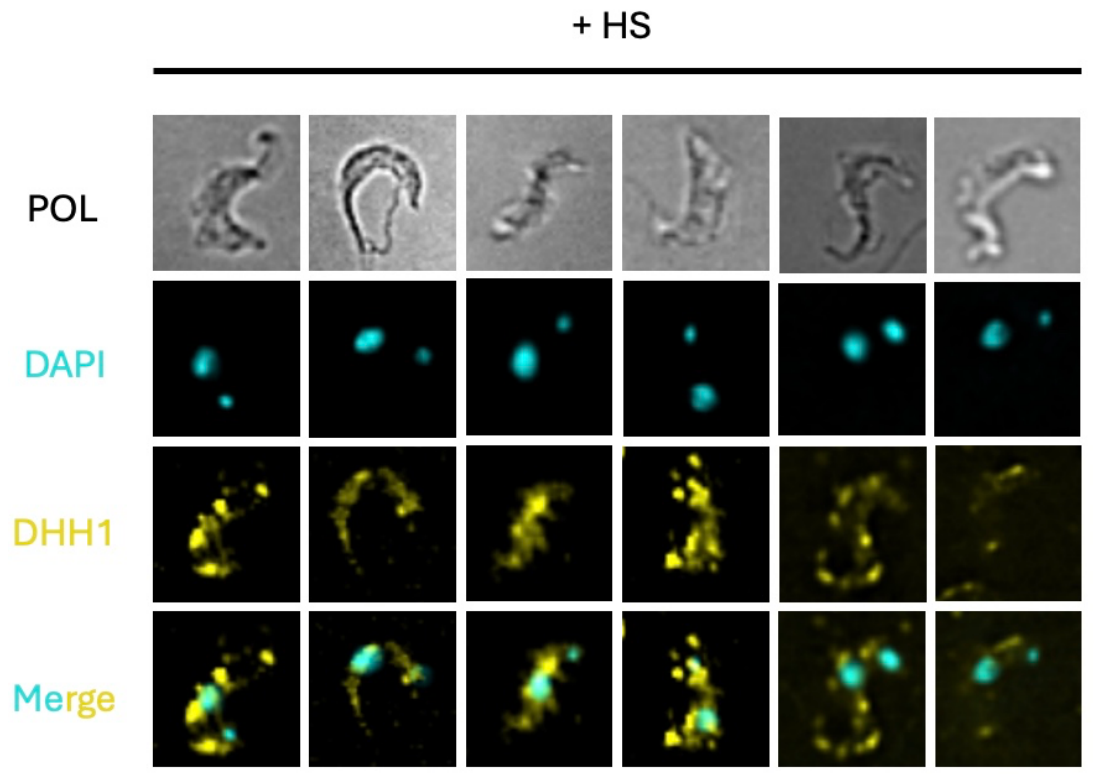

Figure 4.8: BSF *T. brucei* expressing DHH1-Ty after a HS at 41 °C for 1 hour. Cells at a density of ~ 7×10^5 cells/ml were heat shocked prior to fixation using 4% PFA; were stained with anti-Ty rabbit antibody (anti-rabbit FITC secondary) and DAPI via fluoroshield mounting medium. Images were taken using the 60× objective lens on a DeltaVision elite deconvolution microscope and normalised using ImageJ software.

Prior to HS DHH1 in BSF *T. brucei* appears to have a dispersed appearance across the cytoplasm, with some foci in areas of more concentrated DHH1 shown in areas with increased signal. Following HS at 41 °C for 1 hour, DHH1 appears to localise into more punctate areas across the cytoplasm, producing increased foci with greater intensity throughout the cytoplasm and noticeably around the nucleus. This effect of increased abundance of DHH1 foci were observed across two experimental repeats, however the number of foci varied on a cell-to-cell basis, those presented represent the level of variation observed.

4.2 Does HS-induced loss of motility correlate with a growth defect?

To enable future work of assessing the change HS induces upon growth over a shorter experimental time course, rather than completing outgrowth cell counts for growth curve analysis across several days, motility analysis was investigated. This involved testing a hypothesis derived from the work of Broadhead et al (2006), that with a decrease in motility there is a decrease in flagellum movement to support cytokinesis resulting in a growth defect as cells are halted in G2M. As a result, due to the HS-induced lags in growth observed in *T. brucei* it was hypothesised that a growth disturbance may be reflected in a decrease in cell motility limiting cytokinesis following HS. Furthermore, prior to cytokinesis VSG synthesis is at its peak, to support both daughter cells having a complete VSG coat upon their division. As a result, this analysis may provide an indirect readout of cells halted at this stage with increased VSG expression unable to complete cytokinesis, through decreased motility.

The timepoints for each temperature vary from 0-8 hours dependent upon the HS temperature. The rationale for this was the higher the temperature, the HS-induced damage to the cells would occur faster and to capture these events, earlier timepoints

are needed; these timepoints were continued until the culture looked visibly dead with few remaining motile cells. Whilst for less severe HS temperatures (closer to the cell culture temperature), damage is assumed to occur as an accumulation of a longer-term exposure, due to this timepoints were increased with the intention to capture this.

HS-induced motility effects were investigated in 2T1 BSF *T. brucei* using a varied time of HS exposure, placing the cells (> 5×10^5 cells/ml) into a water bath with controlled temperatures of 40 °C, 40.5 °C, 41 °C, 41.5 °C and 42 °C. Icy bioimaging software and Excel were used to plot experimental box and whisker plots to observe the implication of these various HS temperatures alongside their increase of exposure to the maximum speed (Figure 4.9) and average speed (Figure 4.10) achieved by the cells. Statistical significance was determined using a single ANOVA with Tukeys ad hoc post-tests using the Real Statistics plugin (Zaiontz, 2023) and all HS p-values are outlined in the Appendix (9.1).

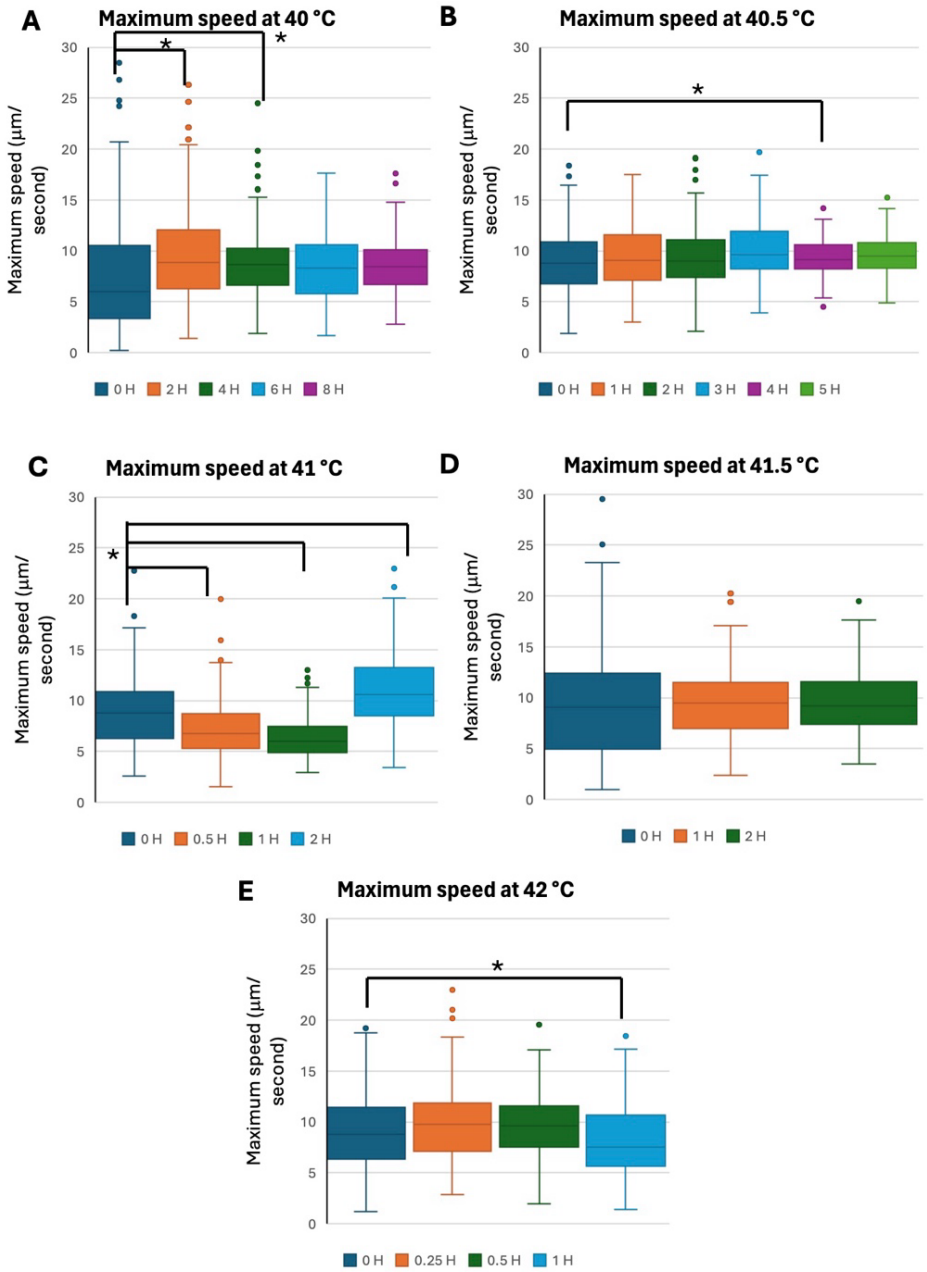

Figure 4.9: The effect of heat shock at 40 °C-42 °C upon the maximum speed of 2T1 *T. brucei* cells. A- cells were placed at 40 °C for 2, 4, 6 and 8 h. B- cells were placed at 41.5°C for 1, 2, 3, 4 and 5 h. C- cells were placed at 41 °C for 0.5, 1 and 2 h. D- cells were placed at 41.5 °C for 1 and 2 h. E- cells were placed at 42 °C for 0.25, 0.5 and 1 h. All cells were recorded in triplicate and were processed using Icy Bioimaging software, producing data for the maximum speed reached by each cell, 200 of which were averaged across the repeats and plotted as box and whisker plots. The data was statistically analysed using a single ANOVA with Tukeys ad hoc post-tests using the Real Statistics plugin (Zaiontz, 2023), data was deemed significant when $p<0.05$ and is highlighted *.

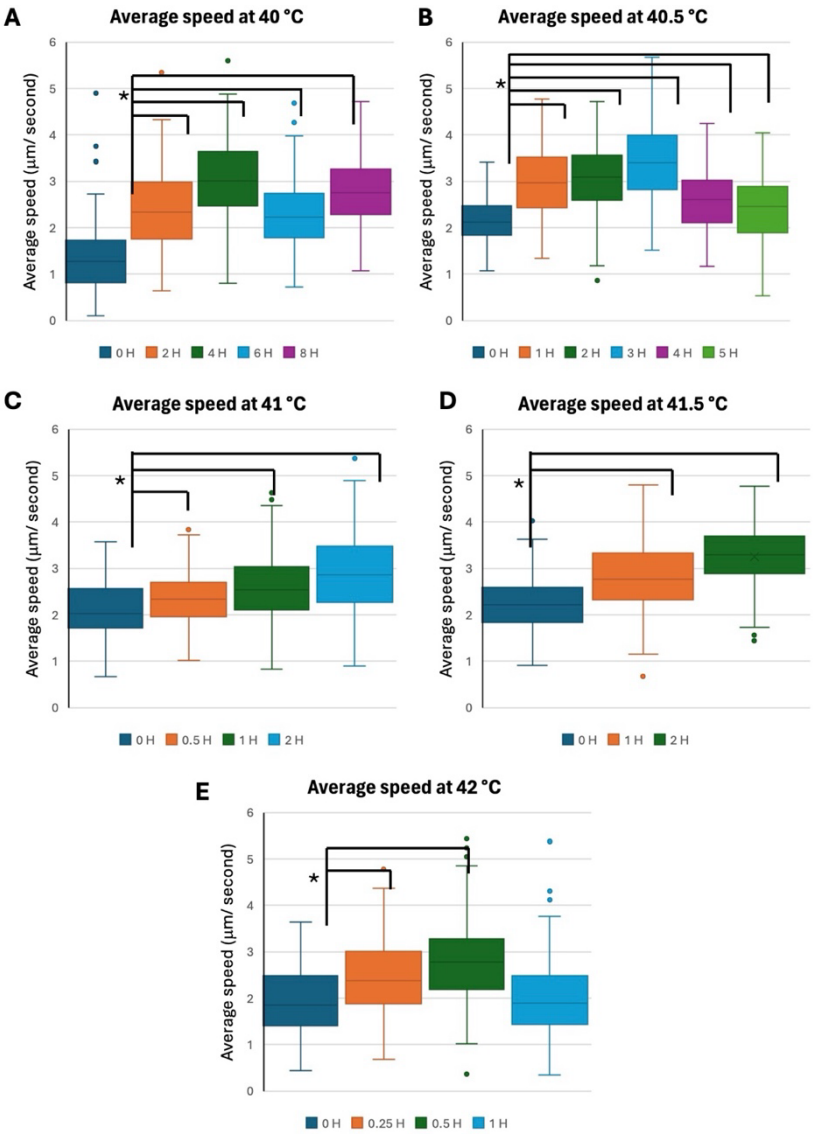

Figure 4.10: The effect of heat shock at 40°C-42°C upon the average speed of 2T1 *T. brucei* cells. A- cells were placed at 40°C for 2, 4, 6 and 8 h. B- cells were placed at 41.5°C for 1, 2, 3, 4 and 5 h. C- cells were placed at 41°C for 0.5, 1 and 2 h. D- cells were placed at 41.5°C for 1 and 2 h. E- cells were placed at 42°C for 0.25, 0.5 and 1 h. All cells were recorded in triplicate and were processed using Icy Bioimaging software, producing data for the average movement completed by each cell, 200 of which were averaged across the repeats and plotted as box and whisker plots.

A HS stimulus between 40 °C and 42 °C caused a lack of a consistent effect upon the maximum speed reached by 2T1 BSF *T. brucei* cells, with the variety of temperatures and timepoints producing little fluctuation from the starting maximum speed of non-HS cells. However, the most noticeable changes occurred to the cells at 41 °C for 2

hours having an increased maximum speed (Figure 4.9C) and at 42 °C for 1 hour causing a decreased maximum speed (Figure 4.9E), indicating the variability of an overall effect occurring. Furthermore, most of the interquartile ranges within Figure 4.9 overlap, suggestive of a high level of similarity across the data.

However, the same HS conditions (40-42 °C) had an effect upon the average speed of cells within the culture, which was consistent across technical replicates, suggesting variation in overall effect upon prolonged HS. HS at both 40.5 °C and 42 °C (Figures 4.10B & D) caused an increase in average speed in the earlier timepoints before then decreasing in subsequent timepoints; thus, indicating a bimodal effect. Variability in a HS-induced trend is observed in the HS at 40 °C (Figure 4.10A), showing an increase in average speed until 4 h, a decrease occurring at 6 h and an increase at 8 h. Whilst the heat shocks at 41 °C and 41.5 °C (Figures 4.10C & D) showed a general increase in the average speed of the cells which was not reflected in the change in maximum speed. This reflects the level of variability motility analysis provides as a read-out of the HS-induced growth defects.

Further equivalent analysis was completed in J1339 BSF *T. brucei* cells using HS temperatures of 41 °C, 41.5 °C and 42 °C to produce box and whisker plots of average and maximum speeds of the cells throughout the duration of HS exposure (Figure 4.11). The representative change in motility observed via the change in track length using the Icy bioimaging software is displayed in Figure 4.12 for each HS and timepoint completed in the J1339 cells. The box plots present the data recorded across three technical replicates, showcasing a wider variety across the dataset as a whole, whilst the tracks shown are from one of these technical replicates.

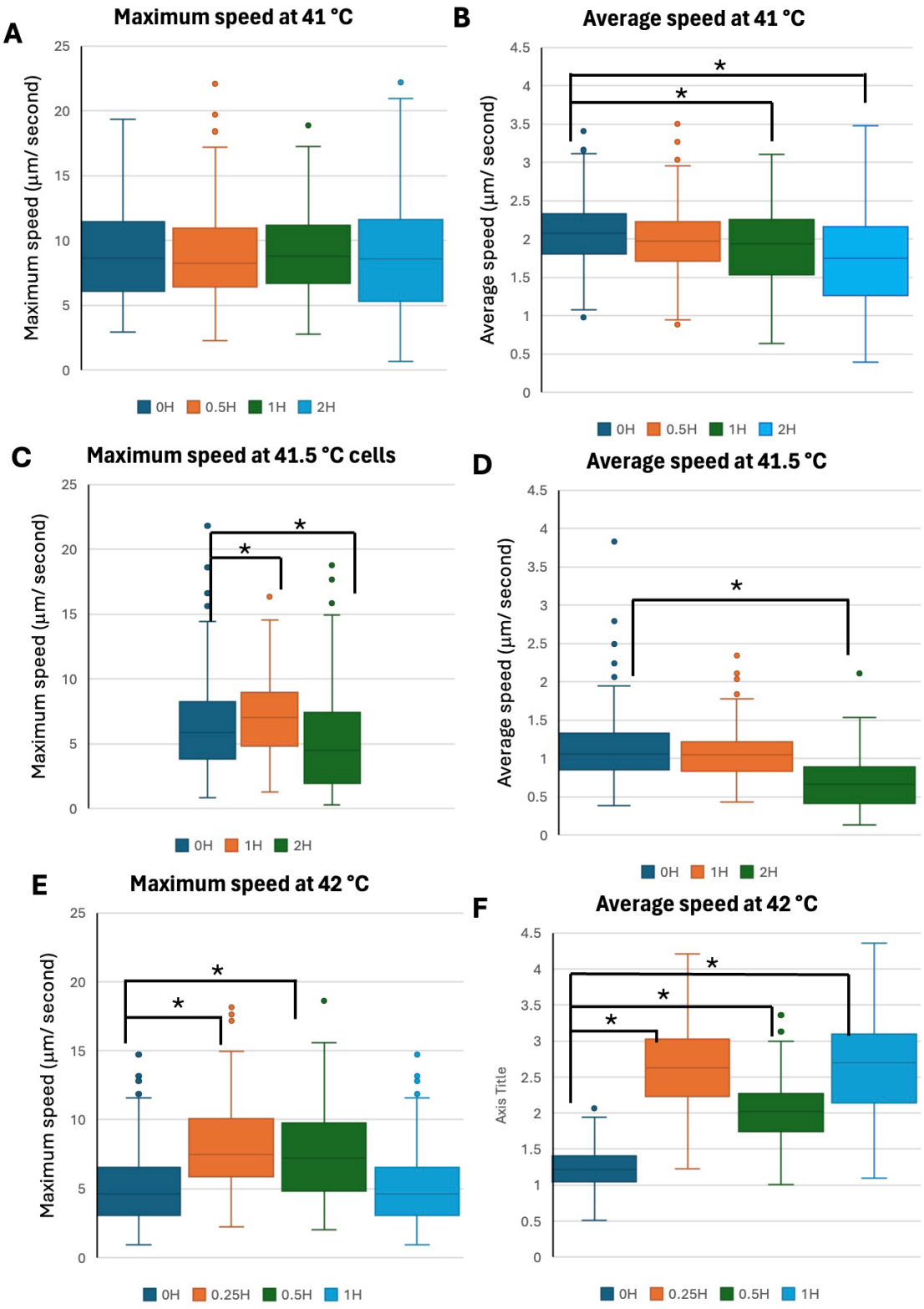

Figure 4.11: The effect of heat shock at 41 °C-42 °C upon the maximum and average speed of J1339 *T. brucei* cells. A and B- cells were placed at 41 °C for 0.5, 1 and 2 h. C and D- cells were placed at 41.5 °C for 1 and 2 h. E and F- cells were placed at 42 °C for 0.25, 0.5 and 1 h. Each timepoint was completed in triplicate and were processed using Icy Bioimaging software,

producing data for the maximum and average speed reached by each cell, 200 of which were averaged across the repeats and plotted as box and whisker plots. The data was statistically analysed using a single ANOVA with Tukeys ad hoc post-tests using the Real Statistics plugin (Zaiontz, 2023), data was deemed significant when $p<0.05$ and is highlighted *.

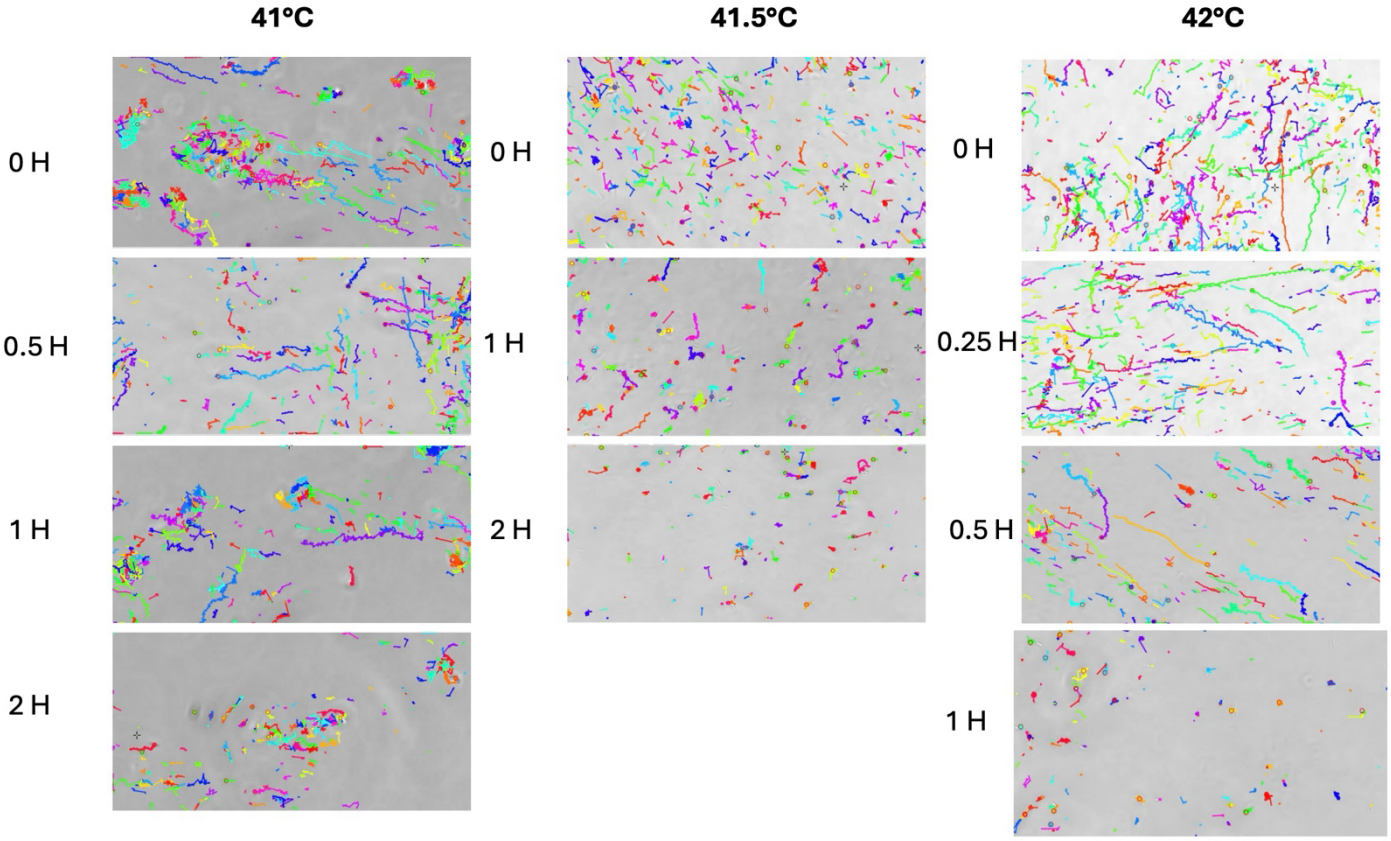

Figure 4.12: Tracks produced by J1339 BSF *T. brucei* cells showing the effect HS has upon motility. HS at 41 °C, 41.5 °C and 42 °C were completed for motility analysis, the tracks are displayed with their various timepoints indicated next to the image. The tracks displayed for each time point are one of each technical triplicate completed that was considered representative of the time point. All tracks were captured using Icy bioimaging software.

Comparative to the equivalent data acquired in 2T1 cells, the motility analysis output of maximum and average cell speeds in J1339 cells showed variability in an overall trend responsive to HS. This is shown by heat shocks at 41 °C and 41.5 °C causing a lack of change in the maximum speed of the cells whilst causing a decrease in average speed, highlighting inconsistency in an overall effect upon motility. Furthermore, HS at 42 °C caused both increases and decreases to the maximum and average speeds at different timepoints, indicating discrepancies in the read-outs of motility and a lack of an overall correlation induced by HS. The data plots present differences to the shown

tracks data as the plots were generated from an average of 3 different panels of tracks for each timepoint, the tracks displayed were selected for being most representative of the triplicate. The tracks data shows that as exposure to a HS stimulus increases, there is a visible decrease in the length of paths taken by the J1339 *T. brucei* cells. This indicates that the motility of the cells is being implicated by HS; that a shorter and more severe HS is able to have the same impact as a lower HS temperature for an increased time of exposure. This is shown by 1 h at 42 °C having short tracks comparable to those observed after 2 h at 41 °C and 2 h at 41.5 °C, presenting a comparable effect induced by differing HS stimuli.

To produce a potential initial read-out of the effect HS has upon the growth of *T. congolense* to compare to that in *T. brucei*, an equivalent motility analysis was completed in *T. congolense* cells. This observed the effect exposure to 41 °C for 0.5 and 1 h has upon the average and maximum speed of *T. congolense* cells (Figure 4.13).

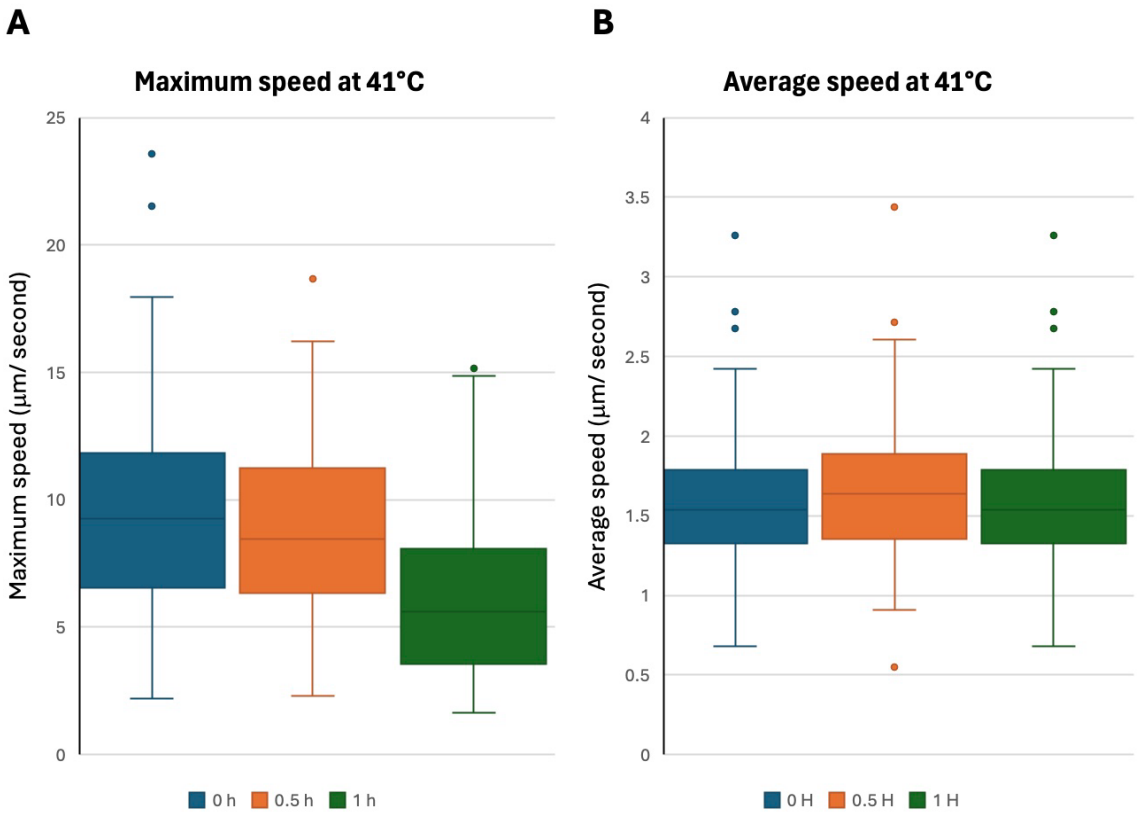

Figure 4.13: Motility analysis of *T. congolense* cells heat shocked at 41 °C. Cells were placed into a 41 °C water bath for 0.5 and 1 hours for their motility to be compared with non-HS cells. Cells were recorded in triplicate for 30 seconds using a DroiX 4K colour camera system set up

on an Oxion Inverso inverted light microscope. The videos were processed using Icy Bioimaging software, producing data for the maximum movement completed by each cell (A) and average speed of each cell (B), these measurements were averaged across the repeats and plotted as box and whisker plots. The plot boxes highlight the interquartile range containing the marked mean and the whiskers represent the range in values, excluding outliers which are also highlighted. The data was statistically analysed using a single ANOVA with Tukeys ad hoc post-tests using the Real Statistics plugin (Zaiontz, 2023), data was deemed significant when $p<0.05$ and is highlighted *.

HS at 41 °C shows to decrease the maximum speed of *T. congolense* cells from 9.56 μm/second to 8.73 μm/second after 0.5 h and a further decrease to 6.07 μm/second after 1 h. Statistical significance was determined using a single ANOVA with Tukeys ad hoc post-tests using the Real Statistics plugin (Zaiontz, 2023) on Excel software (Table 4.1). The greatest difference in maximum speed was observed between 0 h and 1 h shown by the smallest overlap in the interquartile ranges. However, the same trend for reduced motility was not indicated in the average speed of the *T. congolense* cells, as after 0.5 h at 41 °C the cells moved on average 0.14 μm/second faster lacking statistical significance, which was further shown after 1 h with a 0.05 μm/second insignificant average increase from the 0 h cells. The lack of a significant change across the average speed of *T. congolense* cells at 41 °C for 0, 0.5 and 1 h is demonstrated in the overlap of both the ranges excluding outliers and interquartile ranges.

Table 1: p-values produced via single ANOVA with Tukeys ad hoc post-test for the change in motility for *T. congolense* following HS. HS of *T. congolense* was completed at 41°C for 0.5 and 1 hours. Analysis was completed using the Real Statistics plugin (Zaiontz, 2023) on Excel for both the maximum speed and average speed, presented are the p-values at 3 significant figures. *Significant data $p<0.05$.

Comparison	p-value for Maximum speed	p-value for Average speed
0 H – 0.5 H	0.0862 *	0.451
0 H – 1 H	4.16×10^{-10} *	0.393
0.5 H – 1 H	4.86×10^{-10} *	0.9981

To confirm that the changes observed in the maximum and average speeds of both *T. brucei* and *T. congolense* cells occurred due to the HS stimulus, a negative control was completed using BSF *T. brucei* cells maintained at 37 °C. Equivalent analysis across all previous timepoints were completed using both 2T1 and J1339 BSF *T. brucei* cells; Icy bioimaging software and Excel were used to plot box and whisker plots (Figure 4.14). The acquired tracks of the cells were visually analysed to observe whether the flow or drift of the cells induced by a meniscus effect had a significant effect upon the movement of the cells (Figure 4.15). The absence of this effect was determined by a lack of a singular directionality of the tracks completed by the cells influenced by the movement of media.

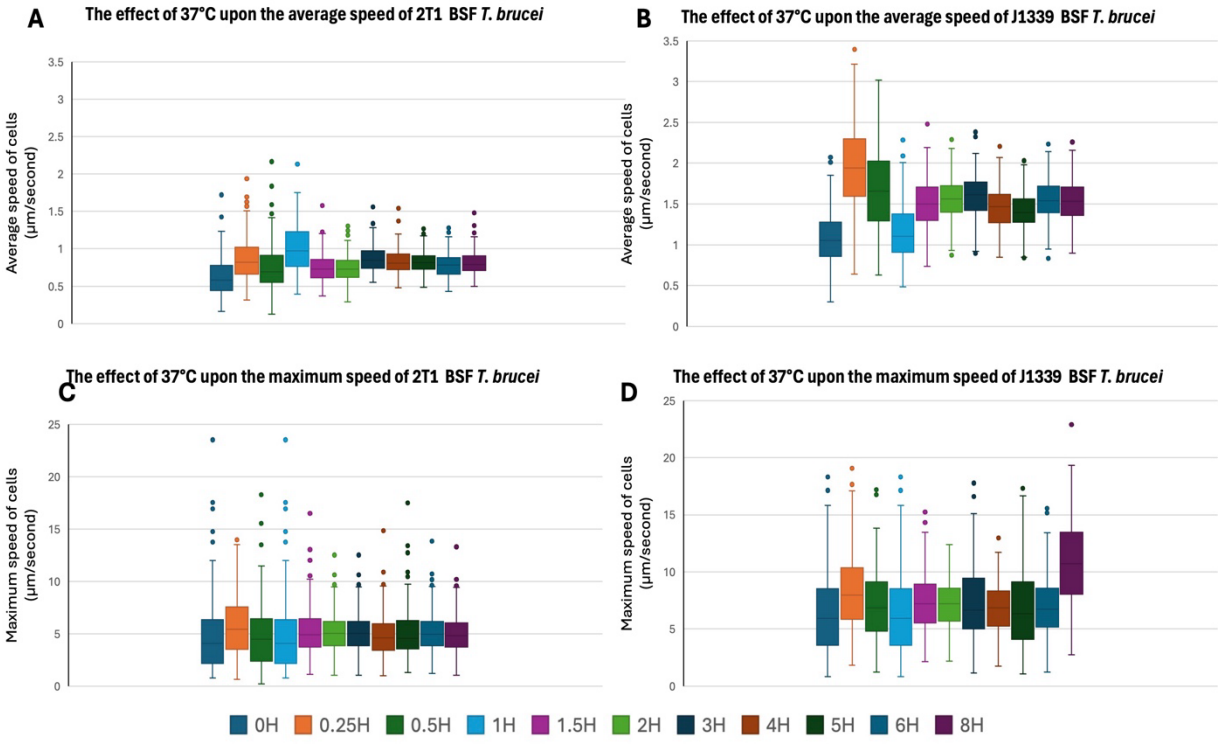

Figure 4.14: Motility analysis of BSF *T. brucei* cells for up to 8 h at 37 °C. The effect of 37 °C across a time course of analysis upon the average speed of 2T1 cells is shown in panel A and of J1339 cells in panel B. The effect of 37 °C across a time course of analysis upon the maximum speed of 2T1 cells is shown in panel C and of J1339 cells in panel D. This data was produced using Icy bioimaging software, to plot the output data of 200 average tracks using Excel.

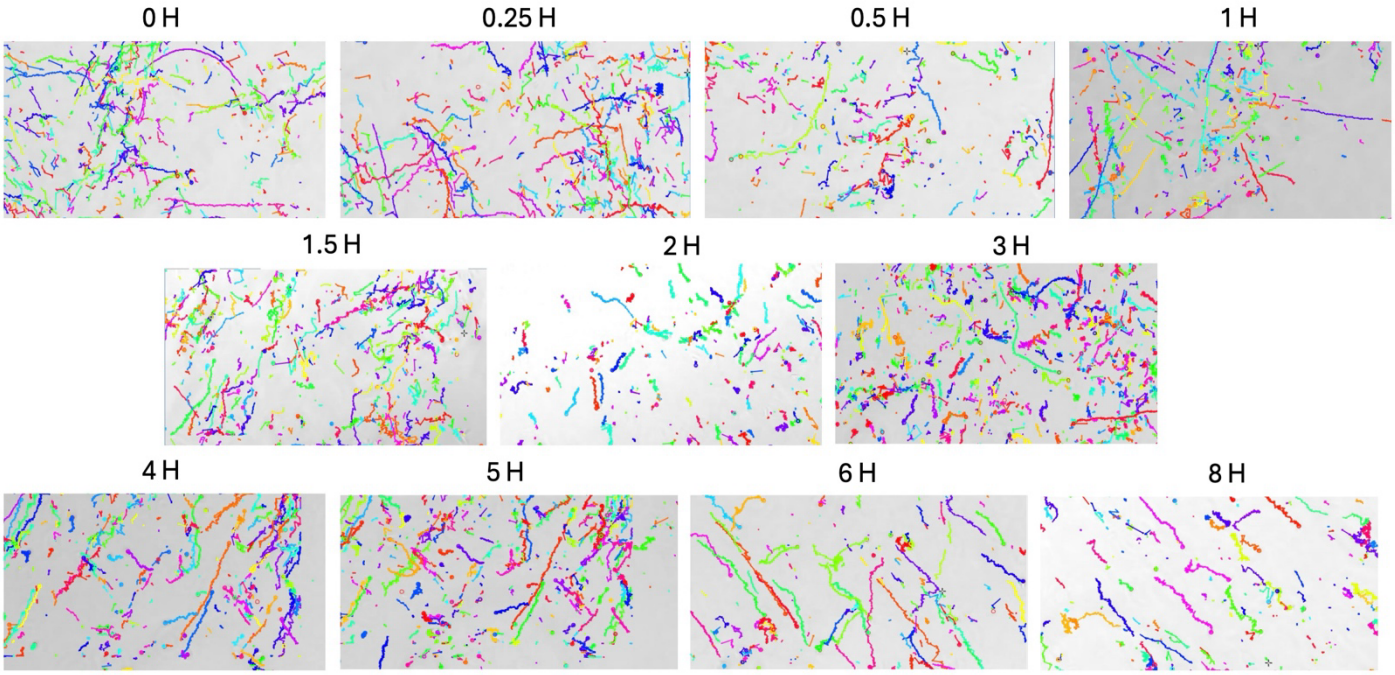

Figure 4.15: Tracks produced by 2T1 BSF *T. brucei* cells up to 8 h of motility analysis being completed with the culture at a constant temperature of 37 °C. The tracks displayed for each time point are one of each technical triplicate completed that was considered representative of the time point. All tracks were captured using Icy bioimaging software.

The box and whisker plots for both the 2T1 and J1339 *T. brucei* cells for average and maximum speed present a lack of significant change throughout the completed time courses, indicated through comparative means and constant overlap in the interquartile ranges. Furthermore, the plots emphasise statistical similarity via overlap in the ranges excluding outliers. The effect of flow or drift was shown to be limited due to there being multiple directions of tracks completed by the 2T1 cells, with a level of visual similarity throughout the time course, indicating that any potential changes observed after HS may be independent of a meniscus-derived effect upon the cells.

Due to the consistency observed in the control, it may suggest that HS implicates trypanosome motility. However overall, motility analysis did not provide a consistent read-out of a HS-induced alteration to motility that could be used to infer a growth defect. As a result, outgrowth analysis remains the most efficient method to observe this effect, without variability due to the lack of influence from uncontrolled temperatures.

4.4 Summary- HS in African trypanosomes induces a lag in growth and a reversible cell cycle arrest

An increase in the exposure of HS up to 2 hours at 41 °C was shown to increase a lag or induce a greater defect in growth of BSF *T. brucei* cells (in both 2T1 and J1339 cell lines). A HS of 1 hour at 41 °C is viewed to be a sufficient HS stimulus to initiate HS recovery, thus enabling the growth rate to lag and then return to a rate equivalent to that in non-HS cells after around 24 hours post-HS in 2T1 and J1339 cells. The first 8 hours post-HS within this lagged growth period were investigated in cell cycle analysis, finding in both cell lines there is an initial S phase enrichment, before shifting to a peak proportion of G2M cells by the 5^{th} or 6^{th} hour of recovery. This peak of G2M cells is completely resolved in the 2T1 cells by the 8^{th} hour of recovery and this proportion is shown to decrease towards the pre-HS level in the J1339 cells. HS at 42 °C is shown to be fatal to 2T1 BSF *T. brucei* cells, shown by a HS-induced increase in <G1 and >G2M cells, which are assumed to subsequently die.

After 1 hour at 41 °C in BSF *T. brucei* there is a shift in localisation of DHH1 from being dispersed throughout the cytoplasm of the cell to being increased within punctate localisations. These accumulations noticeably increased around the nucleus. The increase in foci of DHH1, is the observation of an increase in DHH1-rich P-bodies post-HS.

Despite the association between motility and cell division, the motility analysis observing the effect of HS produced inconsistencies in the read-outs of maximum and average speeds reached by the cells. Therefore, no overall correlation was shown between motility and an increased exposure or severity of a HS stimulus as hypothesised; instead presenting variability in an overall effect. However, the initial tracks data demonstrated a decrease in the length of paths taken by J1339 BSF *T. brucei* cells in increased HS stimuli, suggesting decreased motility for less distance to be covered. But these same tracks were used to produce the data of maximum and average speeds of J1339 *T. brucei* cells, which did not provide evidence to confirm this visual observation. Motility analysis of *T. congolense* cells also showed this same level of inconsistency of a HS-induced effect to the maximum and average cell speeds.

Overall, indicating that motility analysis had limited accuracy as a predictor of cell growth defects caused by HS.

5. Characterising the role of the ZC3H11-MKT1 complex in the HSR

In *T. brucei* ZC3H11 plays an essential role in the HS response, binding to AU-rich elements in HSP mRNAs and stabilising them (Singh et al., 2014). ZC3H11 also interacts with MKT1, a cytosolic and polysome associated protein (Singh et al., 2014). Analysis of phosphorylation sites in *T. brucei* after HS by Ooi et al (2020) suggested that the ZC3H11-MKT1 complex has a role in thermotolerance to stabilise mRNAs essential for the HS response, with an increase in phosphorylation site abundance on DHH1 and PABP that associate with the complex (Ooi et al, Benz and Urbaniak, 2020). To directly confirm the role of the ZC3H11-MKT1 interaction within the HS response, here we perform *in situ* mutagenesis of the HNPY motif on ZC3H11 that is required for it to interact with MKT1 (Singh et al., 2014).

5.1 Characterising ZC3H11 complex formation with MKT1 in the HSR in *T. brucei*

5.1.1 Site-directed mutagenesis of the HNPY motif in ZC3H11

The HNPY consensus interaction motif was identified in ZC3H11 by Singh et al (2014). Singh et al (2014) mutated the interaction motif into either ANPA, AAPY and HNPA, and demonstrated that the motif was required for interaction with MKT1 by immunoprecipitation. Interestingly, they also stated that they could not detect ectopically expressed tagged ZC3H11 mutants in PCF *T. brucei* and suggested that the proteins were unstable. We aimed to confirm whether the ZC3H11-MKT1 interaction was essential for the HS response by generating BSF cells expressing both *in situ* TY1-tagged mutated ZC3H11 (no ectopic expression was used throughout this project, instead a mutated copy of ZC3H11 replaced the endogenous copy) and myc-tagged MKT1 and followed by immunoprecipitation. We completed site-directed mutagenesis

of the ZC3H11 HNPY motif with a different single base substitution mutation, changing the proline (CCC) into an alanine (GCC), altering the motif to HNAY. In this process the mutant ZC3H11 keeps the endogenous 3' UTR, as no modifications were introduced downstream of the coding sequence. The workflow used to generate the pPOTv6 plasmid containing mutated ZC3H11 prior for transfection is shown in Figure 5.1.

The pPOTv6 plasmid was chosen for its compatibility with CRISPR-Cas9 editing, and has a cloning site flanked by three copies of the TY epitope tag to facilitate downstream detection (Paterou et al., 2025). The Cas9 guide RNA was generated *in vitro* during transcription using RNA polymerase from a PCR-amplified DNA template containing both the promoter and guide sequence. Transfection of the pPOTv6-ZC3H11(HNAY) plasmid, using a DN100 program on a Lonza Nucleofector machine, was completed into a 2T1-based parental cell line (previously transfected with a pRPa-dfLUC-Hsp100 3'UTR plasmid, allowing fLUC reporter expression under control of TbHsp100 3'UTR, and with a J1339 plasmid carrying a puromycin resistance marker, the Tet Repressor, T7 RNA polymerase and Cas9 all expressed constitutively; with resistance to phleomycin, hygromycin and puromycin). This cell line was selected because under HS conditions, the fLUC signal increases which can be used as a clear read-out of ZC3H11 activity, and for its compatibility for CRISPR via the J1339 plasmid (Rojas et al., 2019).

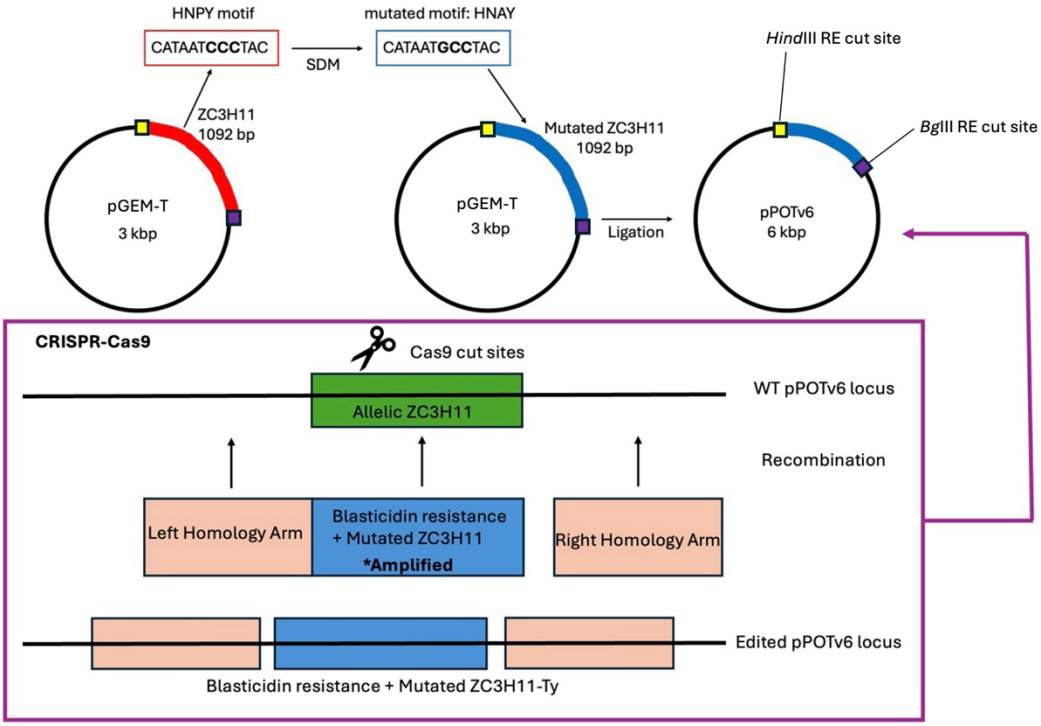

Figure 5.1: Schematic showing production of plasmid pPOTv6-ZC3H11(HNAY). After SDM completion, pGEM-T containing the mutant ZC3H11 gene was digested using *Hind*III and *Bg*III to isolate its insert, allowing ligation of the mutant ZC3H11 gene into a CRISPR-Cas9 edited pPOTv6 plasmid. In CRISPR-Cas9-aided genetic recombination, Cas9 introduces double strand breaks, which induces homologous repair of the DNA, incorporating the selection marker (blasticidin resistance gene) and mutant tagged ZC3H11 via neighbouring homology arms. The activity of Cas9 is guided by sg RNA, that forms a complex with Cas9, to direct double strand breaks to occur at a specific DNA sequence. This process specifically produces the HNAY mutant in transfected cells, but recombination events can occur upstream or downstream from the mutation, which can result in transfected *T. brucei* clones that are resistant to the drug selection marker, which may or may not contain the mutation.

After carrying out the SDM protocol (Figure 5.2), the plasmid pPOTv6-ZC3H11(HNAY) was transformed into bacteria and purified by miniprep. Sequencing of 5 minipreps was completed to detect whether the mutation of interest had been introduced (Table 5.1).

Sequencing of the mutant ZC3H11 ligated into pPOTv6 used T7 primers as it was flanked by a T7 promoter sequence within the pPOTv6 vector backbone, enabling the confirmation of the induced SDM. Whilst the sequencing of the gDNA extracted from transfected cells used a custom primer, that was used because of its location at the start of the ZC3H11 sequence, to allow sequencing to start immediately at the N-terminus of ZC3H11 to confirm the presence or absence of an induced mutation transfected into the cell line.

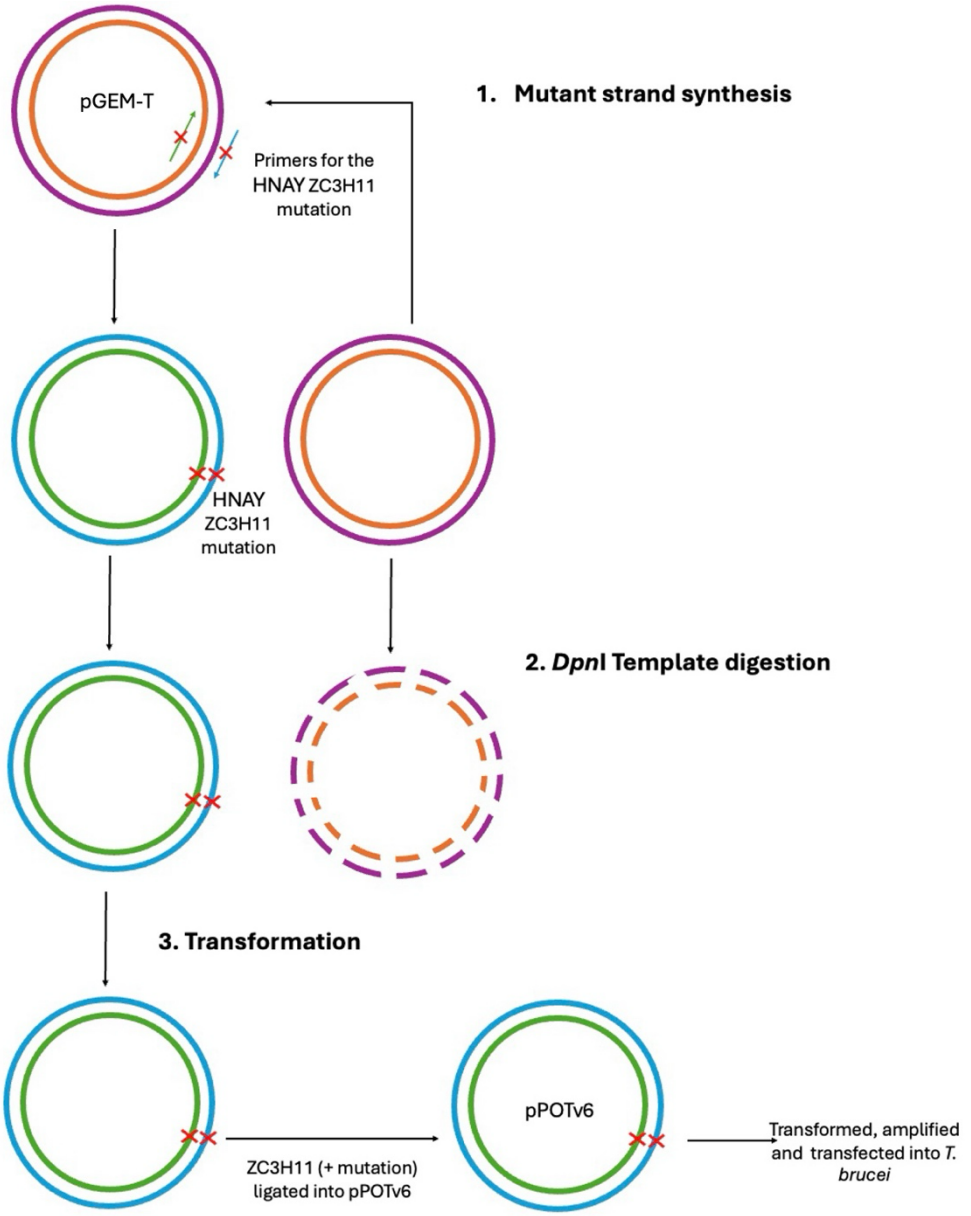

Figure 5.2: A schematic showing the use of SDM in the production of plasmid pPOTv6-ZC3H11(HNAY). Within mutant strand synthesis, the DNA template (ZC3H11-pGEM) is denatured, enabling the annealing of the mutating primers partially complementary to opposite strands of the template, thus enabling their extension, achieved via a PCR programme with DNA polymerase. Treatment with *Dpn*I enabled the digestion of the parental DNA template, due to its specificity to hemimethylated DNA (Agilent, n.d.). The resultant plasmid now containing mutant ZC3H11 was transformed in *E. coli* where the mutation was confirmed by sequencing. Mutant ZC3H11 was digested out of pGEM and ligated into pPOTv6. The mutant

ZC3H11-pPOTv6 was transformed into *E. coli*, miniprepped and sequenced. This Figure is adapted from (Agilent, n.d.).

Table 5.1: Sequencing results from minipreps to confirm the success of the SDM protocol. The T7 primer was used to sequence the pGEM inserts. The region of interest here is the genetic region around the ZC3H11 HNPY motif. The underlined sequence here indicates the coding sequence of the motif with the mutant codon highlighted in bold. Sequencing shown in the 5' to 3' direction.

Clone number	Sequencing result of the region of interest using T7
1	TGGCCGTGTCCGACATAAT**GCC**TACTGCCA
2	TGGCCGTGTCCGACATAAT**GCC**TACTGCCA
3	TGGCCGTGTCCGACATAAT**GCC**TACTGCCA
4	TGGCCGTGTCCGACATAAT**GCC**TACTGCCA
5	TGGCCGTGTCCGACATAATCCCTACTGCCA

In the resulting sequencing data (Table 5.1), minipreps 1-4 showed the presence of a GCC codon within the HNPY motif sequence, whilst clone 5 showed a CCC codon. The chromatogram sequencing data comparing the non-mutant clone 5 with the mutant sequence of clone 1 is shown in Figure 5.3. No other mutation was found within these ZC3H11 sequences.

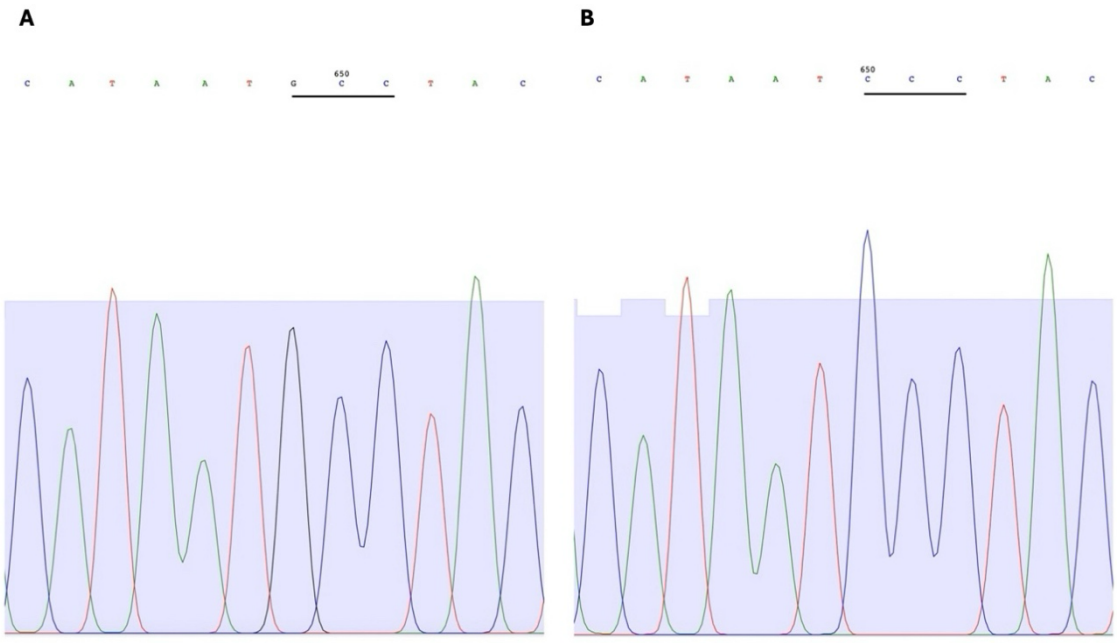

Figure 5.3: Chromatogram sequencing data using T7 comparing the mutant HNAY interaction motif sequence with the non-mutated HNPY sequence in ZC3H11. Panel A presents the sequencing data produced by clone 1, containing the SDM-induced mutation (GCC) indicated by an underline. Panel B presents the sequencing data produced by clone 5, with an unsuccessful SDM indicated by the WT (CCC) HNPY interaction motif sequence, which is underlined. Sequencing shown 5' to 3'.

Miniprep 1 was then used in a RE digest using *Hind*III and *Bg*III alongside pPOTv6 for subsequent ligation. The gel used to confirm their size and for their following gel extraction and subsequent ligation together is shown in Figure 5.4. The REs *Hind*III and *Bg*III were validated for their use in digests as the sequencing data was used to confirm that there were no additional cut sites induced by the mutagenesis of ZC3H11; only a single site for each enzyme used to flank the mutant gene.

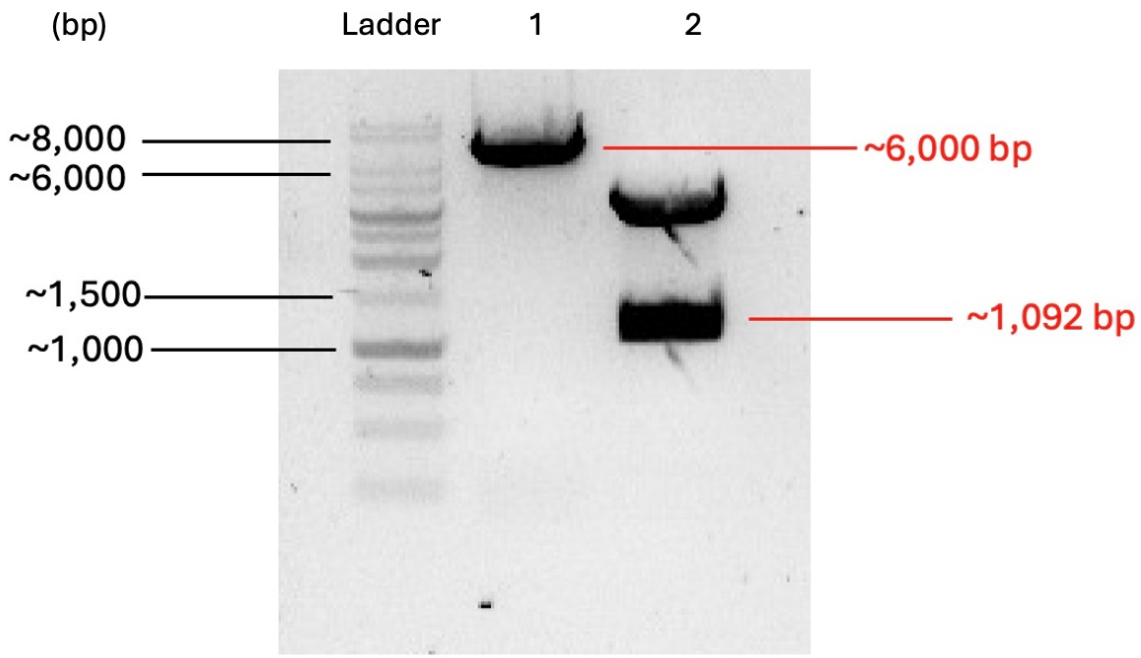

Figure 5.4: Gel electrophoresis gel showing the digest of HNPY mutant ZC3H11-pGEM miniprep 1 and plasmid pPOTv6. The digest used *Hind*III and *Bgl*II, the sites are schematically shown in Figure 5.1. Lane 1 contained pPOTv6 and lane 2 contained SDM-mutated ZC3H11-pGEM. Size of ladder bands are shown in base pairs (bp) and, in red, sizes indicate the bands to be gel extracted. Double digests were only completed and compared to the expected sizes based off the location of RE cut sites, further validation could use uncut plasmid and a single digest for each plasmid.

In Figure 5.4, lane 1 containing the digest of pPOTv6 showed a band of approximately 6,500 bp and a faint band around the lowest band of the ladder at 250 bp. Lane 2, containing the digest of mutant ZC3H11, showed two bands, the lower band being observed between 1,500 and 1,000 bp comparative to the ladder. These indicated locations correspond roughly with the outlined expected sizes of 6,000 bp (pPOTv6) and 1,092 bp (ZC3H11). After extraction of the bands comparable to these sizes, the digested products were ligated together, the resultant plasmid was transformed into *E. coli,* miniprepped and sequenced to confirm the presence of correctly mutated ZC3H11 (data not shown).

To generate amplicons for the transfection of *T. brucei*, PCR reactions were completed to amplify sgRNAs and for the amplification of a segment of DNA containing the

blasticidin resistance cassette and mutated ZC3H11 ORF from pPOTv6-ZC3H11(HNAY). The success of these PCR reactions was determined via gel electrophoresis (Figure 5.5).

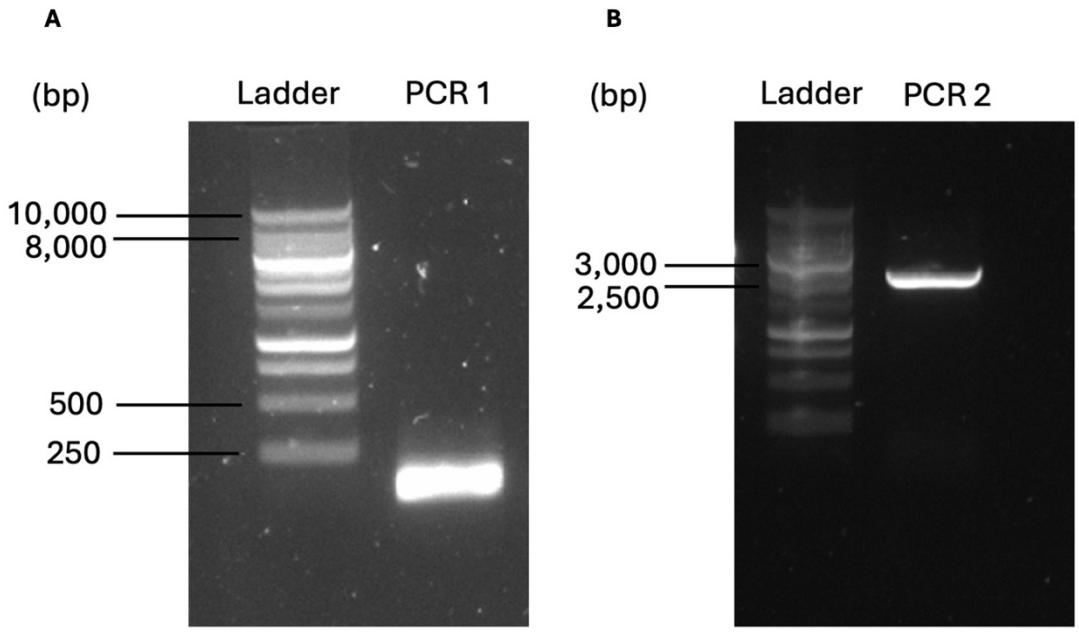

Figure 5.5: Gel electrophoresis results showing the results of PCR reactions prior to ethanol precipitation and transfection. PCR A is for the amplification of sgRNAs, and PCR B is for the amplification of the resistance cassette and ZC3H11 ORFs from pPOTv6-ZC3H11(HNAY).

The gel in Figure 5.5A shows a solid single band of less than 250 bp. In Figure 5.5B the PCR produced a single strong band between 2,500 and 3,000 bp in size. Following transfection of the ethanol precipitated DNA using a DN100 program on a Lonza Nucleofector machine. A total of 8 clones were selected via blasticidin drug selection: initially six clones were selected of which four were unable to grow further in culture upon continued blasticidin selection; a further two clones were then picked which also were unable to grow. gDNA was extracted from the two surviving clones for the amplification of the ZC3H11 gene via PCR (Figure 5.6). This produced bands at 1.1 kb, comparable to the size of ZC3H11, and therefore these were subsequently extracted and sequenced to confirm the presence of the mutated HNAY motif (Table 5.2).

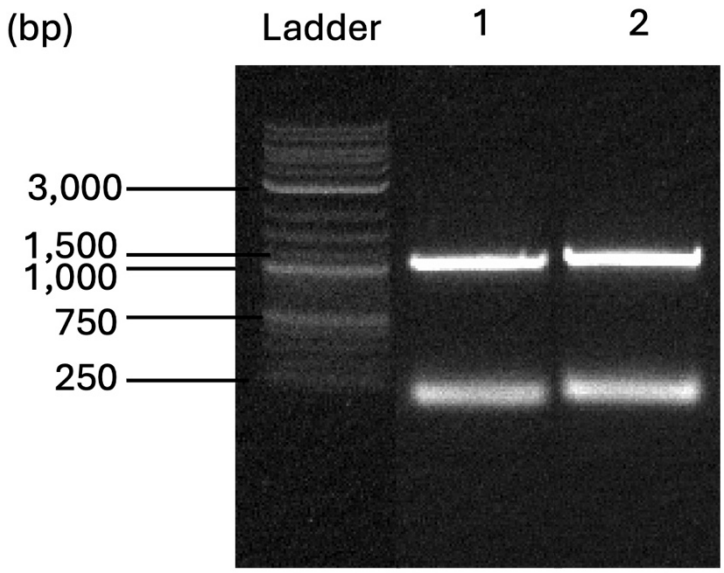

Figure 5.6: Gel electrophoresis result of the PCR amplified ZC3H11 from gDNA extracted from the transfected *T. brucei* clones. Lanes were loaded with 1Kb Promega ladder, followed by samples: (1) ZC3H11 PCR product from clone 1 gDNA and (2) ZC3H11 PCR product from clone 6. Size of bands are indicated in number of base pairs (bp).

Table 5.2: Sequencing results from the PCR amplified ZC3H11 from gDNA extracted from viable *T. brucei* cells post-transfection to confirm the presence of the HNAY mutation in ZC3H11. A custom primer was used, the sequence of which is outlined. The region of interest here is the genetic region around the ZC3H11 HNPY motif. The underlined sequence here indicates the coding sequence of the motif with the mutant codon highlighted in bold (not highlighted to represent its absence). Sequencing shown 5' to 3'.

Clone number	**Sequencing result of the region of interest using TGGTTGCTGCTGCTGCTG**
1	TGGCCGTGTCCGACATAATCCCTACTGCCA
6	TGGCCGTGTCCGACATAATCCCTACTGCCA

The sequencing data in Table 5.2 shows an absence of a mutated HNPY motif within ZC3H11 transfected into the 2T1-based *T. brucei,* with the endogenous CCC codon present instead of the desired GCC mutant sequence. The absence of the mutation is also illustrated in the chromatogram traces: when a heterozygous mutation is confirmed by Sanger sequencing from gDNA, two equal half-size peaks at the mutated genetic location would be present, due to there being one endogenous allele and one mutant allele present in these cells. Instead here, we see a full-size C (WT) base peak in the first position within the codon that should have been mutated (Figure 5.7).

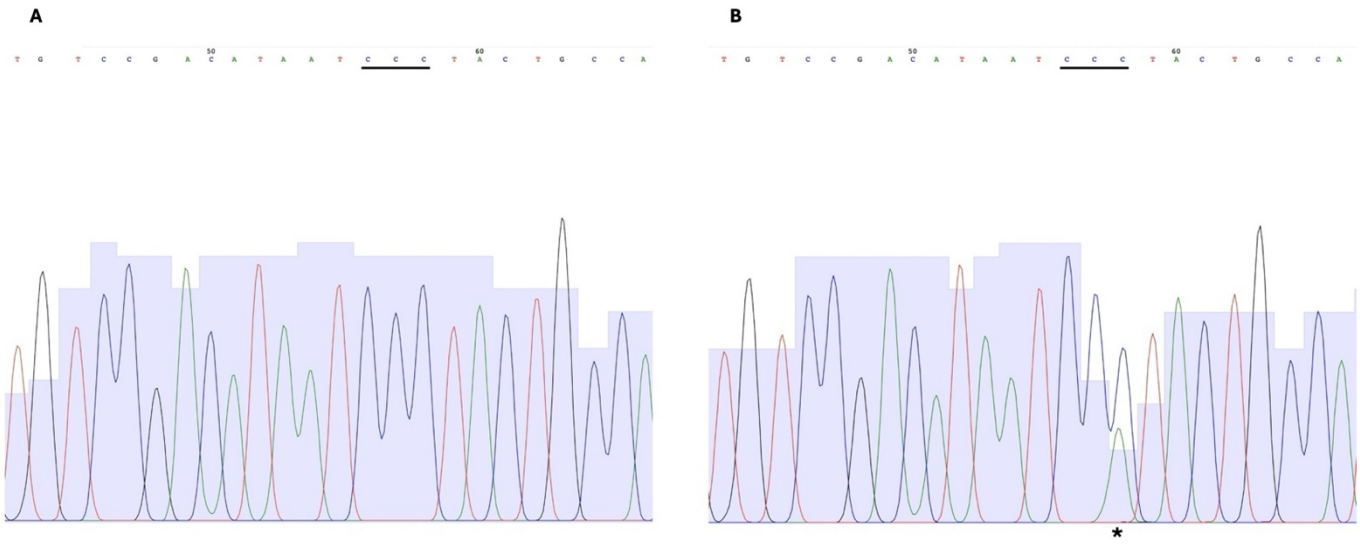

Figure 5.7: Chromatogram produced from sequencing the region around the HNPY motif to confirm the presence of mutated ZC3H11 within *T. brucei* cells. Panel A corresponds to clone 1 and panel B corresponds to clone 6. Underlined sequence indicates the sequence of the motif targeted by SDM. * Indicates traces of a random (non-SDM introduced) mutation present in a subset of cells within the population.

The only mixture of bases evident within either chromatogram is in clone 6, containing both the CCC codon for proline within the HNPY motif, and a less abundant CCA codon. The CCA codon is a redundant change due to it also encoding for proline and therefore, is not a phenotypic mutant. As a result, gDNA analysis of the two surviving transfected *T. brucei* clones confirmed that only ZC3H11 containing the WT HNPY motif was present. Whether the ZC3H11 had been TY1-tagged and if the Ty tag interfered with the endogenous ZC3H11 was not checked as these clones were not to be used in following analysis due to lacking the SDM induced mutation.

5.2 Investigating HS-responsive change in protein expression of ZC3H11 in *T. brucei*

Minia and Clayton (2016) report that upon HS ZC3H11 is stabilised and its expression increases at the protein level by at least 10-fold; this was observed by western blotting (WB). As a result, this study observed the repeatability of this finding by collection of *T. brucei* 3Ty-ZC3H11 2T1 cells without HS treatment, after 1 hour at 41 °C and cells with the addition of a proteosome inhibitor (MG132) for 1 hour at 37 °C for following WB analysis (Figure 5.8).

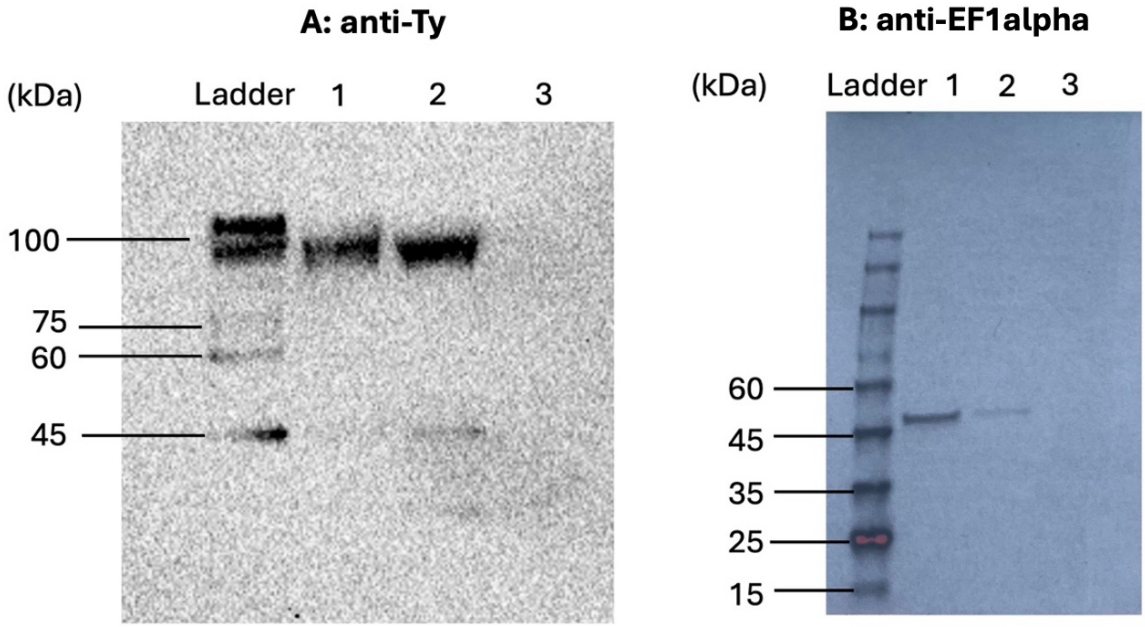

Figure 5.8: Western blotting results of Ty-tagged ZC3H11 stained with anti-Ty antibody. Panel A (anti-Ty) shows the fluorescence detected used for ZC3H11 visualisation and panel B (anti-EF1alpha) is the loading control highlighting the abundance of cells loaded within each lane of the gel. The lanes were loaded as cell samples of (1) no HS, (2) 1 h at 41 °C and (3) the addition of MG132 proteosome inhibitor with 1 h at 37 °C.

The expected size of ZC3H11 was reported by Minia and Clayton (2016) to be 40 kDa and EF1alpha as 43 kDa by Alves, Oliveira and Goldenberg (2015). The WB in Figure 5.8 showed a consistent band in the no HS and 1 h at 41 °C HS cell samples, less than 100 kDa and a further band at around 45 kDa which is fainter in the non-HS sample. This

band at around 45 kDa is consistent with the reported size for ZC3H11, indicating this band as representing ZC3H11.

However, the cell sample that had MG132 treatment showed no banding in this same blot. The MG132 was used to be a positive control to observe how an increase in ZC3H11 protein abundance is observed in the WB. This is because the MG132 blocks the 26S proteasome (Pajonk et al., 2005); therefore, proteins that are normally polyubiquitinated and degraded accumulate. Thus, preventing the degradation of ZC3H11 and increasing the intensity of the expected ZC3H11 band on the blot, which was unable to be observed.

In the loading control (anti-EF1alpha), the no HS sample showed the strongest band above 45 kDa, which also occurred in the 1 h at 41 °C sample but fainter and in the proteosome inhibitor sample no band was visualised; this indicates inconsistencies in the number of cells loaded across the gel. This band migrating slightly higher than the expected 43 kDa of EF1alpha, but its comparability confirming these bands as representing EF1alpha. An increase in ZC3H11 may be interpreted after HS, as despite a visible decrease in the cell load, there is still an increase that seemingly overcomes the load difference. This is shown in the increased band intensity at around 45 kDa post-HS observed in the anti-Ty staining compared to the no HS sample.

Due to time restrictions, confirmation of whether the potential generated HNAY mutant expressed ZC3H11 in absence of HS and if the same increase to ZC3H11 occurs post-HS was unable to be completed.

5.2.2 Tagging of MKT1 for experimental interrogation via co-immunoprecipitation

To experimentally interrogate the formation of the ZC3H11-MKT1 complex *in situ* and its significance in the HS response, we aimed to generate a tagged version of MKT1 that would allow completion of an immunoprecipitation assay with ZC3H11. This requires epitope tagging of MKT1 as the ‘bait’ to pull down ZC3H11. As a result, this study aimed to produce a Myc-tagged MKT1 cell line, and the workflow to generate a MKT1-G418-pPOTv6-myc plasmid (shown in Appendix 9.2) that could be transfected

into a 3Ty-ZC3H11 in a 2T1 cell line is summarised in Figure 5.9. The G418 resistance sequence was added alongside MKT1 into the cell line to confirm the success of the transfection as a selection factor, as puromycin resistance was pre-existing within the cell line.

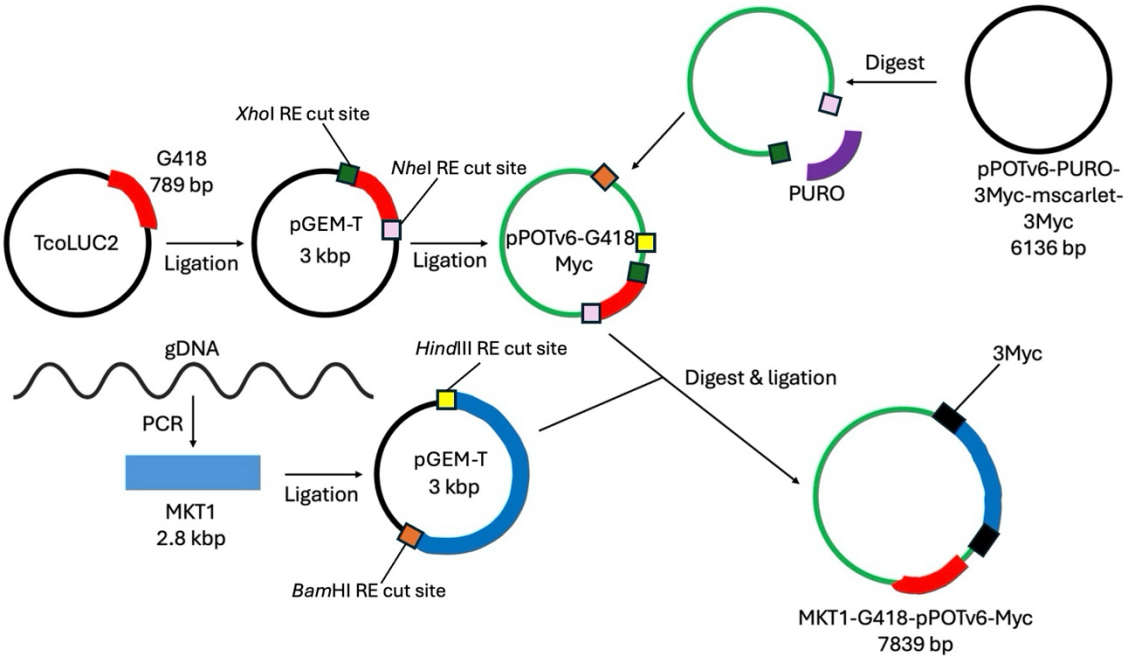

Figure 5.9: Schematic of the aimed workflow to produce a MKT1-G418-pPOTv6-Myc plasmid. The G418 resistance cassette is extracted, following digest using *Xho*I and *Nhe*I (cut sites shown), and ligated into pGEM-T then pPOTv6 plasmid to replace the puromycin resistance cassette. MKT1 was also PCR amplified from gDNA and ligated into p-GEM-T; finally digested using *Hind*III and *Bam*HI (cut sites shown) and ligated into a pPOTv6-G418-Myc to produce a MKT1-G418-pPOTv6-Myc plasmid.

To amplify MKT1 from gDNA a PCR reaction was performed. Optimisation of the conditions was required to achieve specific successful amplification of MKT1; the process of optimisation is outlined in gel electrophoresis results in Figure 5.10.

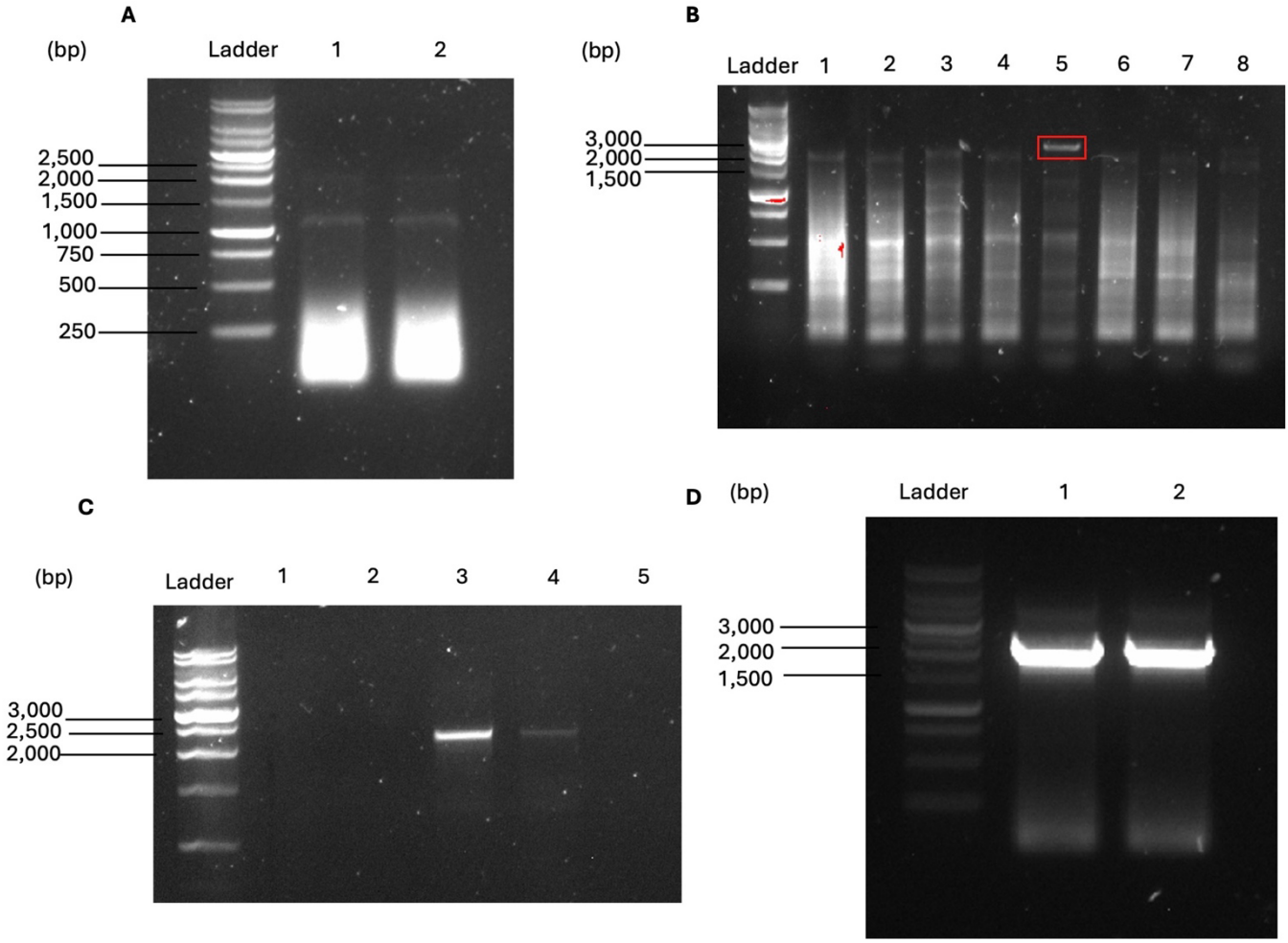

Figure 5.10: Complete optimisation process of MKT1 PCR reactions to achieve amplification of MKT1 with increased yield. A- initial PCR reaction of MKT1 using OneTaq pol and an annealing temperature 48 °C, 25 µl of reaction was run in each well. B- PCR using a temperature gradient of annealing temperatures where the annealing temperature of the lanes were: 1- 65 °C, 2- 64.3 °C, 3- 63 °C, 4- 61.1 °C 5- 58.8 °C, 6- 56.9 °C, 7- 55.7 °C and 8- 55 °C. C- PCRs of MKT1 ran with an annealing temperature at 58.8 °C with different templates of comparable quality where: 1- original SM 427, 2- mNG gDNA, 3- gDNA extracted from a 427 J1339 cell line with the replacement of one copy of PABP2 with a PABP2-S212A mutation and 4- purified extract of gel B lane 5. D- Final PCR of MKT1 using an annealing temperature of 58.8 °C, optimal gDNA template and superfied II polymerase instead of OneTaq.

As the steps of optimisation for the PCR reaction of MKT1 progressed from Figure 5.10A to 5.10B a stronger band is shown to become more apparent smaller than 3,000 bp in size, near to the size of MKT1 at 2.8 kbp. Figure 5.10A demonstrates that an annealing temperature of 48 °C is insufficient through a smear of non-specific DNA being present in the gel and faint bands. Figure 5.10B used a temperature gradient for

a range of annealing temperatures between 55 °C and 65 °C, showing the temperature that specifically amplified DNA near the size of interest occurred at 55.8 °C, highlighted in red, justifying for following PCR reactions for MKT1 to use this annealing temperature. The following step of optimisation was testing the DNA template used within the reaction, Figure 5.10C showed the strongest band using a template of gDNA extracted from a 427 J1339 cell line with the replacement of one copy of PABP2 with a PABP2-S212A mutation; this was therefore, used in future reactions. Finally, Figure 5.10C used a higher fidelity polymerase (Superfi II polymerase) and combined these optimal conditions to produce a strong single band at around 2,000 bp.

The successful MKT1 amplicons were extracted and ligated into pGEM-T and the success of the ligation was confirmed by a diagnostic digest. The digests of four MKT1-pGEM-T ligation reaction products were run on a gel (Figure 5.11), for subsequent extraction and ligation into the pPOT plasmid.

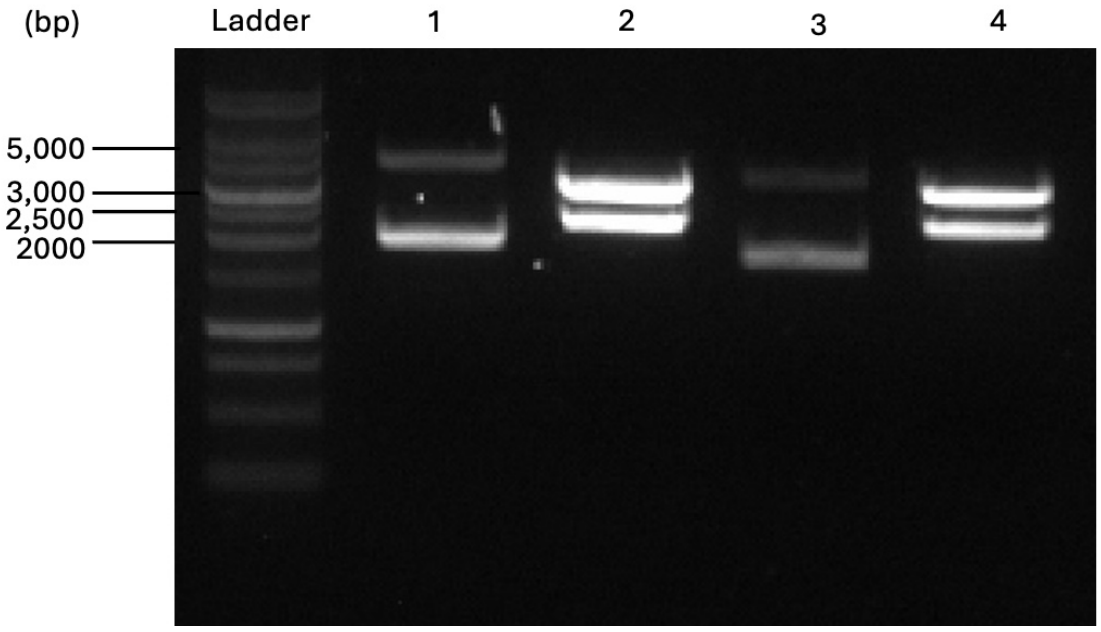

Figure 5.11: Gel electrophoresis of restriction enzyme digests of MKT1-pGEM-T. The digests used *Bam*HI and *Hind*III, their cut sites are schematically shown in Figure 5.9. The lanes were loaded as 1kb Promega ladder and lanes 1-4 as the MKT1-pGEM-T digest repeats. Double digests were only completed and compared to the expected sizes based off the location of RE cut sites, further validation could use uncut plasmid and a single digest for each plasmid.

The digests of MKT1-pGEM-T ligations 1 and 3 present two bands, a fainter upper band exceeding 3,000 bp and a lower stronger band at around 2,000 bp; neither align with the expected size of MKT1 of 2.8 kbp, therefore these ligations could instead be of the vector with truncated MKT1 (~ 2 kbp). Whilst ligation reactions 2 and 4 present two strong bands, the upper band exceeding 3,000 bp and the lower band is observed between 2,500 and 3,000 bp. These lower bands in ligations 2 and 4 align with the expected size of 2.8 kbp of MKT1 and were extracted.

Amplification of the G418 resistance gene was also required to be completed using a PCR reaction with confirmation via gel electrophoresis (Figure 5.12).

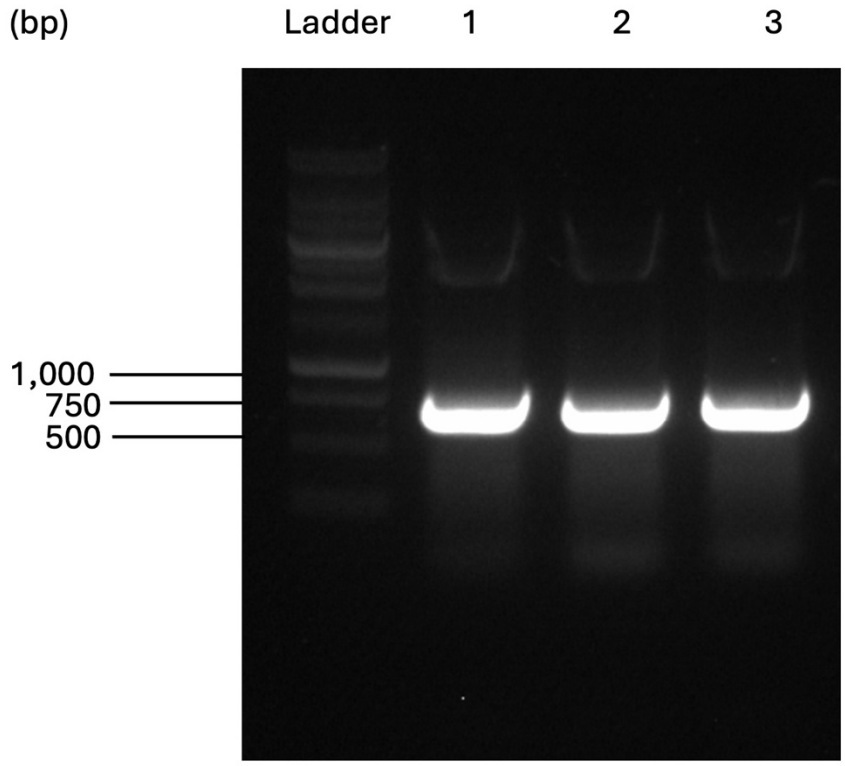

Figure 5.12: Gel electrophoresis result of G418 resistance gene PCR amplification. The PCR amplification used OneTaq polymerase, an annealing temperature of 46 °C and an extension time of 1.5 minutes. The reaction products were run alongside a 1kb Promega ladder.

Following amplification of the G418 resistance cassette, a DNA band is observed between 500 and 750 bp when run via gel electrophoresis (Figure 5.12). This is comparable to the expected size of the G418 resistance sequence of 789 bp. The G418 resistance sequence amplicons were extracted and ligated into pGEM-T with a

diagnostic digest using the restriction enzymes *Xho*I and *Nhe*I. The digests of both G418-pGEM-T and pPOTv6-Myc were run on a gel (Figure 5.13), for subsequent extraction and ligation to produce Myc-tagged G418-pPOTv6.

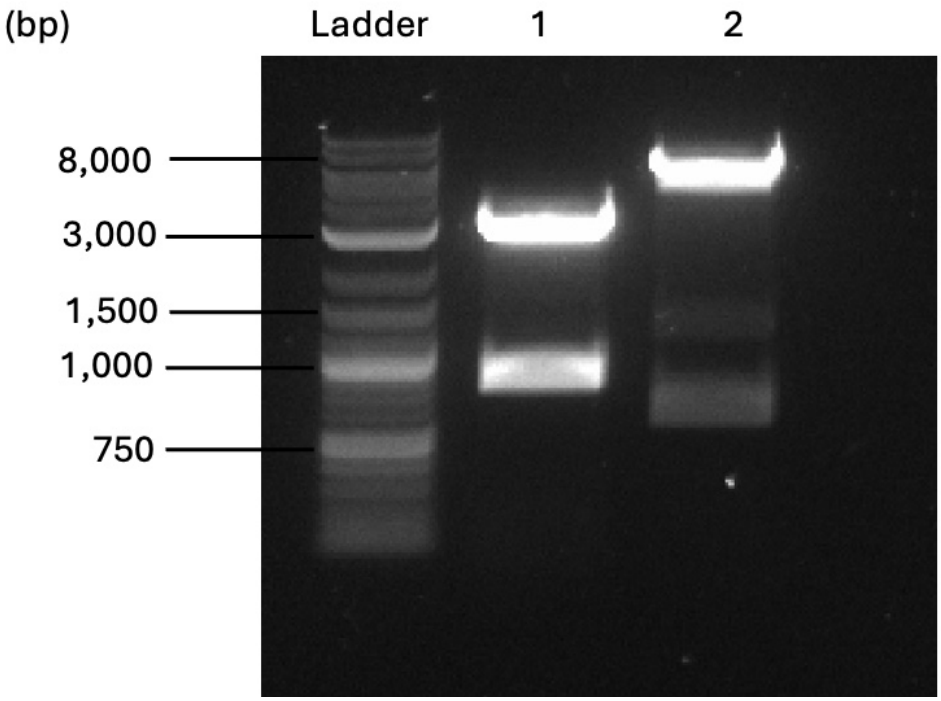

Figure 5.13: Gel electrophoresis result of digested G418-pGEM-T and rSAP treated digest of pPOTv6-Myc. A Promega 1kb ladder was run alongside the digested G418-pGEM-T (20 μl) (lane 1) and digested pPOTv6-Myc plasmid (20 μl) (lane 2). *Xho*I and *Nhe*I were the restriction enzymes used for both digests; their cut sites are schematically shown in Figure 5.9. Double digests were only completed and compared to the expected sizes based off the location of RE cut sites, further validation could use uncut plasmid and a single digest for each plasmid.

The digest of G418-pGEM-T shows a strong upper band exceeding 3,000 bp and a lighter lower band between 750 and 1,000 bp, thought to be the G418 resistance gene at around 789 bp. Whilst the digest of pPOTv6 run on a gel presents a strong upper band between 3,000 and 8,000 bp, assumed as the backbone, and a faint lower band below 1,000 bp. The bands comparable in size to the G418 resistance sequence and the pPOTv6-Myc backbone were extracted and ligated together. The success of the ligation was assessed by a further restriction enzyme digest and gel electrophoresis (Figure 5.14).

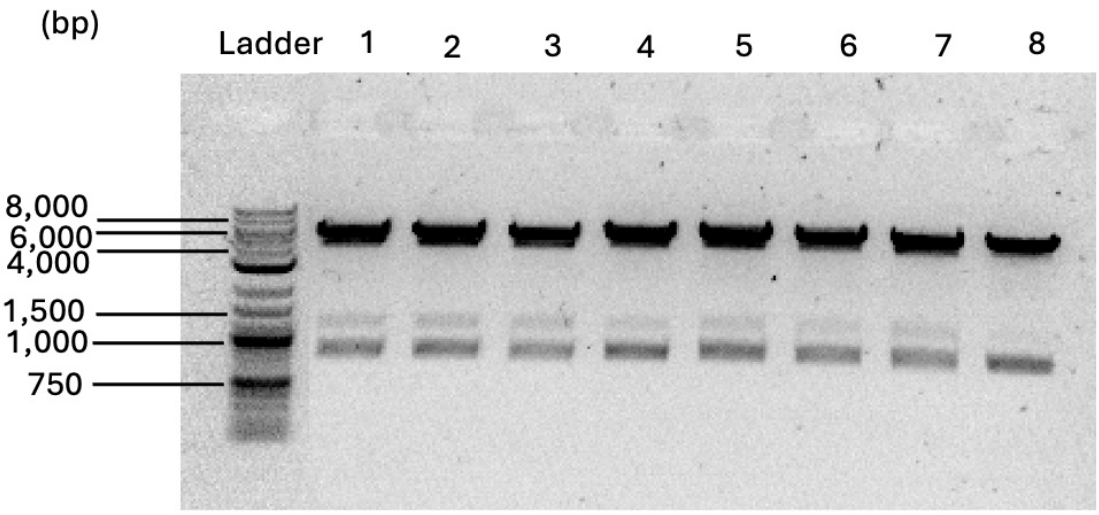

Figure 5.14: Gel electrophoresis result of digested G418-pPOT. A Promega 1kb ladder was run alongside the G418-pPOT digests using *Xho*I and *Nhe*I (12 µl/lane). Lanes 1-4 were loaded as digest repeats from a single ligation reaction and lanes 5-8 were loaded as digest repeats from a second ligation reaction. The RE cut sites are schematically represented in Figure 5.9. Double digests were only completed and compared to the expected sizes based off the location of RE cut sites, further validation could use uncut plasmid and a single digest for each plasmid.

The digests of G418-pPOT gel electrophoresis result presented three consistent bands, the strong upper band appears between 6 and 8 kbp as a band for the pPOT backbone, a faint band is observed between 1,000 and 1,500 bp and a final band between 750 and 1,000 bp. To confirm the identity of this lowest band as being the G418 resistance sequence, sequencing results are required.

5.3 Summary- Investigating the ZC3H11-MKT1 complex in the *T. brucei* HS response

The involvement of the ZC3H11-MKT1 complex, suggested to be an 'integration node' in the HS response by Ooi, Benz and Urbaniak (2020) was aimed to be further characterised.

The desired HNAY mutation of the HNPY motif in ZC3H11 was initially observed in sequencing data in 4 of 5 clones post-SDM. However, following transfection drug resistance was only observed alongside the WT HNPY interaction motif sequence, however PCR and following sequencing data would be required to confirm the

presence of the drug resistance cassette. This potentially indicates that the mutation is not tolerated or that the transfection was unsuccessful. The transfection may have been unsuccessful potentially due to poor health of the cells or quality of the nucleic acids. An increase in WT ZC3H11-TY expression after HS in *T. brucei* was observed via western blotting.

Whilst for the tagging of MKT1, amplification of MKT1 via optimised PCR enabled successful ligation into pGEM-T. The G418 resistance cassette was PCR amplified and ligated into pGEM-T. A digest of pPOTv6-Myc was also completed enabling the ligation of the G418 resistance sequence into pPOTv6, providing the plasmid into which MKT1 could be sub-cloned. Due to the challenges of cloning MKT1 and the G418 resistance cassette, sequencing data for each are required. The completed work contributing to the generation of the plasmids is summarised in Figure 5.15.

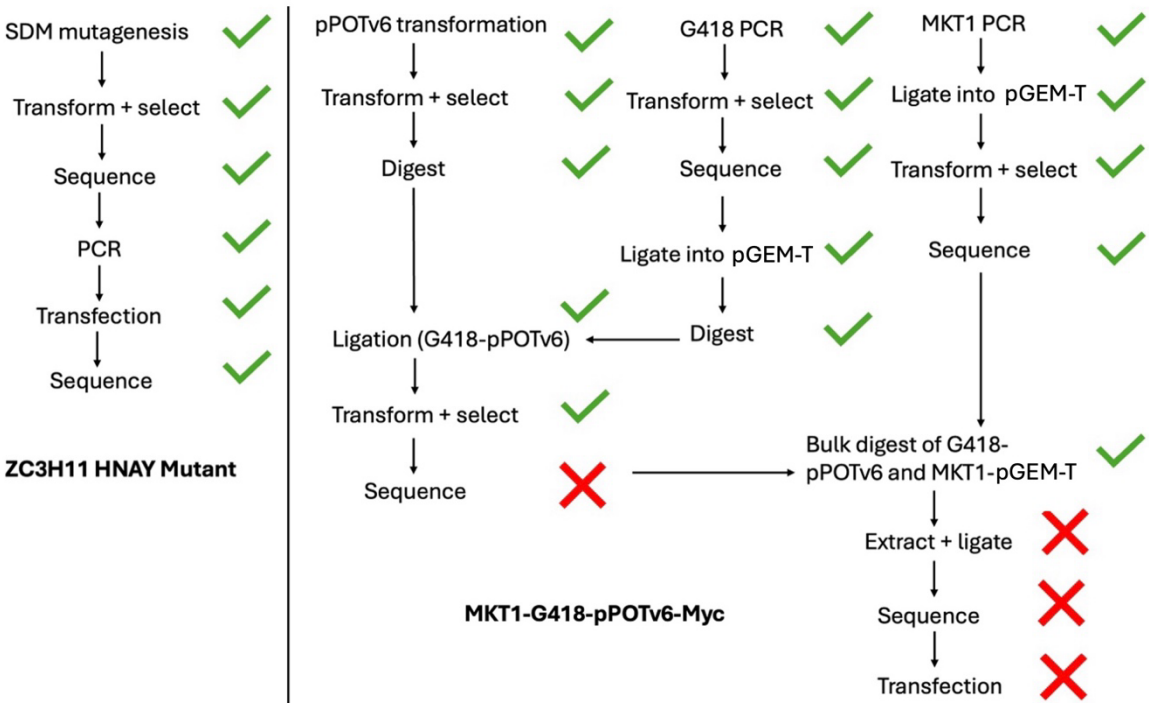

Figure 5.15: Flow chart of work required to produce a ZC3H11 HNAY mutant cell line and MKT1-G418-pPOTv6 cell line. Work completed within this study is indicated by a green tick and incomplete work due to time restrictions is denoted by a red cross.

6. Temporal profiling of global translational arrest and polysome dissolution.

6.1 Validation of the gradient fractionation methodology

Polysome gradient fractionation is completed using sucrose gradients and cell components are sorted accordingly due to their sedimentation velocity within this gradient. Therefore, polysomes are observed as being within the more sucrose-dense fractions lower in the gradient than the smaller monosomes found higher up within the gradient. mRNA found within the more sucrose-dense fractions alongside polysomes indicate that it is actively translated (Chassé et al., 2017). This study completed this method for the first time at Lancaster University; therefore, the equipment and conditions being used required validation. As a result, variables of sucrose gradient preparation were tested.

6.1.1 Gradient mixing device

60% sucrose solution stained with bromophenol blue was layered within an unstained 10% sucrose solution to produce 'unmixed' samples. 'Unmixed' samples were placed in a Biocomp Gradient Master preset for a 15-60% sucrose gradient, producing 'mixed' samples. Finally, 'mixed' samples were placed in an ultracentrifuge at top speed for 1 hour to produce 'spun' samples; this sample production process is summarised in Figure 6.1.

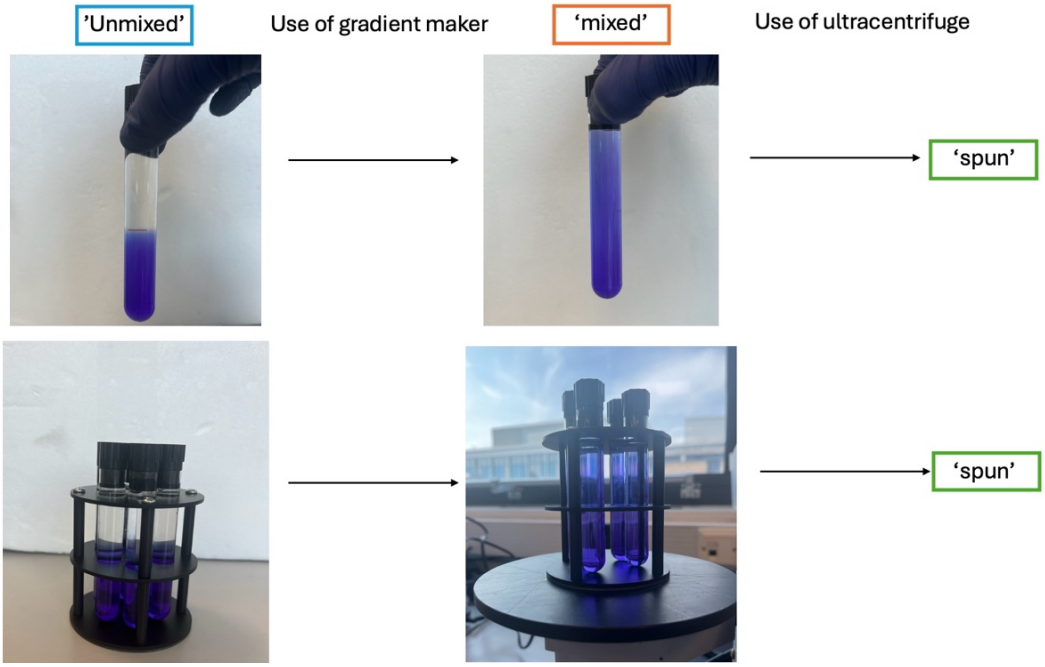

Figure 6.1: A summary of the sample preparation for the three steps of gradient making that were validated using 10% and 60% sucrose solutions with bromophenol blue. Starting gradient solutions were layered and undisturbed ('unmixed'), following use of a Biocomp Gradient maker ('mixed') and an ultracentrifuge at 207,000 ×g for 1 hour ('spun').

'Unmixed', 'mixed' and 'spun' samples were individually run with a Biocomp piston gradient fractionator. Their absorbance at 254 nm was recorded on Biocomp TRIAX software as the piston progressed down the sample tube (Figure 6.2), enabling the collection of fractions starting at the top of the tube (Figure 6.3). The bromophenol blue presence increases the absorbance of a fraction and therefore, upon its fractionation the absorbance is expected to increase. In the 'unmixed' sample where there is a sudden shift in the concentration of bromophenol blue it is expected to result in a sudden increase in the absorbance, whilst in the 'mixed' and 'spun' samples the bromophenol blue occurs across a linear gradient, as a result the absorbance is expected to increase more gradually.

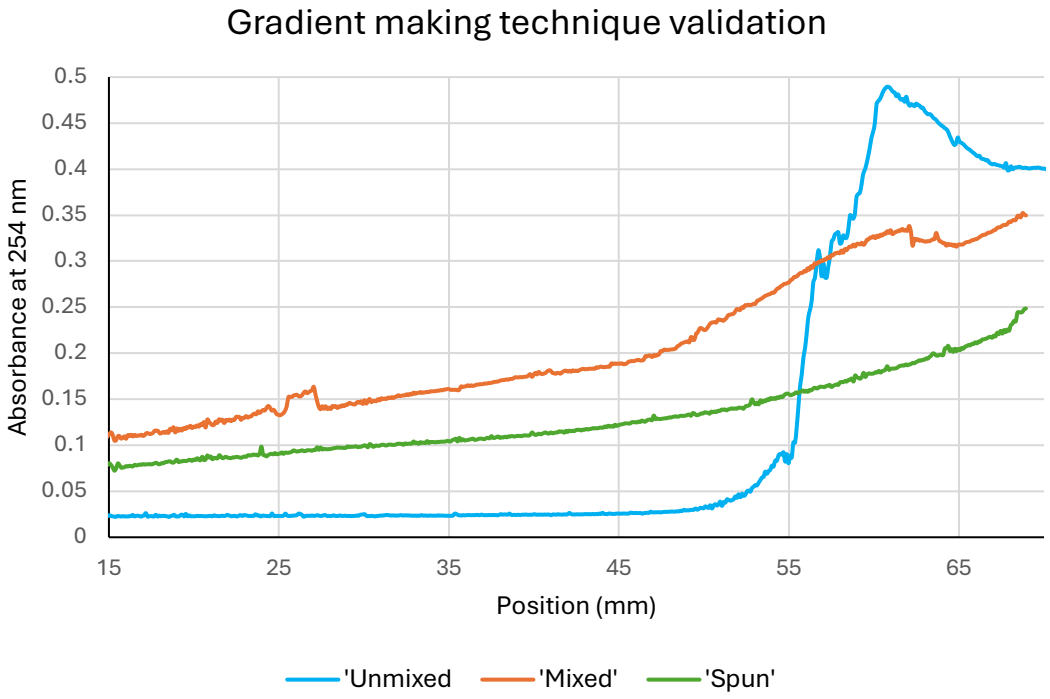

Figure 6.2: Absorbance at 254 nm across the 'unmixed', 'mixed' and 'spun' gradient making step sample tubes. All samples were chilled prior to fractionation using a Biocomp piston gradient fractionator and its associated TRIAX software; the following read outs of the three samples were plotted on a single graph using Excel software. For improved visualisation of all conditions on a single set of axes the 'Unmixed' was scaled by a factor of 0.8.

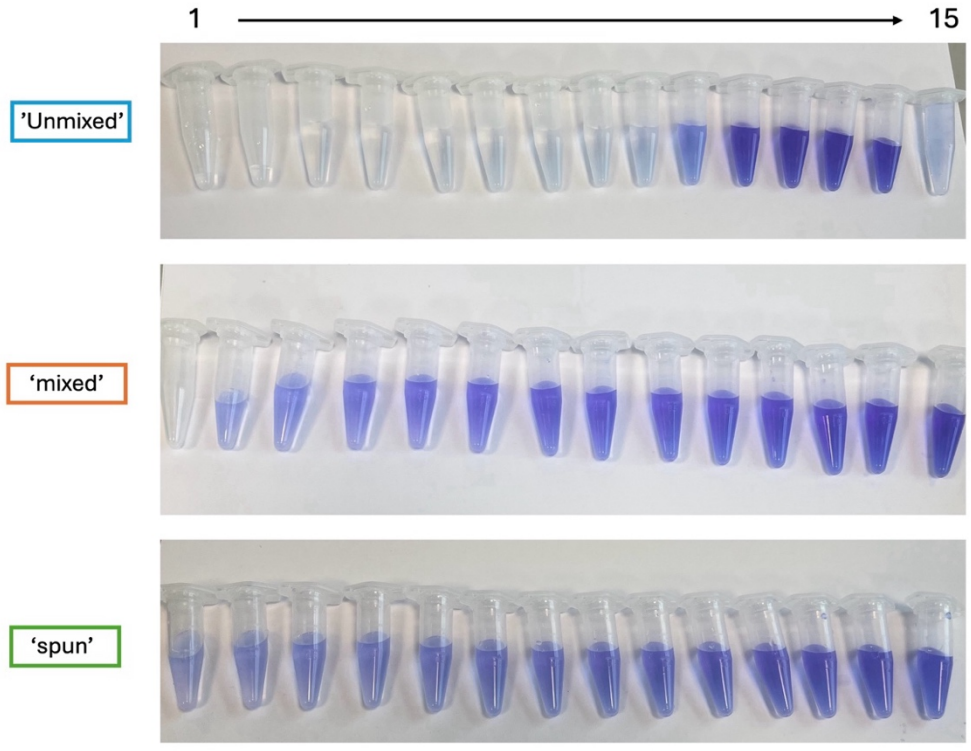

Figure 6.3: Fractions collected within a fraction collector of the fractionated 'unmixed', 'mixed' and spun samples of gradient preparation steps. Shown are the 15 tubes of fractions extracted from each 13.2 ml sample tube using a Biocomp piston gradient fractionator. This figure highlights the colour change across a gradient making condition from the 100 mg/ml bromophenol blue within 60% sucrose solution added to 10% sucrose solution.

The traces of absorbance of the steps of gradient making match the expected results, as the 'unmixed' sample shows a sudden increase in absorbance at a position of around 50 mm. Furthermore, both the 'mixed' and 'spun' samples showed a gradual increase in absorbance, indicating the production of gradients. The 'spun' sample shows a cleaner gradient with less disturbances to the constant increase in absorbance, which are observed in the 'mixed' sample at positions around 25mm and 60 mm as peaks within the overall trend of gradual increased absorbance. This is confirmed in the visual observation of the fractions collected (Figure 6.3), the 'unmixed' sample showing a near sudden presence of bromophenol blue; a gradient of dye being visible in the 'mixed' sample and a cleaner gradient in the 'spun' sample. As a result, this confirmed that using all three steps used in the 'spun' samples would most efficiently produce gradients for fractionation in future experiments.

6.2 Determining the transition from polysome to monosomes within the heat shock response.

Validation of the technique of gradient making confirmed the method of layering the more dense gradient solution within the less dense followed by the use of a Biocomp gradient master and an ultracentrifuge prior to fractionation. For the polysome analysis of cell samples, cell lysates were layered upon the gradients before being placed within an ultracentrifuge to effectively separate cell components according to their size across the gradient.

6.2.1 The effect of HS upon polysome profiling in procyclic form *T. brucei*

Initial polysome profiling was completed upon PCF *T. brucei,* using cell lysates of a cell population before HS and after 1 hour at 41 °C, to enable the direct comparison with

the published data by Kramer et al (2008) and further confirm the validity of the conditions being used. ~2.52 $\times$ 10^8 total cells were collected in both the non-HS and HS samples with a maintained 100 μg/ml cycloheximide concentration throughout lysate preparation. These lysates were placed upon 10-50% sucrose gradients in gradient buffer maintained at 4° C prior to ultracentrifugation and fractionation using a Biocomp piston fractionator. Upon fractionation the absorbance at 254 nm was recorded on Biocomp TRIAX software as the piston progressed down the sample tube (Figure 6.4).

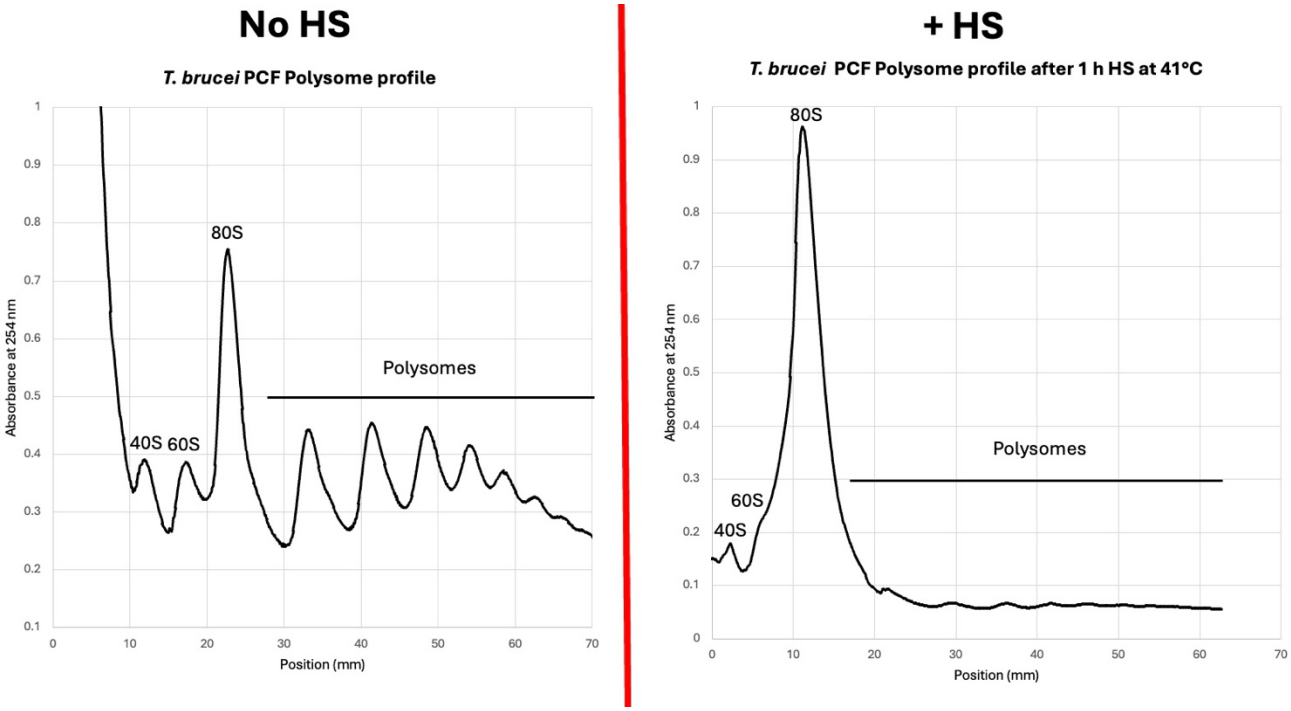

Figure 6.4: Polysome profile of PCF *T. brucei* pre-HS kept at 27 °C (no HS) and after 1 h at 41 °C (+ HS). Fractionation of 10-50% sucrose gradients in gradient buffer with PCF *T. brucei* used a Biocomp piston gradient fractionator and its associated TRIAX software; the produced absorbance values were plotted using Excel software. The HS PCF profile was scaled by a factor of 0.28 to allow visualisation of the top of the 80S peak; +HS values were shifted by 10 mm on the x-axis to present both profiles on the same scale without artefacts or signal noise. The ribosomal subunit (40S, 60S and 80S) and polysome peaks were assigned accordingly using the published data by Kramer et al (2008).

The profiles are interpreted by the peaks present at the lower positions correspond to the smallest components (furthest to the left on the profile) due to being smaller in size and being found higher up within the gradient tube in less sucrose dense fractions.

Therefore, as the position increases (moving right on the profile), the sucrose density of the fractions increases and therefore, the peaks correspond to larger components within these fractions. As a result, the first defined peak is identified as being the 40S ribosomal subunit as the smallest component, followed by 60S and 80S. The increase in subunit size is shown within eukaryotes as the 40S consists of an 18S rRNA and 33 proteins, the 60S contains 5S, 5.8S and 28S rRNA and 47 proteins; the 80S is the largest monosome containing both the 40S and 60S subunits (Weisser and Ban, 2019).

The peaks following the 80S peak are identified as the polysomes, each peak indicating an increase in the number of ribosomes and mRNA associated with the polysome than the previous peak (Kopeina et al., 2008). Therefore, due to increased size through additional ribosomes separate peaks are produced, being found in a more sucrose dense fraction and at a further distance down the gradient tube. For example, according to the ribosome number, peaks are found in the order of disome, trisome, tetrasome from the left of the profile (Kopeina et al., 2008).

Following HS at 41 °C for 1 hour of PCF *T. brucei* cells a collapse in polysome peaks is observed, alongside an increase in the ribosomal subunits, most notably the 80S subunit. The non-HS cells show a ribosomal distribution across polysome fractions and after HS a shift is seen to occur towards the lighter fractions of the profile. These findings corroborate with those by Kramer et al (2008), providing further evidence for the occurrence of the collapse in polysomes as a part of the HS response in PCF *T. brucei.*

6.2.2 The effect of HS upon polysome profiling in bloodstream form *T. brucei*

Following the agreement of findings using the same technique as the published work by Kramer et al (2008), the methodology of polysome gradient fractionation was validated for further use. Therefore, this same experiment was completed using 2T1 BSF *T. brucei* cells to observe whether a comparable effect occurs to the polysome profile after HS and to investigate if a change occurs within the life cycle. Cell lysates were prepared, each with a total of ~1.75×10^8 cells, one sample was kept at 37 °C and

one was heat shocked at 41 °C for 1 hour. The lysates were placed upon 10-50% gradients for following polysome gradient fractionation analysis (Figure 6.5).

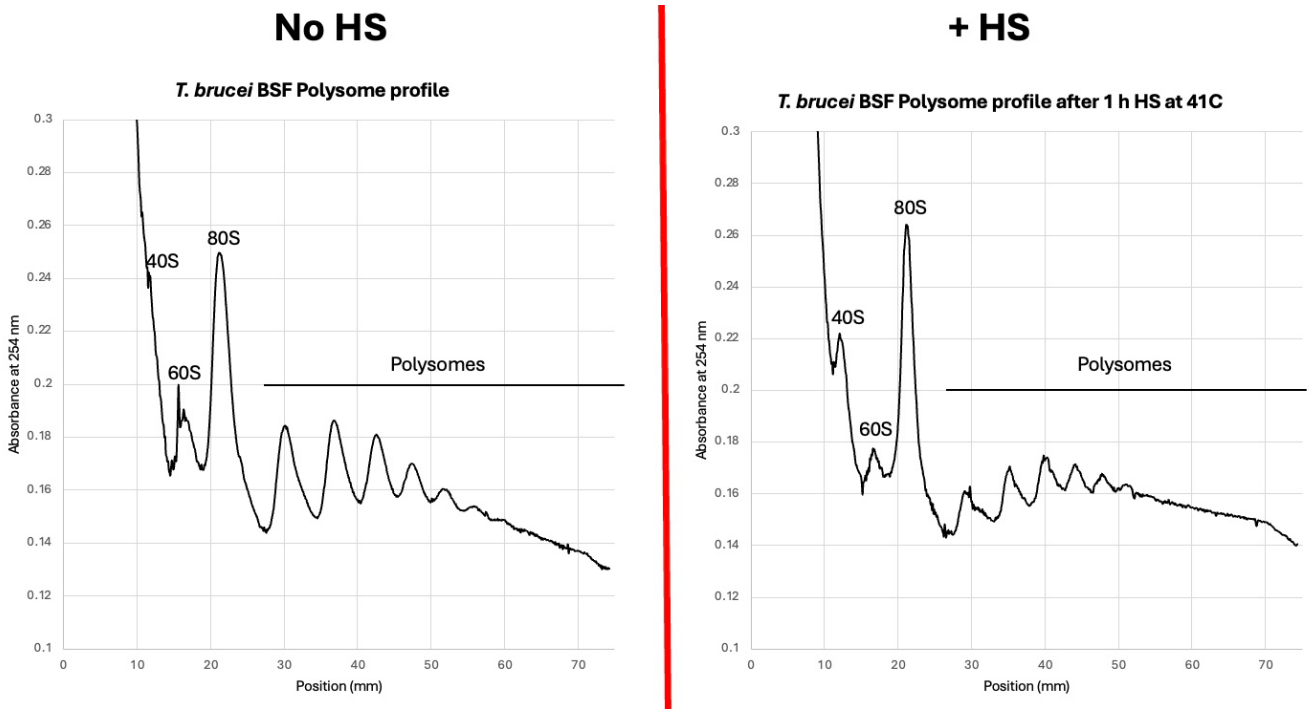

Figure 6.5: Polysome profile of BSF *T. brucei* pre-HS kept at 37 °C (no HS) and after 1 h at 41 °C (+ HS). Fractionation of 10-50% sucrose gradients in gradient buffer with BSF *T. brucei* used a Biocomp piston gradient fractionator and its associated TRIAX software; the produced absorbance values were plotted using Excel software. The ribosomal subunit (40S, 60S and 80S) and polysome peaks were assigned accordingly using the published data of polysome profiles in BSF *T. brucei* by Smith et al (2009).

After 1 hour at 41 °C BSF *T. brucei* shows a decrease in its polysome fractions and a shift in distribution into the lighter 80S fraction compared to the non-HS cells. The polysome peaks in the heat shocked cells are observed as being less defined and peaking at a decreased absorbance, none of which exceeding an absorbance value of 0.18. However, post-HS the 40S and 60S peaks each appear to decrease each by around 0.02 after HS.

6.2.3 The effect of HS upon polysome profiling in *T. congolense*

The role of the collapse of polysomes within the HS of *T. congolense* was also investigated using polysome gradient fractionation. Cell lysate samples were each prepared using a total of 2.52×10^8 cells, one cell population was maintained at 34 °C and the other was placed at 41 °C for 1 hour. The lysates in a 10-50% sucrose gradient were fractionated to produce polysome profiles (Figure 6.6).

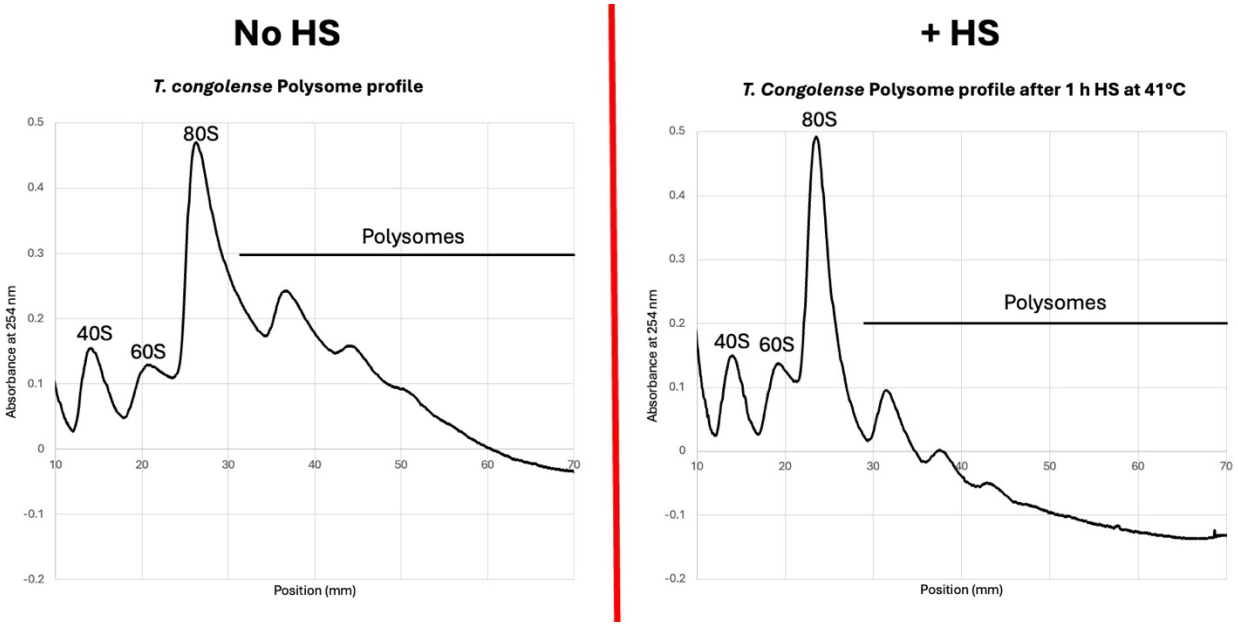

Figure 6.6: Polysome profile of *T. congolense* pre-HS kept at 34 °C (no HS) and after 1 h at 41 °C (+ HS). Fractionation of 10-50% sucrose gradients in gradient buffer with *T. congolense* used a Biocomp piston gradient fractionator and its associated TRIAX software; the produced absorbance values were plotted using Excel software. The non-HS *T. congolense* profile was scaled by a factor of 0.5 to allow visualisation of the top of the 80S peak. The ribosomal subunit (40S, 60S and 80S) and polysome peaks were assigned accordingly using the published data by Kramer et al (2008) and Gandin et al (2014).

Polysome profile analysis of *T. congolense* after HS showed a decrease in the peak absorbance observed across the ribosomal subunit and polysome peaks compared to that of non-HS cells. As, there was no published polysome profile for *T. congolense*, the peaks were assigned using assumed similarity with *T. brucei* (Kramer et al., 2008) and further data within mammalian cells (Gandin et al., 2014), presenting conserved peaks across different species that were able to be defined in the profile of *T. congolense*.

6.3 Summary- Polysomes collapse or decrease in abundance in African trypanosomes in the HS response

HS at 41 °C for 1 hour of PCF *T. brucei* induced a decrease in polysomes, whilst an increase occurred in the 40S, 60S and 80S ribosomal subunits. The same HS in BSF *T. brucei* caused the polysome peaks to reduce in their definition and their peak absorbance value to be decreased post-HS. Furthermore, in BSF *T. brucei* the ribosomal subunit 80S peak increased, whilst the 40S and 60S subunit peaks decreased. Finally, polysome profiling in *T. congolense* after HS found that all polysome and ribosomal peaks decreased compared to the non-HS sample. Overall, this presents that there may be differences in thermotolerance across the cell cycle of *T. brucei*, due to the polysome collapse in PCF cells appearing more severe than that in BSF. The polysome analysis in *T. congolense* showing a decrease in polysomes post-HS*,* like in *T. brucei* may indicate a level of conservation between the two species' HS responses.

7. Discussion

7.1 Analysis of results

7.2.1 Analysis of the implication of HS upon growth and motility

The extent of HS-induced damage to trypanosomes is shown to be both temperature-dependent and time-dependent, determining the severity of a HS stimulus to cell viability. Outgrowth analysis indicated the effect of 41 °C, 2 h of exposure causing a pronounced growth lag for up to ~70 hours, 1 h causing a shorter lag of ~24 hours and 0.5 h causing a less noticeable lag with decreased longevity. These results indicate a threshold of thermal tolerance to complete the HS response and recover from HS-induced cell damage; exposure beyond this threshold causing irreversible cell damage and death, indicated in the 2 h HS due to the decrease in cell number. However, HS at 41 °C for 1 h is shown to be below the threshold of thermotolerance with reversible damage, highlighted by an absence of a decrease in cell number and instead a lag in growth rate. Therefore, justifying 41 °C for 1 h as HS conditions in following

experiments, to develop understanding on how the cells recover within this short-term reversible lagged growth phase.

These findings align with the data produced by Kramer et al (2008) in PCF *T. brucei,* showing that increasing the time of HS exposure at 41 °C increases the severity of growth lag. However, PCF cells appear to be more thermotolerant as after 2 h the cell growth rate is recovered within 36 hours post-HS. PCF *T. brucei* may have a greater range of thermotolerance required for their survival *in vivo,* as BSF cells experience a more stable temperature environment maintained by the mammalian host completing thermostasis, whilst PCF experience a greater flux of temperatures within the tsetse fly.

Motility analysis was used to test the hypothesis that motility could be used as read-out of cell viability post-HS, reducing the necessity to complete longer time courses to complete outgrowth analyses. The variability in maximum and average speeds of *T. brucei* post-HS 40-42 °C, indicated motility as being a poor measure of predictive survival of cells as well as due to disagreement with the effect outlined within the literature. Droll et al (2013) described in PCF *T. brucei* after 1 h at 41 °C that cell motility was 'strongly reduced'. Furthermore, the work of Ooi, Benz and Urbaniak (2020) found that as HS exposure of BSF *T. brucei* at 41 °C increases the cell motility decreases for up to 4 hours, after which no motile cells are observed. The effect of 41 °C upon *T. congolense* motility was also interrogated also finding an absence of a trend in both maximum and average cell speeds, like in *T. brucei* also indicating an unreliable level of variability, however there is no published data to compare to. Overall, motility may be affected when there is a HS-induced growth defect present due to differences observed compared to the negative control cells, but this analysis was complicated by the influence of uncontrolled environmental temperatures.

7.2.2 HS induces a reversible cell cycle arrest

The published work of Droll et al (2013) found that 24 hours after a HS there was no difference in the distribution of cells across the phases of the cell cycle compared to pre-HS. But a halt within the cell cycle was inferred due to the halt in the expression of

proteins required for cell growth and replication highlighted by Kramer et al (2008). Therefore, earlier time points following the HS were completed in the unpublished work by Aelmans (2022) and Taylor (2024) to investigate the occurrence of a cell cycle arrest after a HS. This study corroborated with the previous data in BSF *T. brucei* in presenting a reversible cell cycle arrest, finding a temporary increase of cells within the G2M phase of the cell cycle and these cells arrested within G2M indicate a heat-induced disruption to cytokinesis. This G2M arrest is interesting as BSF *T. brucei* lack a G2M cell cycle checkpoint meaning nucleus and kinetoplast replication can occur without cytokinesis (Hammarton, 2007); this indicates that the arrest observed post-HS is not governed by an impact to a mitotic process.

The previous studies within the Urbaniak lab found that post-HS an equivalent cell cycle arrest does not occur in PCF *T. brucei,* instead Taylor (2024) observed an increase in <G1 or 'zoid' cells lacking nuclear DNA. As a result, the reversible arrest observed uniquely in BSF may be speculated to have a BSF-specific role, for example to support slender to stumpy morphological differentiation. Within the mammalian host, peaks in parasitaemia coincide with peaks of fever, the peak in parasitaemia is also when this differentiation occurs and therefore may be associated with HS (Ross and Thomson, 1910; Silvester, Ivens and Matthews, 2018). Therefore, like in *Leishmania* differentiation (Zinoviev et al., 2011), HS may be used to induce a cell cycle arrest to support the stumpy to slender transition in *T. brucei.*

A further notable difference in PCF to BSF cells is the expression of VSGs via the bloodstream expression sites; therefore, VSGs may influence the cell cycle post-HS in BSF *T. brucei.* This theory is supported by Sheader et al (2005), who showed in the RNAi knockdown of VSG a cell cycle arrest comparable to that observed post-HS with G2M enrichment occurs. But the reversibility of the cell cycle arrest was unable to be compared to that following HS, as the phenotype induced by RNAi is irreversible. This could indicate that HS causes damage and halts VSG expression to prioritise essential mRNA expression, causing a cell cycle arrest until VSG expression is restored allowing cells to complete cell cycle progression.

However, Taylor (2024) observed an increase in *T. brucei* VSG mRNA post-HS via the upregulation of VSG2 during an active HS. This presents that the cell cycle arrest is not

driven by the decrease in VSG expression after HS, but potentially by an active dysregulation in the normal VSG mechanisms, which is unable to occur in PCF cells. Such dysregulation of VSGs may occur due to the HS-induced damage to the endosomes and Golgi apparatus, that are responsible for the endocytosis and recycling of VSGs (Umaer, Bush and Bangs, 2018). This theory is supported by studies within mammalian cells showing that HS causes damage to a transport receptor protein ERGIC-53, which is conserved in *T. brucei* in the p24 family (Spatuzza et al., 2004; Nihei and Nakanishi, 2021). Damage to ERGIC-53 impairs the intracellular transport of glycoproteins (Spatuzza et al., 2004), upon which in *T. brucei* would cause VSG disruptions and could interfere with cell cycle regulation. However, such conclusions are limited due to the lack of comparative work in trypanosomes and the change in VSG post-HS was only observed at the mRNA level and not the protein level.

7.2.3 The formation of P-bodies in BSF *T. brucei* after 41 °C for 1 hour

The formation of DHH1-rich localisations recognised as HS-induced P-bodies in BSF *T. brucei* after 1 hour at 41 °C agrees with previous data in both PCF and BSF within the Urbaniak lab and published data by Kramer et al (2008). This study agrees with past work that following HS, DHH1 migrates to granule-like areas with increased concentration often in proximity to the nucleus. The behaviour of XRNA a further P-body protein, an exoribonuclease involved in mRNA metabolism (Cassola, 2011), has also been analysed by these groups, finding its localisation to areas at the posterior of the cell and perinuclear regions. This study observed an increase in DHH1 signal also in perinuclear regions, indicating the formation of P-bodies containing both DHH1 and XRNA occur near to the nucleus. Localisation in this area has importance for P-body function, as proximity to the nucleus increases access to mRNAs damaged by the HS. This facilitates the P-bodies to remove mRNAs for storage or degradation and contain them away from translational machinery, enabling the prioritisation of 'survival' mRNAs to be expressed. This response is reflected in the outcome of change in mRNA levels post-HS, for there to be a decrease in mRNAs required for cell division and an increase in HSP mRNAs, favouring survival following a HS (Schwede, Kramer and Carrington, 2011).

7.2.4 The importance of the ZC3H11 HNPY interaction motif

The induced SDM GCC mutation was not observed in the *T. brucei* cells after transfection, this may have occurred due to an unsuccessful transfection. However, due to the number of clonal populations that were unable to grow, it may suggest that the mutated HNPY to HNAY is unstable within BSF *T. brucei* and indicating that the proline residue within the motif has an essential role for the function of ZC3H11 for complex formation with MKT1. Due to the use of specific primers, it may suggest that the few surviving post-transfection clones were able to survive due to genetic re-arrangement supporting the loss of the HNAY mutation, whilst retaining the drug resistance.

Singh et al (2014) described the mutation of the interaction motif to AAPY and HNAA as being 'extremely unstable' in *T. brucei* and these mutants were unable to be used in tethering studies. Therefore, the completion of SDM to produce a HNAY mutant, enabled the interrogation of if its phenotype is more or less lethal than the previous mutants. The structural significance of the proline residue within the WT motif to enable interactions may be questioned, as prolines can interfere with hydrogen bonding that occurs in alpha-helices or beta-sheet protein structures and cause sharp bends in the polypeptide chain (Morgan and Rubenstein, 2013). Therefore, the toxicity of the mutation may have occurred due to the absence of the proline to influence the structure of the motif; but this requires downstream mapping to determine the structural role proline has within the motif.

The work of Ooi, Benz and Urbaniak (2020) showed that *T. brucei* utilise the complex of ZC3H11-MKT1 as a vital 'signal integration node' within the HS response due to the increase in HS-responsive phosphorylation events that occur to ZC3H11 and the binding partners of MKT1, including UPL3, NEK6, ZC3H32 and CK1.2. Therefore, HS increases the complex abundance of ZC3H11-MKT1, governed by HS-induced phosphorylation events.

7.2.5 The HS-induced change in ZC3H11 protein expression

In this study the HS-responsive change in ZC3H11 protein abundance was investigated by western blotting using a Ty-tagged ZC3H11 WT cell line. An increase in intensity of a band at around the expected size of 40 kDa (Singh et al., 2014) post-HS is indicative

of its increased protein expression, however this observation was limited due to the variations in sample load across the blot. Furthermore, due to inconsistency in the load no bands were able to be observed in the positive control sample treated by protease inhibitor.

This increase in ZC3H11 abundance after HS is confirmed by the previous work of Droll et al (2013) via probing for ZC3H11 through the use probes against its Myc and V5 tags on a western blot with equivalent samples of PCF *T. brucei* cells. The result presenting an increased intensity of a band at the molecular weight of ZC3H11, indicating its increased abundance. This increased intensity of the ZC3H11 band was further shown in PCF *T. brucei* by Minia and Clayton (2016) using anti-ZC3H11, with an increase occurring at a HS temperature of 37 °C and a further increase after a HS at 41 °C.

7.2.6 The significance of the collapse of polysomes within the HS response of *T. brucei* and *T. congolense*

In this study a polysome profile showing the effect of heat shock upon PCF *T. brucei* has been produced with improved resolution than the existing published data (Kramer et al., 2008). This furthering our understanding of the global translational arrest that occurs in the HS response. The profile showing a shift in absorbance towards the monomer ribosomal subunits, with a decrease in polysome peaks. The observed shift indicates a decrease in mRNA-ribosome complexes and subsequent dissociation of polysomes into monosomes, such components are smaller and fractioned out earlier (Panda, Martindale and Gorospe, 2017). This shift in peaks demonstrates a global translational arrest as there is a decrease in polysomes able to actively translate mRNAs and an increase in non-translative ribosomal subunits with their recruitment to elongation being halted (Sivan, Kedersha and Elroy-Stein, 2007).

Furthermore, we observed the effect of HS upon the polysome profile of BSF *T. brucei*. After HS all the profile peaks decreased, other than 80S which increased. This could suggest that the HS caused impairment to translation initiation, as an increase in 80S indicates that 80S complexes have assembled but are unable to progress to elongation

(Sivan, Kedersha and Elroy-Stein, 2007). As a result, the profile suggests that HS in BSF *T. brucei* induces a global translational arrest, reducing protein synthesis.

These results support the timeline of events of the HS response in BSF *T. brucei* that polysomes collapse and release mRNAs enabling the formation of stress granules and P-bodies for mRNA storage or degradation (Kramer et al., 2008). This is shown within this study as at the same timepoint immediately after 1 h at 41 °C a global translational arrest coincided with DHH1-accumulations as P-bodies, presenting a release of mRNAs from active translation to then localise alongside DHH1 for their following fate. The collapse of polysomes in reducing the active translation of heat shocked cells may explain the disruption to growth and cell cycle arrest observed within this study. The decrease in protein expression may result in a lack of cell cycle-essential proteins and thus facilitating limited progression in the cell cycle and subsequent growth.

This collapse observed in BSF *T. brucei* is less severe than that in PCF, this may be explained in that 41 °C is a greater HS stimulus to procyclic cells. As BSF cells are cultured at 37 °C and PCF cells are cultured at 27 °C; therefore, the HS temperature is closer to the physiological temperature range for BSF cells, potentially causing a smaller collapse in polysomes (Briggs et al., 2023). Furthermore, the physiological conditions of BSF *T. brucei* within the mammalian host, means that these cells are more likely to experience temperatures as high as 41 °C (within a human host) due to the fever response and therefore have reduced sensitivity to the HS (Sinha et al., 1999). BSF *T. brucei* are also shown to require a constant level of translation to meet expression demands, for example of VSGs; therefore, less of a polysome collapse may occur to sustain this translation (Vasquez et al., 2014; Vieira-da-Rocha et al., 2019). Whilst during the PCF life cycle stage, cells have a reduced demand for continuous global translation, with reduced translational efficiency, and this may enable a more severe collapse in polysomes to occur more readily than BSF cells heat shocked at 41 °C (Vasquez et al., 2014).

Finally, this study completed polysome profiling in *T. congolense* for the first time and interrogated the changes in peaks following HS. The peaks for the ribosomal subunits and polysomes decrease post-HS, showing an overall decrease in the polysome to

monosome ratio. This suggests a decreased proportion of ribosomes actively completing translation via inhibited initiation through a decrease in ribosomal stability, or due to a reduced number of ribosomes (Xie et al., 2024). A HS-induced decrease in polysomes is comparable to that observed in *T. brucei* and therefore, this may allude to evolutionary conservation in the HS responses between the two species.

7.3 Limitations

7.3.1 Cell counts and motility analysis

The use of using an automated cell counter to measure cell growth as a read-out of viability has its limitations, including that counts produced did not distinguish and filter out any dead cells or debris, these being incorporated into the cell counts. Furthermore, the counts used 10 μl of culture and this relies upon the assumption that this volume is representative of the density of the complete culture.

Furthermore, issues of motility analysis include the change in temperature of the cells upon visualisation, with the cells being placed on a microscope stage at an uncontrolled temperature; this may influence cell motility and cause variability between experiments. A further issue of motility analysis was the drift experienced by the cells throughout the media, drift having the ability to falsely increase the movement of cells and produce more variation.

7.3.2 Immunofluorescence imaging

Limitations of the immunofluorescence images observing the change in localisation of DHH1 include issues of background in the immunofluorescent pictures, the potential for non-specific antibody binding and normalisation issues. These factors have the potential to make an effect look more or less prominent.

7.3.3 Polysome gradient analysis

Issues with the polysome gradient fractionation analysis include difficulty in producing results with reproducibility, as some experiments presented traces with an absence of

peaks. Therefore, further optimisation would involve developing an understanding around the inconsistency generated by the method. A further aspect to optimise the experiment would be to generate a minimum cell number threshold of sensitivity that is able to produce a standard polysome profile. This would ensure that the number of cells being used in following experiments would be known as not being a limiting factor, as well as scaling to be completed across different cell types. For the direct comparison between non-HS and HS profiles, rather than the limitation of adjusting axes to view the shift in peaks, normalising to the area under the peaks would enable an increased accuracy to observe the effect of HS upon polysomes.

Furthermore, a limitation included the use of Biocomp long caps which were used in producing the gradients. These caps meant that a section of the tube was unable to be filled, meaning the samples were unable to completely fill the whole of the 13.2 ml tubes. As a result, detection at the top of the tube produced noise on the profiles (that was cropped out from the presented figures due to not representing the sample); therefore, shorter caps in future could be used to efficiently capture the absorbance of the early fractions.

7.4 Future work

7.4.1 Enhancing understanding of cell viability post-HS

To produce cell counts representative of viable cells, future experiments could use a haemocytometer to only count motile cells or incorporate live/dead staining for example using calcein AM to directly quantify the viable cells after a HS and to compare the proportion of cells irreversibly damaged via death across the different HS conditions.

To maximise the accuracy of the motility analysis data, the flow effect requires reduction, but providing more time for the meniscus to settle upon the stage was a compromise in enabling the culture to further decrease in temperature from the HS conditions. Therefore, to optimise future motility experiments, a single vessel to HS and image the cells alongside the use of a heated microscope stage could be used, enabling greater control of the environmental temperature and providing more time

for the flow effect to settle. Furthermore, the initial track length data visualised aligned with both the published and hypothesised trend reflecting decreased motility with further HS exposure; therefore, further repeats are required to assess the validity of track length as a read-out of motility.

7.4.2 Further investigation of HS-induced cell cycle events and their role *in vivo*

For comparative analysis of the mechanism of HS recovery in *T. brucei* and *T. congolense* flow cytometry analysis could be used in future work to observe whether an equivalent reversible cell cycle arrest characterised by a peak in G2M enrichment occurs. To achieve this, sample preparation for the fixation of *T. congolense* using methanol requires optimisation.

For the flow cytometry analysis in the 2T1 and J1339 cells post-HS there was a difference in the precise timing of the peak G2M enrichment within the arrest. This may have occurred due to the uncontrolled difference of the input of cells across the cell cycle and in future work this could be controlled using cell cycle synchronised populations, enabling the development of understanding of the timing of events within *T. brucei* HS recovery.

Future experiments could also address the role of HS in the slender to stumpy differentiation pathway. Via the completion of equivalent flow cytometry analysis using pleomorphic BSF *T. brucei* cells that are able to differentiate; it would enable the observation of whether a G2M enrichment coincides with differentiation. Or the theory of dynamic dysregulation of VSGs influencing the cell cycle arrest could also be tested further via completion of this flow cytometry analysis in *T. brucei* cells that have RNAi knockout of EGIC-53. Enabling the observation of if disruption to VSG transport and recycling pathways alone is able to induce a cell cycle arrest with enriched G2M comparable to the post-HS observation.

7.4.3 Future visualisation of P-bodies

Future analysis of the change in DHH1 localisation upon HS would require more repeats to validate the observed effect in this study. Furthermore, an improved resolution could also be used in future work to observe the precise location of P-bodies in relation to the nucleus and enable counts to quantify the increase in P-bodies compared to the pre-HS state. The completion of this IFA for longer time points post-HS in future work would also be beneficial to observe the timing for the dissolution of P-bodies in HS recovery and to observe whether this coincides with the observed resolution of the cell cycle arrest. The use of another P-body marker, for example XRNA may strengthen the observation of P-body formation further in future work, through the observation of the P-body proteins directly co-localising within the observed accumulations post-HS.

Equivalent analysis in *T. congolense,* via initially the production of a DHH1-tagged WT cell line, would allow comparisons of the role of P-body formation in the HS response relative to *T. brucei*. Similarity in the increase of punctate localisations post-HS may indicate a further level of conservation in the response between the two species.

7.4.4 Interrogating the ZC3H11-MKT1 interaction in the *T. brucei* HS response

To confirm the instability of the HNAY mutation of the ZC3H11 interaction motif, future work would require the repetition of the transfection and following sequencing of the selected clonal cell populations. If all sequenced motifs have the WT CCC codon, this would strengthen the observation that the mutant GCC codon promotes instability for growth. Furthermore, ectopic expression could be used to determine the lethality of the mutated ZC3H11 via the use of tetracycline-inducible episomal expression, thus using Tet-regulation to test its stability and investigate dose dependence of the potential observed effect of HNAY ZC3H11 toxicity.

Upon the production of a stable HNPY mutant cell line, future work could address whether ZC3H11 phosphorylation is impacted by the HNAY mutation. Or whether HS and its induced phosphorylation acts to rescue the HNAY mutant phenotype and that

the proline may no longer be required for the ZC3H11-MKT1 interaction to occur. To investigate whether ZC3H11-MKT1 complex formation is required for the HS response, if the mutant is unable to support the interaction, HS-induced cell cycle and growth disturbances could be compared in the mutant to the WT. The use of growth analysis would enable the comparison of the extent of a HS-induced lag in growth and the rate of recovery between the mutant and WT cell lines after HS. Additionally, cell cycle analysis could compare whether the reversible cell cycle arrest is able to occur and to the same level of G2M enrichment in the mutant cells as in the WT cells. These analyses could present the extremity of the HNAY mutant phenotype within the HS response or if it is comparable to the WT, it could demonstrate that the proline residue is not a requirement of the interaction motif for its functionality.

A confirmed HNAY ZC3H11 mutant cell line could also be used alongside a tagged-MKT1 cell line for the completion of co-immunoprecipitation (co-IP) assays to directly observe the mutation-driven effects upon their interaction. To produce a MKT1-tagged cell line for this, further ligation reactions and sequencing are required with the MKT1 amplicon to produce a MKT1-G418-pPOTv6-Myc plasmid for following transfection to form a cell line (required steps shown in Figure 5.15). Upon the completion of the MKT1-tagged cell line, a co-IP may enable the mutant complex formation of ZC3H11 (HNAY) with MKT1 to be compared to the WT (HNPY). Reciprocal pull-downs could also be used to eliminate any antibody-driven effects contributing to the results showing that the same effect may be observed in both directions, swapping ZC3H11 and MKT1 to be the ‘bait’ protein or the ‘prey’ protein (Huang and Kim, 2023). If the level of protein observed is the same in both the mutant and non-mutant ZC3H11 co-IPs with MKT1, it could indicate that the substitution of alanine does not induce a mis-folding effect and that the mutated interaction motif is able to form the same complexes as the WT. However, if the levels are observed to be different it suggests that proline has a vital role in governing the structure that enables binding at the interaction motif.

7.4.4 Furthering the output of polysome gradient analysis

An aspect to investigate in the future work would be the treatment of cells with cycloheximide, in this study cycloheximide was used to preserve polysomes in their

states upon lysate preparation. Kramer et al (2008) presented that a more severe collapse in polysomes occurs in the absence of post-HS cycloheximide treatment and the addition of cycloheximide pre-HS prevented the decrease in polysome fractions. Cycloheximide treatment prior to HS was also shown by Kramer et al (2008) to inhibit the formation of P-bodies and HS granules. Therefore, future work could involve observing the effect of the absence of cycloheximide, its treatment pre-HS and post-HS upon polysome profiles in PCF and BSF *T. brucei* as a repeat, and for the first time in *T. congolense.* This could be combined with the study of the downstream effect of cycloheximide treatment on P-bodies and stress granules in all three cell types via immunofluorescence microscopy.

Furthermore, to observe the complete process of HS recovery it would be interesting to prepare further lysates at more time points post-HS to observe when a complete resolution of HS occurs. This being characterised by the decrease in ribosomal subunits and increase in polysomes observed in the fractionation analysis. This enabling the observation of whether polysome reformation corresponds to the resolution of cell growth and the cell cycle arrest shown within this study. This analysis of post-HS resolution of polysomes could also correspond with the future work of viewing when P-bodies dissolve post-HS, to view whether P-body dissolution corresponds with monosome polymerisation supported by the incorporation of components released from the P-bodies. Thus, enabling comparison to the mammalian work indicating that polysomes begin to re-appear in recovery rapidly, with near-complete resolution reported within 60 minutes of cells being returned to 37 °C; coinciding with the dissolution of stress granules and P-bodies (Duncan and John W.B. Hershey, 1989; Kedersha et al., 2005).

Future analysis could also use the fractions produced by polysome gradient fractionation for quantitative PCR (qPCR) analysis, enabling quantification of specific mRNA from each fraction (Han et al., 2021). qPCR analysis could indicate which mRNAs of interest, for example that of HSPs, are being most actively translated in the more dense fractions in association with the ribosomes and polysomes; the proportion of mRNAs in these fractions could be compared pre- and post-HS. If an equivalent increase or decrease of multiple mRNAs in these fractions is observed, it could also

inform of potential co-regulation mechanisms in response to HS. However, issues would arise regarding a negative control of an mRNA that remains unchanged after HS, as HS is shown to cause a decrease in the expression of housekeeping genes and increase in stress response genes (Kramer et al., 2008).

7.5 Conclusions

Overall, this study completed work to characterise the HS response in *T. brucei*, with initial comparative data in *T. congolense.* HS at 41 °C for 1 hour was shown to influence the growth of BSF *T. brucei* cells prior to recovery, defined by a reversible cell cycle arrest observed within a period of lagged cell growth. This cell cycle arrest was viewed as an initial lag of S-phase cells prior to a peak of G2M cells at the 5th or 6th hour of recovery post-HS, which subsequently returned to the pre-HS proportions.

Site-directed mutagenesis was completed to produce a mutant HNAY interaction motif in ZC3H11, which was not observed post-transfection alongside the associated drug resistance. Thus, arising further questions regarding the success of the transfection or the stability of the mutant and whether the substituted proline residue within the HNPY motif has an essential role in ZC3H11-MKT1 complex formation. Due to time constraints, initial steps were completed to produce an MKT1-tagged *T. brucei* cell line and upon its complete generation it would enable further questions to be addressed regarding the significance of the WT HNPY interaction motif and the ZC3H11-MKT1 complex within the HS response.

Finally, polysome gradient analysis was completed pre- and post-HS for PCF and BSF *T. brucei,* with improved resolution compared to the published data. HS of PCF cells was shown to induce a more severe collapse in polysomes and increase in ribosomal subunits than that in BSF. This same analysis was also completed in *T. congolense* for the first time, also finding a decrease in polysomes and potentially indicating a comparative HS-induced decrease in ribosomal stability to that in *T. brucei;* alluding to a level of conservation in the HS response. This technique was completed and optimised for the first time at Lancaster University and opens the opportunity for more

questions to be answered in future work, relating to HS recovery and the translated status of mRNAs during the response.

8. References

Adams, E.R., Hamilton, P.B. and Gibson, W.C. (2010). African trypanosomes: celebrating diversity. *Trends in Parasitology*, 26(7), pp.324–328. doi: 10.1016/j.pt.2010.03.003.

Aelmans, M. (2022). *Characterising the heat shock response in Trypanosoma congolense*. Unpublished MSc by Research thesis, Available at: https://eprints.lancs.ac.uk/id/eprint/185047/1/2023aelmansmres.pdf.

Agilent (n.d.). QuikChange II Site-Directed Mutagenesis Kits - Details & Specifications | Agilent. www.agilent.com. Available at: https://www.agilent.com/en/quikchange-ii-site-directed-mutagenesis-kits-details [Accessed 24 Sep. 2025].

Agilent (n.d.). *QuickChange Primer Design*. Agilent.com. Available at: https://www.agilent.com/store/primerDesignProgram.jsp.

Alagar Boopathy, L.R., Jacob-Tomas, S., Alecki, C. and Vera, M. (2022). Mechanisms tailoring the expression of heat shock proteins to proteostasis challenges. Journal of Biological Chemistry, 298(5), p.101796. doi: 10.1016/j.jbc.2022.101796.

Alsford, S., Kawahara, T., Glover, L. and Horn, D. (2005). Tagging a *T. brucei* RRNA locus improves stable transfection efficiency and circumvents inducible expression position effects. Molecular and Biochemical Parasitology, 144(2), pp.142–148. doi: 10.1016/j.molbiopara.2005.08.009.

Alves, L.R., Oliveira, C. and Goldenberg, S. (2015). Eukaryotic translation elongation factor-1 alpha is associated with a specific subset of mRNAs in *Trypanosoma cruzi.* BMC Microbiology, 15(1). doi: 10.1186/s12866-015-0436-2.

American Chemical Society (2017). *Pentamidine - American Chemical Society*. American Chemical Society. Available at: https://www.acs.org/molecule-of-the-week/archive/p/pentamidine.html [Accessed 23 Aug. 2025].

Appenheimer, M.M. and Evans, S.S. (2018). Temperature and adaptive immunity. Handbook of Clinical Neurology, 156, pp.397–415. doi: 10.1016/B978-0-444-63912-7.00024-2.

Archile Paguem, Abanda, B., Dieudonné Ndjonka, Weber, J.S., Henriette, C., Kingsley Tanyi Manchang, Mamoudou Adoulmoumini, Eisenbarth, A., Renz, A., Kelm, S. and Mbunkah Daniel Achukwi (2019). Widespread co-endemicity of

Trypanosoma species infecting cattle in the Sudano-Sahelian and Guinea Savannah zones of Cameroon. BMC Veterinary Research, 15(1). doi: 10.1186/s12917-019-2111-6.

Aslett, M., Aurrecoechea, C., Berriman, M., Brestelli, J., Brunk, B.P., Carrington, M., Depledge, D.P., Fischer, S., Gajria, B., Gao, X., Gardner, M.J., Gingle, A., Grant, G., Harb, O.S., Heiges, M., Hertz-Fowler, C., Houston, R., Innamorato, F., Iodice, J. and Kissinger, J.C. (2009). TriTrypDB: a functional genomic resource for the Trypanosomatidae. Nucleic Acids Research, 38(suppl_1), pp.D457–D462. doi: 10.1093/nar/gkp851.

Awuah-Mensah, G., McDonald, J., Steketee, P.C., Autheman, D., Whipple, S., D'Archivio, S., Brandt, C., Clare, S., Harcourt, K., Wright, G.J., Morrison, L.J., Gadelha, C. and Wickstead, B. (2021). Reliable, scalable functional genetics in bloodstream-form *Trypanosoma congolense* in vitro and in vivo. PLoS Pathogens, 17(1). doi: 10.1371/journal.ppat.1009224.

Aye, H.M., Li, F.-J. and He, C.Y. (2024). Dynamic composition of stress granules in *Trypanosoma brucei*. PLoS Pathogens, 20(10), pp.e1012666–e1012666. doi: 10.1371/journal.ppat.1012666.

Babokhov, P., Sanyaolu, A.O., Oyibo, W.A., Fagbenro-Beyioku, A.F. and Iriemenam, N.C. (2013). A current analysis of chemotherapy strategies for the treatment of human African trypanosomiasis. *Pathogens and Global Health*, 107(5), pp.242–252. doi: 10.1179/2047773213Y.0000000105.

Baker, N., de Koning, H.P., Mäser, P. and Horn, D. (2013). Drug resistance in African trypanosomiasis: the melarsoprol and pentamidine story. Trends in Parasitology, 29(3), pp.110–118. doi: 10.1016/j.pt.2012.12.005.

Balli, S., Sharan, S. and Shumway, K.R. (2023). Physiology, fever. PubMed. Available at: https://www.ncbi.nlm.nih.gov/books/NBK562334/ [Accessed 11 Apr. 2025].

Bargul, J.L., Jung, J., McOdimba, F.A., Omogo, C.O., Adung'a, V.O., Krüger, T., Masiga, D.K. and Engstler, M. (2016). Species-Specific Adaptations of Trypanosome Morphology and Motility to the Mammalian Host. PLOS Pathogens, 12(2), p.e1005448. doi: 10.1371/journal.ppat.1005448.

Bastin, P. (2019). The trypanosome journey in the tsetse fly. *Comptes Rendus Biologies*, 342(7-8), pp.273–275. doi: 10.1016/j.crvi.2019.09.026.

Bauer, B., Holzgrefe, B., Mahama, C.I., Baumann, M.P.O., Mehlitz, D. and Clausen, P.-H. (2011). Managing Tsetse Transmitted Trypanosomosis by Insecticide Treated Nets - an Affordable and Sustainable Method for Resource Poor Pig Farmers in Ghana. PLoS Neglected Tropical Diseases, 5(10), p.e1343. doi: 10.1371/journal.pntd.0001343.

Benoit, B., Mitou, G., Chartier, A., Temme, C., Zaessinger, S., Wahle, E., Busseau, I. and Simonelig, M. (2005). An Essential Cytoplasmic Function for the Nuclear Poly(A) Binding Protein, PABP2, in Poly(A) Tail Length Control and Early Development in *Drosophila*. Developmental Cell, 9(4), pp.511–522. doi: 10.1016/j.devcel.2005.09.002.

Bentley, S.J. and Boshoff, A. (2019). *Trypanosoma brucei* J-Protein 2 Functionally Co-Operates with the Cytosolic Hsp70 and Hsp70.4 Proteins. International Journal of Molecular Sciences, 20(23), p.5843. doi: 10.3390/ijms20235843.

Bentley, S.J., Jamabo, M. and Boshoff, A. (2018). The Hsp70/J-protein machinery of the African trypanosome, *Trypanosoma brucei.* Cell Stress and Chaperones, 24(1), pp.125–148. doi: 10.1007/s12192-018-0950-x.

Benz, C., Dondelinger, F., McKean, P.G. and Urbaniak, M.D. (2017). Cell cycle synchronisation of *Trypanosoma brucei* by centrifugal counter-flow elutriation reveals the timing of nuclear and kinetoplast DNA replication. *Scientific Reports*, 7(1). doi: 10.1038/s41598-017-17779-z.

Berriman, M. (2005). The Genome of the African Trypanosome *Trypanosoma brucei.* Science, 309(5733), pp.416–422. doi: 10.1126/science.1112642.

Bertiaux, E., Mallet, A., Rotureau, B. and Bastin, P. (2020). Intraflagellar transport during assembly of flagella of different length in *Trypanosoma brucei* isolated from tsetse flies. Journal of Cell Science, 133(18). doi: 10.1242/jcs.248989.

BioRender (n.d.). *Biorender*. BioRender. Available at: https://www.biorender.com [Accessed 28 Apr. 2025].

Boes, K.M. and Durham, A.C. (2022). Pathologic Basis of Veterinary Disease. 7th ed. St Louis Etc.: Elsevier, Cop, pp.724–804. Available at:https://www.sciencedirect.com/science/chapter/edited-volume/pii/B9780323357753000138 [Accessed 6 Dec. 2025].

Bose, J., Kloesener, M.H. and Schulte, R.D. (2016). Multiple-genotype infections and their complex effect on virulence. *Zoology*, 119(4), pp.339–349. doi: 10.1016/j.zool.2016.06.003.

Briggs, E.M., Marques, C.A., Oldrieve, G.R., Hu, J., Otto, T.D. and Matthews, K.R. (2023). Profiling the bloodstream form and procyclic form *Trypanosoma brucei* cell cycle using single-cell transcriptomics*. eLife,* 12, p.e86325. doi: 10.7554/eLife.86325.

Broadhead, R., Dawe, H.R., Farr, H., Griffiths, S., Hart, S.R., Portman, N., Shaw, M.K., Ginger, M.L., Gaskell, S.J., McKean, P.G. and Gull, K. (2006). Flagellar motility is required for the viability of the bloodstream trypanosome. Nature, 440(7081), pp.224–227. doi: 10.1038/nature04541.

Burger, A., Ludewig, M.H. and Boshoff, A. (2014). Investigating the Chaperone Properties of a Novel Heat Shock Protein, Hsp70.c, from *Trypanosoma brucei*. Journal of Parasitology Research, 2014, pp.1–12. doi: 10.1155/2014/172582.

Burri, C. and Brun, R. (2003). Eflornithine for the treatment of human African trypanosomiasis. Parasitology Research, 90(S1), pp.S49–S52. doi: 10.1007/s00436-002-0766-5.

Bush, L.M. and Vazquez-Pertejo, M.T. (2024). *Fever*. MSD Manual Professional Edition. Available at: https://www.msdmanuals.com/professional/infectious-diseases/biology-of-infectious-disease/fever#Geriatrics-Essentials_v997477 [Accessed 11 Apr. 2025].

Cassola, A. (2011). RNA Granules Living a Post-Transcriptional Life: the Trypanosome's Case. *Current Chemical Biology*, 5(2), pp.108–117. doi: 10.2174/2212796811105020108.

Centers for Disease Control and Prevention (2019). *CDC - DPDx - Trypanosomiasis, African*. Centers for Disease Control and Prevention. Available at: https://www.cdc.gov/dpdx/trypanosomiasisafrican/index.html [Accessed 2 Jan. 2025].

Chantal, I., Minet, C. and Berthier, D. (2021). In vitro cultivation of *Trypanosoma congolense* bloodstream forms: State of the art and advances. Veterinary Parasitology, 299, p.109567. doi: 10.1016/j.vetpar.2021.109567.

Chassé, H., Boulben, S., Costache, V., Cormier, P. and Morales, J. (2017). Analysis of translation using polysome profiling. Nucleic Acids Research, 45(3), pp.e15–e15. doi: 10.1093/nar/gkw907.

Ciganda, M., José Sotelo-Silveira, Dubey, A.P., Pandey, P., Smith, J.T., Shen, S., Qu, J., Smircich, P. and Read, L.K. (2023). Translational control by *Trypanosoma brucei* DRBD18 contributes to the maintenance of the procyclic state. *RNA*, 29(12), pp.1881–1895. doi: 10.1261/rna.079625.123.

Clayton, C. (2013). The Regulation of Trypanosome Gene Expression by RNA-Binding Proteins. PLoS Pathogens, 9(11), p.e1003680. doi: 10.1371/journal.ppat.1003680.

Clayton, C. (2019). Regulation of gene expression in trypanosomatids: living with polycistronic transcription. Open Biology, 9(6), p.190072. doi: 10.1098/rsob.190072.

Cortazzo da Silva, L., Aoki, J. and Floeter Winter, L. (2022). Finding Correlations Between mRNA and Protein Levels in *Leishmania* Development*:* Is There a Discrepancy? ResearchGate. Available at: https://www.researchgate.net/publication/361955257_Finding_Correlations_Between_mRNA_and_Protein_Levels_in_Leishmania_Development_Is_There_a_Discrepancy [Accessed 5 Jan. 2025].

Coustou, V., Guegan, F., Plazolles, N. and Baltz, T. (2010). Complete In Vitro Life Cycle of *Trypanosoma congolense:* Development of Genetic Tools. PLoS Neglected Tropical Diseases, 4(3), p.e618. doi: 10.1371/journal.pntd.0000618.

Daniels, J.-P. ., Gull, K. and Wickstead, B. (2010). Cell Biology of the Trypanosome Genome. Microbiology and Molecular Biology Reviews, 74(4), pp.552–569. doi: 10.1128/mmbr.00024-10.

Darby, J. (2017). *Kucers' The Use of Antibiotics*. 7th ed. Boca Raton: CRC Press, pp.195–211. doi: 10.1201/9781498747967.

Das, A., Banday, M. and Bellofatto, V. (2007). RNA Polymerase Transcription Machinery in Trypanosomes. Eukaryotic Cell, 7(3), pp.429–434. doi: 10.1128/ec.00297-07.

Das, S., Santos, L., Failla, A.V. and Ignatova, Z. (2022). mRNAs sequestered in stress granules recover nearly completely for translation. RNA Biology, 19(1), pp.877–884. doi: 10.1080/15476286.2022.2094137.

Davis, M.W. and Jorgensen, E.M. (2022). ApE, A Plasmid Editor: A Freely Available DNA Manipulation and Visualization Program. Frontiers in Bioinformatics, 2. doi: 10.3389/fbinf.2022.818619.

Day, R., Bennion, B.J., Ham, S. and Daggett, V. (2002). Increasing Temperature Accelerates Protein Unfolding Without Changing the Pathway of Unfolding. Journal of Molecular Biology, 322(1), pp.189–203. doi10.1016/S0022-2836(02)00672-1.

de Chaumont, F., Dallongeville, S., Chenouard, N., Hervé, N., Pop, S., Provoost, T., Meas-Yedid, V., Pankajakshan, P., Lecomte, T., Le Montagner, Y., Lagache, T., Dufour, A. and Olivo-Marin, J.-C. (2012). Icy: an open bioimage informatics platform for extended reproducible research. Nature Methods, 9(7), pp.690–696. doi: 10.1038/nmeth.2075.

Desquesnes, M. and Dávila, A.M.R. (2002). Applications of PCR-based tools for detection and identification of animal trypanosomes: a review and perspectives. Veterinary Parasitology, 109(3-4), pp.213–231. doi10.1016/s0304-4017(02)00270-4.

Dewar, C.E., MacGregor, P., Cooper, S., Gould, M.K., Matthews, K.R., Savill, N.J. and Schnaufer, A. (2018). Mitochondrial DNA is critical for longevity and metabolism of transmission stage *Trypanosoma brucei*. PLOS Pathogens, 14(7), p.e1007195. doi: 10.1371/journal.ppat.1007195.

Dewhirst, M.W., Jones, E., Samulski, T., Vujaskovic, Z., Li, C. and Prosnitz, L. (2003). *The Biology of Hyperthermia*. www.ncbi.nlm.nih.gov. Available at: https://www.ncbi.nlm.nih.gov/books/NBK13357/ [Accessed 7 Dec. 2025].

Donelson, J. (1998). Multiple mechanisms of immune evasion by African trypanosomes. Molecular and Biochemical Parasitology, 91(1), pp.51–66. doi: 10.1016/s0166-6851(97)00209-0.

Droll, D., Minia, I., Fadda, A., Singh, A., Stewart, M., Queiroz, R. and Clayton, C. (2013). Post-Transcriptional Regulation of the Trypanosome Heat Shock Response by a Zinc Finger Protein. PLoS Pathogens, 9(4), p.e1003286. doi: 10.1371/journal.ppat.1003286.

Drug Bank (2025). Suramin. go.drugbank.com. Available at: https://go.drugbank.com/drugs/DB04786#.

Drugs for Neglected Diseases initiative (2003). Nifurtimox-eflornithine combination therapy (NECT) | *DNDi*. dndi.org. Available at: https://dndi.org/research-development/portfolio/nect/ [Accessed 23 Aug. 2025].

Drugs for Neglected Diseases initiative (2004). *Fexinidazole for T.b. gambiense* | *DNDi*. dndi.org. Available at: https://dndi.org/research-development/portfolio/fexinidazole/ [Accessed 23 Aug. 2025].

Duncan, R. and John W.B. Hershey (1989). Protein synthesis and protein phosphorylation during heat stress, recovery, and adaptation. 109(4), pp.1467–1481. doi: 10.1083/jcb.109.4.1467.

Dunn, N., Wang, S. and Adigun, R. (2018). African trypanosomiasis. Europepmc.org. Available at: https://europepmc.org/article/med/30137864 [Accessed 2 Jan. 2025].

Engstler, M., Pfohl, T., Herminghaus, S., Boshart, M., Wiegertjes, G., Heddergott, N. and Overath, P. (2007). Hydrodynamic Flow-Mediated Protein Sorting on the Cell Surface of Trypanosomes. *Cell*, 131(3), pp.505–515. doi: 10.1016/j.cell.2007.08.046.

Erdaw, M.M (2023). Contribution, prospects and trends of livestock production in sub-Saharan Africa: a review. International Journal of Agricultural Sustainability, 21(1). doi: 10.1080/14735903.2023.2247776.

Evans, S.S., Repasky, E.A. and Fisher, D.T. (2015). Fever and the thermal regulation of immunity: the immune system feels the heat. *Nature Reviews Immunology*, 15(6), pp.335–349. doi: 10.1038/nri3843.

Eyford, B.A., Sakurai, T., Smith, D., Loveless, B., Hertz-Fowler, C., Donelson, J.E., Inoue, N. and Pearson, T.W. (2011). Differential protein expression throughout the life cycle of *Trypanosoma congolense*, a major parasite of cattle in Africa. Molecular and Biochemical Parasitology, 177(2), pp.116–125. doi: 10.1016/j.molbiopara.2011.02.009.

Fèvre, E.M., Wissmann, B. v., Welburn, S.C. and Lutumba, P. (2008). The Burden of Human African Trypanosomiasis. PLoS Neglected Tropical Diseases, 2(12), p.e333. doi: 10.1371/journal.pntd.0000333.

Food and Agriculture Organization and World Health Organisation (2001). The disease | Programme Against African Trypanosomosis (PAAT*)* | Food and Agriculture Organization of the United Nations. www.fao.org. Available at:

https://www.fao.org/paat/the-programme/the-disease/en/ [Accessed 22 Aug. 2025].

Forthal, D.N. (2014). Functions of Antibodies. *Microbiology spectrum*, 2(4), p.1. Available at: https://pmc.ncbi.nlm.nih.gov/articles/PMC4159104/ [Accessed 6 Dec. 2025].

Franco, J.R., Cecchi, G., Paone, M., Diarra, A., Grout, L., Kadima Ebeja, A., Simarro, P.P., Zhao, W. and Argaw, D. (2022). The elimination of human African trypanosomiasis: Achievements in relation to WHO road map targets for 2020. PLOS Neglected Tropical Diseases, 16(1), p.e0010047. doi: 10.1371/journal.pntd.0010047.

Friedheim, E.A.H. (1949). Mel B in the Treatment of Human Trypanosomiasis. The American journal of tropical medicine., s1-29(2), pp.173–180. doi: 10.4269/ajtmh.1949.s1-29.173.

Fritz, M., Vanselow, J.T., Sauer, N., Lamer, S., Goos, C., T. Nicolai Siegel, Subota, I., Schlosser, A., Carrington, M. and Kramer, S. (2015). Novel insights into RNP granules by employing the trypanosome's microtubule skeleton as a molecular sieve. Nucleic Acid Research, 43(16), pp.8013–8032. doi: 10.1093/nar/gkv731.

Fullerton, M., Singha, U.K., Duncan, M. and Chaudhuri, M. (2015). Down regulation of Tim50 in *Trypanosoma brucei* increases tolerance to oxidative stress. Molecular and biochemical parasitology, 199(1-2), pp.9–18. doi: 10.1016/j.molbiopara.2015.03.002.

Gandin, V., Sikström, K., Alain, T., Morita, M., McLaughlan, S., Larsson, O. and Topisirovic, I. (2014). Polysome Fractionation and Analysis of Mammalian Translatomes on a Genome-wide Scale. Journal of Visualized Experiments, (87). doi: 10.3791/51455.

Gardiner, P.R. and Mahmoud Musa Mahmoud (1992). Salivarian Trypanosomes Causing Disease in Livestock Outside Sub-Saharan Africa. Elsevier eBooks, 2, pp.277–314. doi: 10.1016/b978-0-08-092413-7.50010-6.

Gauri Deák, Wapenaar, H., Sandoval, G., Chen, R., Taylor, M.R.D., Burdett, H., Watson, J.A., Tuijtel, M.W., Webb, S. and Wilson, M.D. (2023). Histone divergence in trypanosomes results in unique alterations to nucleosome structure. Nucleic Acids Research, 51(15), pp.7882–7899. doi: 10.1093/nar/gkad577.

Geerts, M., Van Reet, N., Leyten, S., Berghmans, R., Rock, K.S., Coetzer, T.H.T., Eyssen, L.E-A. and Büscher, P. (2020). *Trypanosoma brucei gambiense*-iELISA: A Promising New Test for the Post-Elimination Monitoring of Human African Trypanosomiasis. Clinical Infectious Diseases. doi: 10.1093/cid/ciaa1264.

Gummery, L., Jallow, S., Raftery, A.G., Bennet, E., Rodgers, J. and Sutton, D. (2020). Comparison of loop-mediated isothermal amplification (LAMP) and PCR for the diagnosis of infection with *Trypanosoma brucei* ssp. in equids in The Gambia. PLoS ONE, 15(8), pp.e0237187–e0237187. doi: 10.1371/journal.pone.0237187.

Hammarton, T.C. (2007). Cell cycle regulation in *Trypanosoma brucei.* Molecular and Biochemical Parasitology, 153(1-4), pp.1–8. doi: 10.1016/j.molbiopara.2007.01.017.

Han, C., Sun, L., Pan, Q., Sun, Y., Wang, W. and Chen, Y. (2021). Polysome profiling followed by quantitative PCR for identifying potential micropeptide encoding long non-coding RNAs in suspension cell lines. STAR Protocols, 3(1), p.101037. doi: 10.1016/j.xpro.2021.101037.

Hartl, F.U. (1996). Molecular chaperones in cellular protein folding. Nature, 381(6583), pp.571–580. doi: 10.1038/381571a0.

Hendriks, E.F. (2001). A novel CCCH protein which modulates differentiation of *Trypanosoma brucei* to its procyclic form. The EMBO Journal, 20(23), pp.6700–6711. doi: 10.1093/emboj/20.23.6700.

Heyer, Erin E. and Moore, Melissa J. (2016). Redefining the Translational Status of 80S Monosomes. Cell, 164(4), pp.757–769. doi: 10.1016/j.cell.2016.01.003.

Hill, K.L. (2003). Biology and Mechanism of Trypanosome Cell Motility. *Eukaryotic Cell*, 2(2), pp.200–208. doi: 10.1128/ec.2.2.200-208.2003.

Hirumi, H. and Hirumi, K. (1989). Continuous cultivation of *Trypanosoma brucei* blood stream forms in a medium containing a low concentration of serum protein without feeder cell layers. The Journal of Parasitology, 75(6), pp.985–989. Available at: https://pubmed.ncbi.nlm.nih.gov/2614608/ [Accessed 2 Jan. 2025].

Hu, C., Yang, J., Qi, Z., Wu, H., Wang, B., Zou, F., Mei, H., Liu, J., Wang, W. and Liu, Q. (2022). Heat shock proteins: Biological functions, pathological roles, and therapeutic opportunities. *MedComm*, 3(3). doi: 10.1002/mco2.161.

Huang, B.X. and Kim, H.-Y. (2023). Protocol for identifying physiologically relevant binding proteins of G-protein-coupled receptors. STAR Protocols, 4(4), p.102691. doi: 10.1016/j.xpro.2023.102691.

Huntingford, F., Rey, S. and Quaggiotto, M.-M. (2020). Behavioural fever, fish welfare and what farmers and fishers know. *Applied Animal Behaviour Science*, 231, p.105090. doi:10.1016/j.applanim.2020.105090.

Ibrahim, E.A.A., Elmahal, M.G.E.M., Ahmed, K.A.H.M., Hasabo, E.A. and Omer, M.E.A. (2022). Unusual neurological presentation of second stage African trypanosomiasis in a young boy: a case report. *BMC Pediatrics*, 22(1). doi: 10.1186/s12887-022-03313-2.

Igor Minia, Merce, C., Terrao, M. and Clayton, C. (2016). Translation Regulation and RNA Granule Formation after Heat Shock of Procyclic Form *Trypanosoma brucei*: Many Heat-Induced mRNAs Are also Increased during Differentiation to Mammalian-Infective Forms. PLOS Neglected Tropical Diseases, 10(9), pp.e0004982–e0004982. doi: 10.1371/journal.pntd.0004982.

Iroungou, B.A., Boundenga, L., Guignali Mangouka, L., Bivigou-Mboumba, B., Nzenze, J.R. and Maganga, G.D. (2020). Human African trypanosomiasis in two historical foci of the estuaire province, gabon: A case report. *SAGE open medical case reports*, 8, p.2050313X20959890. doi: 10.1177/2050313X20959890.

Jacobs, R.T., Nare, B., Wring, S.A., Orr, M.D., Chen, D., Sligar, J.M., Jenks, M.X., Noe, R.A., Bowling, T.S., Mercer, L.T., Rewerts, C., Gaukel, E., Owens, J., Parham, R., Randolph, R., Beaudet, B., Bacchi, C.J., Yarlett, N., Plattner, J.J. and Freund, Y. (2011). SCYX-7158, an Orally-Active Benzoxaborole for the Treatment of Stage 2 Human African Trypanosomiasis. *PLoS Neglected Tropical Diseases*, 5(6), p.e1151. doi: 10.1371/journal.pntd.0001151.

Jagadeesh Kumar Uppala, Ghosh, C., Sathe, L. and Dey, M. (2018). Phosphorylation of translation initiation factor eIF2α at Ser51 depends on site- and context-specific information. *FEBS Letters*, 592(18), pp.3116–3125. doi: 10.1002/1873-3468.13214.

Jia, X., He, X., Huang, C., Li, J., Dong, Z. and Liu, K. (2024). Protein translation: biological processes and therapeutic strategies for human diseases. Signal Transduction and Targeted Therapy, 9(1), pp.1–17. doi: 10.1038/s41392-024-01749-9.

Katabazi, A., Aliero, A.A., Witto, S.G., Odoki, M. and Musinguzi, S.P. (2021). Prevalence of *Trypanosoma congolense* and *Trypanosoma vivax* in Lira District, Uganda. BioMed Research International, 2021, pp.1–7. doi: 10.1155/2021/7284042.

Kay, C., Williams, T.A. and Gibson, W. (2020). Mitochondrial DNAs provide insight into trypanosome phylogeny and molecular evolution. BMC Evolutionary Biology, 20(1). doi: 10.1186/s12862-020-01701-9.

Kazusa Database (n.d.). *Codon usage table*. Kazusa.or.jp. Available at: http://www.kazusa.or.jp/codon/cgi-bin/showcodon.cgi?species=5691 [Accessed 26 Apr. 2025].

Kearly, A., Nelson, A.D.L., Aleksandra Skirycz and Chodasiewicz, M. (2024). Composition and function of stress granules and P-bodies in plants. Seminars in cell & developmental biology, 156, pp.167–175. doi: 10.1016/j.semcdb.2022.11.008.

Kedersha, N., Cho, M.R., Li, W., Yacono, P.W., Chen, S., Gilks, N., Golan, D.E. and Anderson, P. (2000). Dynamic Shuttling of Tia-1 Accompanies the Recruitment of mRNA to Mammalian Stress Granules. Journal of Cell Biology, 151(6), pp.1257–1268. doi: 10.1083/jcb.151.6.1257.

Kedersha, N., Stoecklin, G., Ayodele, M., Yacono, P., Lykke-Andersen, J., Fritzler, M.J., Scheuner, D., Kaufman, R.J., Golan, D.E. and Anderson, P. (2005). Stress granules and processing bodies are dynamically linked sites of mRNP remodeling. Journal of Cell Biology, 169(6), pp.871–884. doi: 10.1083/jcb.200502088.

Kedersha, N.L., Gupta, M., Li, W., Miller, I. and Anderson, P. (1999). RNA-Binding Proteins Tia-1 and Tiar Link the Phosphorylation of Eif-2α to the Assembly of Mammalian Stress Granules. Journal of Cell Biology, 147(7), pp.1431–1442. doi: 10.1083/jcb.147.7.1431.

Kelly, S., Ivens, A., Manna, P.T., Gibson, W. and Field, M.C. (2014). A draft genome for the African crocodilian trypanosome *Trypanosoma grayi*. *Scientific Data*, 1(1). doi: 10.1038/sdata.2014.24.

Kieft, R., Cliffe, L., Yan, H., Schmitz, R.J., Hajduk, S.L. and Sabatini, R. (2024a). Mono-allelic epigenetic regulation of polycistronic transcription initiation by RNA polymerase II in *Trypanosoma brucei*. *mBio*. doi: 10.1128/mbio.02328-24.

Kieft, R., Zhang, Y., Yan, H., Schmitz, R.J. and Sabatini, R. (2024b). Protein phosphatase PP1 regulation of RNA polymerase II transcription termination and

allelic exclusion of VSG genes in trypanosomes. Nucleic Acids Research, 52(12), pp.6866–6885. doi: 10.1093/nar/gkae392.

Kizza, D., Ocaido, M., Mugisha, A., Azuba, R., Nalule, S., Onyuth, H., Musinguzi, S.P., Okwasiimire, R. and Waiswa, C. (2021). Prevalence and risk factors for trypanosome infection in cattle from communities surrounding the Murchison Falls National Park, Uganda. Parasites & Vectors, 14(1). doi: 10.1186/s13071-021-04987-w.

Koch, H., Raabe, M., Urlaub, H., Bindereif, A. and Preußer, C. (2016). The polyadenylation complex of *Trypanosoma brucei:* Characterization of the functional poly(A) polymerase. RNA Biology, 13(2), pp.221–231. doi:10.1080/15476286.2015.1130208.

Kolev, N.G., Franklin, J.B., Carmi, S., Shi, H., Michaeli, S. and Tschudi, C. (2010). The transcriptome of the human pathogen *Trypanosoma brucei* at single-nucleotide resolution. PLoS pathogens, 6(9), p.e1001090. doi: 10.1371/journal.ppat.1001090.

Kolev, N.G., Ramey-Butler, K., Cross, G.A.M., Ullu, E. and Tschudi, C. (2012). Developmental Progression to Infectivity in *Trypanosoma brucei* Triggered by an RNA-Binding Protein. Science (New York, N.Y.), 338(6112), pp.1352–1353. doi: 10.1126/science.1229641.

Kolev, N.G., Ullu, E. and Tschudi, C. (2014). The emerging role of RNA-binding proteins in the life cycle of *Trypanosoma brucei*. Cellular Microbiology, 16(4), pp.482–489. doi: 10.1111/cmi.12268.

Kopeina, G.S., Afonina, Z.A., Gromova, K.V., Shirokov, V.A., Vasiliev, V.D. and Spirin, A.S. (2008). Step-wise formation of eukaryotic double-row polyribosomes and circular translation of polysomal mRNA. Nucleic Acids Research, 36(8), pp.2476–2488. doi: 10.1093/nar/gkm1177.

Kramer, S. (2017). The ApaH-like phosphatase TbALPH1 is the major mRNA decapping enzyme of trypanosomes. *PLoS pathogens*, 13(6), p.e1006456. doi: 10.1371/journal.ppat.1006456.

Kramer, S. and Carrington, M. (2011). Trans-acting proteins regulating mRNA maturation, stability and translation in trypanosomatids. Trends in Parasitology, 27(1), pp.23–30. doi: 10.1016/j.pt.2010.06.011.

Kramer, S., Marnef, A., Standart, N. and Carrington, M. (2012). Inhibition of mRNA maturation in trypanosomes causes the formation of novel foci at the nuclear

periphery containing cytoplasmic regulators of mRNA fate. Journal of Cell Science, 125(12). doi: 10.1242/jcs.099275.

Kramer, S., Piper, S., Estevez, A. and Carrington, M. (2016). Polycistronic trypanosome mRNAs are a target for the exosome. Molecular and Biochemical Parasitology, 205(1-2), pp.1–5. doi: 10.1016/j.molbiopara.2016.02.009.

Kramer, S., Queiroz, R., Ellis, L., Hoheisel, J.D., Clayton, C. and Carrington, M. (2010). The RNA helicase DHH1 is central to the correct expression of many developmentally regulated mRNAs in trypanosomes. Journal of Cell Science, 123(Pt 5), pp.699–711. doi: 10.1242/jcs.058511.

Kramer, S., Queiroz, R., Ellis, L., Webb, H., Hoheisel, J.D., Clayton, C. and Carrington, M. (2008). Heat shock causes a decrease in polysomes and the appearance of stress granules in trypanosomes independently of eIF2(alpha) phosphorylation at Thr169. Journal of Cell Science, 121(Pt 18), pp.3002–3014. doi: 10.1242/jcs.031823.

Krüger, T., Hofweber, M. and Kramer, S. (2013). SCD6 induces ribonucleoprotein granule formation in trypanosomes in a translation-independent manner, regulated by its Lsm and RGG domains. Molecular Biology of the Cell, 24(13), pp.2098–2111. doi: 10.1091/mbc.e13-01-0068.

Langousis, G. and Hill, K.L. (2014). Motility and more: the flagellum of *Trypanosoma brucei. Nature Reviews Microbiology*, 12(7), pp.505–518. doi: 10.1038/nrmicro3274.

Larburu, N., Adams, C.J., Chen, C.-S., Nowak, P.R. and Ali, M.M.U. (2020). Mechanism of Hsp70 specialized interactions in protein translocation and the unfolded protein response. Open Biology, 10(8), p.200089. doi: 10.1098/rsob.200089.

Larcombe, S.D., Briggs, E.M., Savill, N., Balazs Szoor and Matthews, K.R. (2023). The developmental hierarchy and scarcity of replicative slender trypanosomes in blood challenges their role in infection maintenance. Proceedings of the National Academy of Sciences of the United States of America, 120(42). doi: 10.1073/pnas.2306848120.

Lejon, V., Bentivoglio, M. and Franco, J.R. (2013). Chapter 11 - Human African trypanosomiasis. ScienceDirect. Available at: https://www.sciencedirect.com/science/article/abs/pii/B978044453490300011X [Accessed 3 Jan. 2025].

Li, B. and Zhao, Y. (2021). Regulation of Antigenic Variation by *Trypanosoma brucei* Telomere Proteins Depends on Their Unique DNA Binding Activities. *Pathogens*, 10(8), p.967. doi: 10.3390/pathogens10080967.

Liang, X., Haritan, A., Uliel, S. and Michaeli, S. (2003). trans and cis Splicing in Trypanosomatids: Mechanism, Factors, and Regulation. Eukaryotic Cell, 2(5), pp.830–840. doi: 10.1128/EC.2.5.830-840.2003.

Lindner, A.K., Veerle Lejon, Barrett, M.P., Blumberg, L., Bukachi, S.A., Chancey, R.J., Edielu, A., Matemba, L., Tihitina Mesha, Mwanakasale, V., Pasi, C., Tapunda Phiri, Seixas, J., Akl, E.A., Katrin Probyn, Villanueva, G., Simarro, P.P., Augustin Kadima Ebeja, Franco, J.R. and Priotto, G. (2024). New WHO guidelines for treating rhodesiense human African trypanosomiasis: expanded indications for fexinidazole and pentamidine. The Lancet Infectious Diseases. doi: 10.1016/s1473-3099(24)00581-4.

Logan-Henfrey, L.L., Gardiner, P.R. and Mahmoud, M.M. (1992). Parasitic Protozoa. Elsevier, pp.157–276. Available at: https://www.sciencedirect.com/science/article/abs/pii/B978008092413750009X.

Lord, J.S., Hargrove, J.W., Torr, S.J. and Vale, G.A. (2018). Climate change and African trypanosomiasis vector populations in Zimbabwe's Zambezi Valley: A mathematical modelling study. *PLOS Medicine*, 15(10), p.e1002675. doi: 10.1371/journal.pmed.1002675.

Love, S. and Mair, T.S. (2012). Nagana - an overview | ScienceDirect Topics. www.sciencedirect.com. Available at: https://www.sciencedirect.com/topics/pharmacology-toxicology-and-pharmaceutical-science/nagana [Accessed 2 Jan. 2025].

Lukeš, J., Butenko, A., Hashimi, H., Maslov, D.A., Votýpka, J. and Yurchenko, V. (2018). Trypanosomatids Are Much More than Just Trypanosomes: Clues from the Expanded Family Tree. Trends in Parasitology, [online] 34(6), pp.466–480. doi: 10.1016/j.pt.2018.03.002.

Lundkvist, G.B., Kristensson, K. and Bentivoglio, M. (2004). Why Trypanosomes Cause Sleeping Sickness. Physiology, 19(4), pp.198–206. doi: 10.1152/physiol.00006.2004.

Luo, Y., Na, Z. and Slavoff, S.A. (2018). P-Bodies: Composition, Properties, and Functions. Biochemistry, 57(17), pp.2424–2431. doi: 10.1021/acs.biochem.7b01162.

Macaluso, G., Grippi, F., Di Bella, S., Blanda, V., Gucciardi, F., Torina, A., Guercio, A. and Cannella, V. (2023). A Review on the Immunological Response against *Trypanosoma cruzi*. Pathogens, 12(2), p.282. doi: 10.3390/pathogens12020282.

Magez, S., Stijlemans, B., Baral, T. and De Baetselier, P. (2002). VSG-GPI anchors of African trypanosomes: their role in macrophage activation and induction of infection-associated immunopathology. Microbes and Infection, 4(9), pp.999–1006. doi: 10.1016/s1286-4579(02)01617-9.

Magona, J.W., Walubengo, J., Olaho-Mukani, W., Jonsson, N.N. and Eisler, M.C. (2008). Diagnostic value of rectal temperature of African cattle of variable coat colour infected with trypanosomes and tick-borne infections. Veterinary Parasitology, 160(3-4), pp.301–305. doi: 10.1016/j.vetpar.2008.11.020.

Mahat, Dig B., Salamanca, H. Hans, Duarte, Fabiana M., Danko, Charles G. and Lis, John T. (2016). Mammalian Heat Shock Response and Mechanisms Underlying Its Genome-wide Transcriptional Regulation. Molecular Cell, 62(1), pp.63–78. doi: 10.1016/j.molcel.2016.02.025.

Marcelo, A., Koppenol, R., de Almeida, L.P., Matos, C.A. and Nóbrega, C. (2021). Stress granules, RNA-binding proteins and polyglutamine diseases: too much aggregation*? Cell Death & Disease*, 12(6), pp.1–17. doi: 10.1038/s41419-021-03873-8.

Masocha, W., Robertson, B., Rottenberg, M.E., Mhlanga, J., Sorokin, L. and Kristensson, K. (2004). Cerebral vessel laminins and IFN-γ define *Trypanosoma brucei brucei* penetration of the blood-brain barrier. Journal of Clinical Investigation, 114(5), pp.689–694. doi: 10.1172/jci22104.

Masser, A.E., Ciccarelli, M. and Andréasson, C. (2020). Hsf1 on a leash – controlling the heat shock response by chaperone titration. Experimental Cell Research, 396(1), p.112246. doi: 10.1016/j.yexcr.2020.112246.

McCarthy, J.S., Wortmann, G.W. and Kirchhoff, L.V. (2015). *41* - Drugs for Protozoal Infections Other Than Malaria. ScienceDirect. Available at: https://www.sciencedirect.com/science/article/abs/pii/B9781455748013000412 [Accessed 3 Jan. 2025].

Meyer, K.J. and Shapiro, T.A. (2013). Potent Antitrypanosomal Activities of Heat Shock Protein 90 Inhibitors In Vitro and In Vivo. The Journal of Infectious Diseases, 208(3), pp.489–499. doi: 10.1093/infdis/jit179.

Milord, F., Pépin, J., Ethier, L., Milord, F., Loko, L., Ethier, L. and Mpia, B. (1992). Efficacy and toxicity of eflornithine for treatment of *Trypanosoma brucei gambiense* sleeping sickness. The Lancet, 340(8820), pp.652–655. doi: 10.1016/0140-6736(92)92180-n.

Minia, I. and Clayton, C. (2016). Regulating a Post-Transcriptional Regulator: Protein Phosphorylation, Degradation and Translational Blockage in Control of the Trypanosome Stress-Response RNA-Binding Protein ZC3H11. PLOS Pathogens, 12(3), p.e1005514. doi: 10.1371/journal.ppat.1005514.

Morgan, A.A. and Rubenstein, E. (2013). Proline: The Distribution, Frequency, Positioning, and Common Functional Roles of Proline and Polyproline Sequences in the Human Proteome. PLoS ONE, 8(1), p.e53785. doi: 10.1371/journal.pone.0053785.

Mugler, C.F., Hondele, M., Heinrich, S., Sachdev, R., Vallotton, P., Koek, A.Y., Chan, L.Y. and Weis, K. (2016). ATPase activity of the DEAD-box protein Dhh1 controls processing body formation. eLife, 5, p.e18746. doi: 10.7554/eLife.18746.

Mugnier, M.R., Stebbins, C.E. and Papavasiliou, F.N. (2016). Masters of Disguise: Antigenic Variation and the VSG Coat in *Trypanosoma brucei*. PLoS Pathogens, 12(9). doi: 10.1371/journal.ppat.1005784.

Mugo, E. and Clayton, C. (2017). Expression of the RNA-binding protein RBP10 promotes the bloodstream-form differentiation state in *Trypanosoma brucei*. PLOS Pathogens, 13(8), p.e1006560. doi: 10.1371/journal.ppat.1006560.

Muhich, M.L. and Boothroyd, J.C. (1989). Synthesis of trypanosome hsp70 mRNA is resistant to disruption of trans-splicing by heat shock. The Journal of biological chemistry, 264(13), pp.7107–10. Available at: https://pubmed.ncbi.nlm.nih.gov/2708359/ [Accessed 6 May 2025].

Muhich, M.L., Hsu, M.P. and Boothroyd, J.C. (1989). Heat-shock disruption of trans-splicing in trypanosomes: effect on Hsp70, Hsp85 and tubulin mRNA synthesis. Gene, 82(1), pp.169–175. doi: 10.1016/0378-1119(89)90042-5.

Mulindwa, J., Ssentamu, G., Matovu, E., Kamanyi Marucha, K., Aresta-Branco, F., Helbig, C. and Clayton, C. (2021). In vitro culture of freshly isolated *Trypanosoma brucei brucei* bloodstream forms results in gene copy-number changes. PLOS Neglected Tropical Diseases, 15(9), p.e0009738. doi: 10.1371/journal.pntd.0009738.

Naguleswaran, A., Fernandes, P., Bevkal, S., Rehmann, R., Nicholson, P. and Roditi, I. (2021). Developmental changes and metabolic reprogramming during establishment of infection and progression of *Trypanosoma brucei brucei* through its insect host. *PLOS* Neglected Tropical Diseases, 15(9), p.e0009504. doi: 10.1371/journal.pntd.0009504.

Namkoong, S., Ho, A., Woo, Y.M., Kwak, H. and Lee, J.H. (2018). Systematic Characterization of Stress-Induced RNA Granulation. Molecular Cell, 70(1), pp.175-187.e8. doi: 10.1016/j.molcel.2018.02.025.

New England Biolabs (n.d.). NEB Tm Calculator. tmcalculator.neb.com. Available at: https://tmcalculator.neb.com/# [Accessed 26 Apr. 2025].

Nihei, C. and Nakanishi, M. (2021). Cargo selection in the early secretory pathway of African trypanosomes. Parasitology International, 84, p.102379. doi: 10.1016/j.parint.2021.102379.

Oldenburg, S. (2021). TrypanoFluidique : compartimentation, culture et analyse de la microfluidique de gouttes de *Trypanosoma brucei*. [online] Research Gate. Available at: https://www.researchgate.net/publication/356941807_TrypanoFluidique_compartimentation_culture_et_analyse_de_la_microfluidique_de_gouttes_de_Trypanosoma_brucei [Accessed 9 Apr. 2025].

Ooi, C.-P., Benz, C. and Urbaniak, M.D. (2020). Phosphoproteomic analysis of mammalian infective *Trypanosoma brucei* subjected to heat shock suggests atypical mechanisms for thermotolerance. Journal of Proteomics, 219, pp.103735–103735. doi: 10.1016/j.jprot.2020.103735.

Ooi, C.-P., Schuster, S., Cren-Travaillé, C., Bertiaux, E., Cosson, A., Goyard, S., Perrot, S. and Rotureau, B. (2016). The Cyclical Development of *Trypanosoma vivax* in the Tsetse Fly Involves an Asymmetric Division. Frontiers in Cellular and Infection Microbiology, 6. doi: 10.3389/fcimb.2016.00115.

Pagabeleguem, S., Ravel, S., Dicko, A.H., Vreysen, M.J.B., Parker, A., Takac, P., Huber, K., Sidibé, I., Gimonneau, G. and Bouyer, J. (2016). Influence of temperature and relative humidity on survival and fecundity of three tsetse strains. Parasites & Vectors, 9(1). doi: 10.1186/s13071-016-1805-x.

Pajonk, F., Arndt van Ophoven, Weissenberger, C. and McBride, W.H. (2005). The proteasome inhibitor MG-132 sensitizes PC-3 prostate cancer cells to ionizing

radiation by a DNA-PK-independent mechanism. BMC Cancer, 5(1). doi:10.1186/1471-2407-5-76.

Panda, A., Martindale, J. and Gorospe, M. (2017). Polysome Fractionation to Analyze mRNA Distribution Profiles. BIO-PROTOCOL, 7(3), p.https://pmc.ncbi.nlm.nih.gov/articles/PMC5431591/. doi: 10.21769/bioprotoc.2126.

Paterou, A., Sáez Conde, J., Týč, J., Sunter, J.D., Vaughan, S., Gull, K. and Dean, S. (2025). A comprehensive toolkit for protein localization and functional analysis in trypanosomatids. Open biology, 15(4), p.240361. doi: 10.1098/rsob.240361.

Peacock, L., Cook, S., Ferris, V., Bailey, M. and Gibson, W. (2012). The life cycle of *Trypanosoma* (Nannomonas) *congolense* in the tsetse fly. *Parasites & Vectors*, 5(1), p.109. doi: 10.1186/1756-3305-5-109.

Prasanna, P. and Upadhyay, A. (2021). Heat Shock Proteins as the Druggable Targets in Leishmaniasis: Promises and Perils. Infection and Immunity, 89(2), pp.e00559-20. doi: 10.1128/IAI.00559-20.

Reineke, L.C. and Lloyd, R.E. (2013). Diversion of stress granules and P-bodies during viral infection. Virology, 436(2), pp.255–267. doi: 10.1016/j.virol.2012.11.017.

Reithmeier, R.A.F. (1996). Chapter 16 - Assembly of proteins into membranes. [online] ScienceDirect. Available at: https://www.sciencedirect.com/science/article/abs/pii/S0167730608605232 [Accessed 5 Jul. 2025].

Pereira, S.S, Mariana De Niz, Serre, K., Ouarné, M., Coelho, J., Franco, C.A. and Figueiredo, L.M. (2022). Immunopathology and *Trypanosoma congolense* parasite sequestration cause acute cerebral trypanosomiasis. eLife, 11. doi: 10.7554/elife.77440.

Reuter, C., Hauf, L., Imdahl, F., Sen, R., Vafadarnejad, E., Fey, P., Finger, T., Jones, N.G., Walles, H., Barquist, L., Saliba, A.-E., Groeber-Becker, F. and Engstler, M. (2023). Vector-borne *Trypanosoma brucei* parasites develop in artificial human skin and persist as skin tissue forms. Nature Communications, 14(1), p.7660. doi: 10.1038/s41467-023-43437-2.

Riggs, C.L., Kedersha, N., Ivanov, P. and Anderson, P. (2020). Mammalian stress granules and P bodies at a glance. Journal of Cell Science, 133(16), p.jcs242487. doi: 10.1242/jcs.242487.

Roditi, I. and Lehane, M.J. (2008). Interactions between trypanosomes and tsetse flies. Current Opinion in Microbiology, 11(4), pp.345–351. doi: 10.1016/j.mib.2008.06.006.

Rogers, K. (2024). eflornithine | drug | Britannica. www.britannica.com. Available at: https://www.britannica.com/science/eflornithine [Accessed 3 Jan. 2025].

Rojas, F., Silvester, E., Young, J., Milne, R., Tettey, M., Houston, D.R., Walkinshaw, M.D., Pérez-Pi, I., Auer, M., Denton, H., Smith, T.K., Thompson, J. and Matthews, K.R. (2019). Oligopeptide Signaling through TbGPR89 Drives Trypanosome Quorum Sensing. Cell, 176(1-2), pp.306-317.e16. doi: 10.1016/j.cell.2018.10.041.

Ross, R. and Thomson, D. (1910). A Case of Sleeping Sickness showing Regular Periodical Increase of the Parasites Disclosed. BMJ, 1(2582), pp.1544–1545. doi: 10.1136/bmj.1.2582.1544.

Ryan, E.T., Gutman, J.R. and Chancey, R.J. (2022). Antiparasitic Agents. In: S.S. Long, ed., Principles and Practice of Pediatric Infectious Diseases. Elsevier, pp.1598-1617.e2. doi: 10.1016/B978-0-323-75608-2.00296-2.

Sabalette, K.B., Sotelo-Silveira, J.R., Smircich, P. and De, J.G. (2023). RNA-Seq reveals that overexpression of TcUBP1 switches the gene expression pattern toward that of the infective form of *Trypanosoma cruzi*. Journal of Biological Chemistry, 299(5), pp.104623–104623. doi: 10.1016/j.jbc.2023.104623.

Saha, S. (2020). Histone Modifications and Other Facets of Epigenetic Regulation in Trypanosomatids: Leaving Their Mark. mBio, 11(5). doi: 10.1128/mbio.01079-20.

Sakharkar, M.K., Chow, V.T.K. and Kangueane, P. (2004). Distributions of exons and introns in the human genome. In Silico Biology, 4(4), pp.387–393. Available at: https://pubmed.ncbi.nlm.nih.gov/15217358/ [Accessed 5 Jan. 2025].

Sands, M., Kron, M.A. and Brown, R.B. (1985). Pentamidine: a review. Reviews of infectious diseases, 7(5), pp.625–34. doi: 10.1093/clinids/7.5.625.

Sarge, K.D., Murphy, S.P. and Morimoto, R.I. (1993). Activation of Heat Shock Gene Transcription by Heat Shock Factor 1 Involves Oligomerization, Acquisition of DNA-Binding Activity, and Nuclear Localization and Can Occur in the Absence of

Stress. Molecular and Cellular Biology, 13(3), pp.1392–1407. doi: 10.1128/mcb.13.3.1392-1407.1993.

Scholar, E. (2008). Nifurtimox. In: S.J. Enna and D.B. Bylund, eds., xPharm*: The* Comprehensive Pharmacology Reference. Elsevier, pp.1–5. doi: 10.1016/B978-008055232-3.62282-2.

Schwede, A., Kramer, S. and Carrington, M. (2011). How do trypanosomes change gene expression in response to the environment? Protoplasma, 249(2), pp.223–238. doi: 10.1007/s00709-011-0282-5.

Sharma, A.K., Dhasmana, N., Dubey, N., Kumar, N., Gangwal, A., Gupta, M. and Singh, Y. (2016). Bacterial Virulence Factors: Secreted for Survival. Indian Journal of Microbiology, 57(1), pp.1–10. doi: 10.1007/s12088-016-0625-1.

Sheader, K., Vaughan, S., Minchin, J., Hughes, K., Gull, K. and Rudenko, G. (2005). Variant surface glycoprotein RNA interference triggers a precytokinesis cell cycle arrest in African trypanosomes. Proceedings of the National Academy of Sciences, 102(24), pp.8716–8721. doi: 10.1073/pnas.0501886102.

Shi, H., Butler, K. and Tschudi, C. (2018). Differential expression analysis of transcriptome data of *Trypanosoma brucei* RBP6 induction in procyclics leading to infectious metacyclics and bloodstream forms in vitro. Data in Brief, 20, pp.978–980. doi: 10.1016/j.dib.2018.08.169.

Shimogawa, M.M., Ray, S.S., Kisalu, N., Zhang, Y., Geng, Q., Ozcan, A. and Hill, K.L. (2018). Parasite motility is critical for virulence of African trypanosomes. Scientific Reports, 8(1). doi: 10.1038/s41598-018-27228-0.

Silvester, E., Ivens, A. and Matthews, K.R. (2018). A gene expression comparison of *Trypanosoma brucei* and *Trypanosoma congolense* in the bloodstream of the mammalian host reveals species-specific adaptations to density-dependent development. PLOS Neglected Tropical Diseases, 12(10), p.e0006863. doi: 10.1371/journal.pntd.0006863.

Singh, A., Igor Minia, Droll, D., Fadda, A.A., Clayton, C. and Erben, E. (2014). Trypanosome MKT1 and the RNA-binding protein ZC3H11: interactions and potential roles in post-transcriptional regulatory networks. Nucleic Acids Journal, 42(7), pp.4652–4668. doi: 10.1093/nar/gkt1416.

Sivan, G., Kedersha, N. and Elroy-Stein, O. (2007). Ribosomal Slowdown Mediates Translational Arrest during Cellular Division. Molecular and Cellular Biology, 27(19), pp.6639–6646. doi: 10.1128/mcb.00798-07.

Smith, T.K., Nadina Vasileva, Gluenz, E., Terry, S., Portman, N., Kramer, S., Carrington, M., Michaeli, S., Gull, K. and Rudenko, G. (2009). Blocking Variant Surface Glycoprotein Synthesis in *Trypanosoma brucei* Triggers a General Arrest in Translation Initiation. PLoS ONE, 4(10), pp.e7532–e7532. doi: 10.1371/journal.pone.0007532.

Spatuzza, C., Renna, M., Raffaella Faraonio, Cardinali, G., Martire, G., Stefano Bonatti and Paolo Remondelli (2004). Heat Shock Induces Preferential Translation of ERGIC-53 and Affects Its Recycling Pathway. Journal of Biological Chemistry, 279(41), pp.42535–42544. doi: 10.1074/jbc.m401860200.

Srivastava, A., Nitika Badjatia, Ju Huck Lee, Hao, B. and Günzl, A. (2017). An RNA polymerase II-associated TFIIF-like complex is indispensable for SL RNA gene transcription in *Trypanosoma brucei*. Nucleic Acids Research, 46(4), pp.1695–1709. doi: 10.1093/nar/gkx1198.

Steketee, P.C., Dickie, E.A., Iremonger, J., Crouch, K., Paxton, E., Jayaraman, S., Alfituri, O.A., Awuah-Mensah, G., Ritchie, R., Schnaufer, A., Rowan, T., Harry, Gadelha, C., Wickstead, B., Barrett, M.P. and Morrison, L.J. (2021). Divergent metabolism between *Trypanosoma congolense* and *Trypanosoma brucei* results in differential sensitivity to metabolic inhibition. PLOS pathogens, 17(7), pp.e1009734–e1009734. doi: 10.1371/journal.ppat.1009734.

Steverding, D. (2010). The development of drugs for treatment of sleeping sickness: a historical review. Parasites & Vectors, 3(1), p.15. doi: 10.1186/1756-3305-3-15.

Stoecklin, G. and Kedersha, N. (2013). Relationship of GW/P-bodies with stress granules. Advances in experimental medicine and biology, 768, pp.197–211. doi: 10.1007/978-1-4614-5107-5_12.

Stuart, K., Brun, R., Croft, S., Fairlamb, A., Gürtler, R.E., McKerrow, J., Reed, S. and Tarleton, R. (2008). Kinetoplastids: related protozoan pathogens, different diseases. Journal of Clinical Investigation, 118(4), pp.1301–1310. doi: 10.1172/jci33945.

Subota, I., Rotureau, B., Blisnick, T., Ngwabyt, S., Durand-Dubief, M., Engstler, M. and Bastin, P. (2011). ALBA proteins are stage regulated during trypanosome

development in the tsetse fly and participate in differentiation. Molecular Biology of the Cell, 22(22), pp.4205–4219. doi: 10.1091/mbc.e11-06-0511.

Subramaniam, C., Veazey, P., Redmond, S., Hayes-Sinclair, J., Chambers, E., Carrington, M., Gull, K., Matthews, K., Horn, D. and Field, M.C. (2006). Chromosome-Wide Analysis of Gene Function by RNA Interference in the African Trypanosome. Eukaryotic Cell, 5(9), pp.1539–1549. doi: 10.1128/ec.00141-06.

Sweet, T., Kovalak, C. and Coller, J. (2012). The DEAD-Box Protein Dhh1 Promotes Decapping by Slowing Ribosome Movement. PLoS Biology, 10(6), p.e1001342. doi: 10.1371/journal.pbio.1001342.

Tarral, A., Blesson, S., Mordt, O.V., Torreele, E., Sassella, D., Bray, M.A., Hovsepian, L., Evène, E., Gualano, V., Felices, M. and Strub-Wourgaft, N. (2014). Determination of an Optimal Dosing Regimen for Fexinidazole, a Novel Oral Drug for the Treatment of Human African Trypanosomiasis: First-in-Human Studies. Clinical Pharmacokinetics, 53(6), pp.565–580. doi: 10.1007/s40262-014-0136-3.

Tarral, A., Hovsepian, L., Duvauchelle, T., Yves Donazzolo, Latreille, M., Mathieu Felices, Gualano, V., Delhomme, S., Olaf Valverde Mordt, Séverine Blesson, P Voiriot and Strub-Wourgaft, N. (2023). Determination of the Optimal Single Dose Treatment for Acoziborole, a Novel Drug for the Treatment of Human African Trypanosomiasis: First-in-Human Study. Clinical Pharmacokinectics, 62(3), pp.481–491. doi: 10.1007/s40262-023-01216-8.

Tavassolifar, M. javad, Vodjgani, M., Salehi, Z. and Izad, M. (2020). The Influence of Reactive Oxygen Species in the Immune System and Pathogenesis of Multiple Sclerosis. Autoimmune Diseases, 2020, pp.1–14. doi: 10.1155/2020/5793817.

Taylor, A. (2024). Investigating the heat shock response of bloodstream and procyclic forms of *Trypanosoma* spp. Unpublished Msc by Research thesis.

Taylor, C. and Lyman, C. (1972). Heat storage in running antelopes: independence of brain and body temperatures. *American Journal of Physiology-Legacy Content*, 222(1), pp.114–117. doi: 10.1152/ajplegacy.1972.222.1.114.

Teixeira, S.M., Paiva, R.M.C. de, Kangussu-Marcolino, M.M. and DaRocha, W.D. (2012). Trypanosomatid comparative genomics: contributions to the study of parasite biology and different parasitic diseases. Genetics and Molecular Biology, 35(1), pp.1–17. doi: 10.1590/s1415-47572012005000008.

Thermo Scientific (n.d.). GeneJet PCR Purification Kit. www.thermofisher.com. Available at: https://www.thermofisher.com/document-connect/document-connect.html?url=https://assets.thermofisher.com/TFS-Assets%2FLSG%2Fmanuals%2FMAN0012662_GeneJET_PCR_Purification_UG.pdf [Accessed 27 Feb. 2024].

Timur Baymukhametov, Lyabin, D.N., Chesnokov, Y.M., Sorokin, I.I., Pechnikova, E.V., Vasiliev, A.L. and Afonina, Z.A. (2022). Polyribosomes of circular topology are prevalent in mammalian cells. Nucleic Acids Research, 51(2), pp.908–918. doi: 10.1093/nar/gkac1208.

Trenaman, A., Glover, L., Hutchinson, S. and Horn, D. (2019). A post-transcriptional respiratome regulon in trypanosomes. Nucleic Acids Research, 47(13), pp.7063–7077. doi: 10.1093/nar/gkz455.

Trépout, S. (2020). In situ structural analysis of the flagellum attachment zone in *Trypanosoma brucei* using cryo-scanning transmission electron tomography. Journal of Structural Biology: X, 4, p.100033. doi: 10.1016/j.yjsbx.2020.100033.

Trindade, S., Rijo-Ferreira, F., Carvalho, T., Pinto-Neves, D., Guegan, F., Aresta-Branco, F., Bento, F., Young, Simon A., Pinto, A., Van Den Abbeele, J., Ribeiro, Ruy M., Dias, S., Smith, Terry K. and Figueiredo, Luisa M. (2016). *Trypanosoma brucei* Parasites Occupy and Functionally Adapt to the Adipose Tissue in Mice. Cell Host & Microbe, 19(6), pp.837–848. doi: 10.1016/j.chom.2016.05.002.

Týč, J., Klingbeil, M.M. and Lukeš, J. (2015). Mitochondrial Heat Shock Protein Machinery Hsp70/Hsp40 Is Indispensable for Proper Mitochondrial DNA Maintenance and Replication. mBio, 6(1). doi: 10.1128/mbio.02425-14.

Umaer, K., Bush, P.J. and Bangs, J.D. (2018). Rab11 mediates selective recycling and endocytic trafficking in *Trypanosoma brucei*. Traffic, 19(6), pp.406–420. doi: 10.1111/tra.12565.

Vasquez, J.-J., Hon, C.-C., Vanselow, J.T., Schlosser, A. and Siegel, T.N. (2014). Comparative ribosome profiling reveals extensive translational complexity in different *Trypanosoma brucei* life cycle stages. Nucleic Acids Research, 42(6), pp.3623–3637. doi: 10.1093/nar/gkt1386.

Vaughan, S. and Gull, K. (2015). Basal body structure and cell cycle-dependent biogenesis in *Trypanosoma brucei*. Cilia, 5(1). doi: 10.1186/s13630-016-0023-7.

Verghese, J., Abrams, J., Wang, Y. and Morano, K.A. (2012). Biology of the Heat Shock Response and Protein Chaperones: Budding Yeast (Saccharomyces cerevisiae) as a Model System. Microbiology and Molecular Biology Reviews, 76(2), pp.115–158. doi: 10.1128/mmbr.05018-11.

Vieira-da-Rocha, J.P., Passos-Silva, D.G., Mendes, I.C., Rocha, E.A., Gomes, D.A., Machado, C.R. and McCulloch, R. (2019). The DNA damage response is developmentally regulated in the African trypanosome. DNA Repair, 73, pp.78–90. doi: 10.1016/j.dnarep.2018.11.005.

Vourchakbé, J., Tiofack, Z.A.A., Kante, T.S., Mpoame, M. and Simo, G. (2020). Molecular identification of *Trypanosoma brucei gambiense* in naturally infected pigs, dogs and small ruminants confirms domestic animals as potential reservoirs for sleeping sickness in Chad. Parasite, 27, p.63. doi: 10.1051/parasite/2020061.

W. Masocha, Amin, D.N., K. Kristensson and Rottenberg, M.E. (2008). Differential Invasion of *Trypanosoma brucei brucei* and Lymphocytes into the Brain of C57BL/6 and 129Sv/Ev Mice. Scandinavian Journal of Immunology, 68(5), pp.484–491. doi: 10.1111/j.1365-3083.2008.02170.x.

Weidner, J., Wang, C., Prescianotto-Baschong, C., Estrada, A.F. and Spang, A. (2014). The polysome-associated proteins Scp160 and Bfr1 prevent P body formation under normal growth conditions. Journal of Cell Science, 127. doi: 10.1242/jcs.142083.

Weisser, M. and Ban, N. (2019). Extensions, Extra Factors, and Extreme Complexity: Ribosomal Structures Provide Insights into Eukaryotic Translation. Cold Spring Harbor Perspectives in Biology,] 11(9), p.a032367. doi: 10.1101/cshperspect.a032367.

Wheeler, R.J., Gull, K. and Sunter, J.D. (2019). Coordination of the Cell Cycle in Trypanosomes. Annual Review of Microbiology, 73(1), pp.133–154. doi: 10.1146/annurev-micro-020518-115617.

Wiedemar, N., Hauser, D.A. and Mäser, P. (2020). 100 Years of Suramin. Antimicrobial Agents and Chemotherapy, 64(3). doi: 10.1128/AAC.01168-19.

World Health Organization (2023). Trypanosomiasis, Human African (sleeping sickness). WHO. Available at: https://www.who.int/news-room/fact-sheets/detail/trypanosomiasis-human-african-(sleeping-sickness) [Accessed 2 Jan. 2025].

Wurst, M., Robles, A.I., June, Luu, V.-D., Brems, S., Marentije, M., Savrina Stoitsova, Quijada, L., Hoheisel, J., Stewart, M., Hartmann, C. and Clayton, C. (2009). An RNAi screen of the RRM-domain proteins of *Trypanosoma brucei*. Molecular and Biochemical Parasitology, 163(1), pp.61–65. doi: 10.1016/j.molbiopara.2008.09.001.

Xie, Y., Shu, T., Liu, T., Spindler, M.-C., Mahamid, J., Hocky, G.M., Gresham, D. and Holt, L.J. (2024). Polysome collapse and RNA condensation fluidize the cytoplasm. Molecular Cell, 84(14), pp.2698-2716.e9. doi: 10.1016/j.molcel.2024.06.024.

Yun, O., Priotto, G., Tong, J., Flevaud, L. and Chappuis, F. (2010). NECT Is Next: Implementing the New Drug Combination Therapy for *Trypanosoma brucei gambiense* Sleeping Sickness. PLoS Neglected Tropical Diseases, 4(5), p.e720. doi: 10.1371/journal.pntd.0000720.

Zaiontz, C. (2023). Real Statistics Using Excel. Real-statistics.com. Available at: https://real-statistics.com [Accessed 7 Aug. 2025].

Zheng, J., Guo, N., Huang, Y., Guo, X. and Wagner, A. (2024). High temperature delays and low temperature accelerates evolution of a new protein phenotype. Nature Communications, 15(1), p.2495. doi: 10.1038/s41467-024-46332-6.

Zinoviev, A., Léger, M., Wagner, G. and Shapira, M. (2011). A novel 4E-interacting protein in *Leishmania* is involved in stage-specific translation pathways. Nucleic Acids Research, 39(19), pp.8404–8415. doi: 10.1093/nar/gkr555.

Zoltner, M., Krienitz, N., Field, M.C. and Kramer, S. (2018). Comparative proteomics of the two *T. brucei* PABPs suggests that PABP2 controls bulk mRNA. PLoS neglected tropical diseases, 12(7), pp.e0006679–e0006679. doi: 10.1371/journal.pntd.0006679.

Zügel, U. and Kaufmann, S.H.E. (1999). Role of Heat Shock Proteins in Protection from and Pathogenesis of Infectious Diseases. Clinical Microbiology Reviews, 12(1), pp.19–39. doi: 10.1128/CMR.12.1.19.

9. Appendix

9.1 P-values for motility analysis

Table 9.1: p-values for HS of 2T1 BSF *T. brucei* maximum speed motility analysis. The p-values correspond to each stated timepoint within each temperature statistically compared to the 0 h data. The data was statistically analysed using a single ANOVA with Tukeys ad hoc post-tests using the Real Statistics plugin (Zaiontz, 2023), data was deemed significant when $p<0.05$ and is highlighted *.

HS temperature	p-values
40 °C	0 h – 2 h: 7.53×10^{-6} * 0 h – 4 h: 0.01258 * 0 h – 6 h: 0.07659 0 h – 8 h: 0.1247
40.5 °C	0 h – 1 h: 0.5211 0 h – 2 h: 0.8558 0 h – 3 h: 0.00352 * 0 h – 4 h: 0.9988 0 h – 5 h: 0.9997
41 °C	0 h – 0.5 h: 6.14×10^{-9} * 0 h – 1 h: 0 * 0 h – 2 h: 0 *
41.5 °C	0 h – 1 h: 0.7492 0 h – 2 h: 0.8176
42 °C	0 h – 0.25 h: 0.09195 0 h – 0.5 h: 0.5134 0 h – 1 h: 0.04831 *

Table 9.2: p-values for HS of 2T1 BSF *T. brucei* average speed motility analysis. The p-values correspond to each stated timepoint within each temperature statistically compared to the 0 h data. The data was statistically analysed using a single ANOVA with Tukeys ad hoc post-tests using the Real Statistics plugin (Zaiontz, 2023), data was deemed significant when $p<0.05$ and is highlighted *.

HS temperature	p-values
40 °C	0 h – 2 h: 1.69×10^{-10} * 0 h – 4 h: 1.69×10^{-10} * 0 h – 6 h: 1.69×10^{-10} * 0 h – 8 h: 1.69×10^{-10} *
40.5 °C	0 h – 1 h: 1.72×10^{-10} *

	0 h – 2 h: 1.72×10^{-10} * 0 h – 3 h: 1.72×10^{-10} * 0 h – 4 h: 1.16×10^{-8} * 0 h – 5 h: 0.01866
41 °C	0 h – 0.5 h: 0.006523 * 0 h – 1 h: 0 * 0 h – 2 h: 0 *
41.5 °C	0 h – 1 h: 6.03×10^{-10} * 0 h – 2 h: 6.03×10^{-10} *
42 °C	0 h – 0.25 h: 0 * 0 h – 0.5 h: 0 * 0 h – 1 h: 0.6303

Table 9.3: p-values for HS of J1339 BSF *T. brucei* average and maximum cell speed motility analysis. The p-values correspond to each stated timepoint within each temperature statistically compared to the 0 h data. The data was statistically analysed using a single ANOVA with Tukeys ad hoc post-tests using the Real Statistics plugin (Zaiontz, 2023), data was deemed significant when $p<0.05$ and is highlighted *.

HS temperature	Max. speed p-values	Av. speed p-values
41 °C	0 h – 0.5 h: 0.8113 0 h – 1 h: 0.9998 0 h – 2 h: 0.5649	0 h – 0.5 h: 0.1514 0 h – 1 h: 0.00137 * 0 h – 2 h: 0 *
41.5 °C	0 h – 1 h: 0.0347 * 0 h – 2 h: 0.001118 *	0 h – 1 h: 0.09052 0 h – 2 h: 5.52×10^{-10} *
42 °C	0 h – 0.25 h: 0 * 0 h – 0.5 h: 0 * 0 h – 1 h: 0 *	0 h – 0.25 h: 0 * 0 h – 0.5 h: 0 * 0 h – 1 h: 1

9.2 Plasmid map

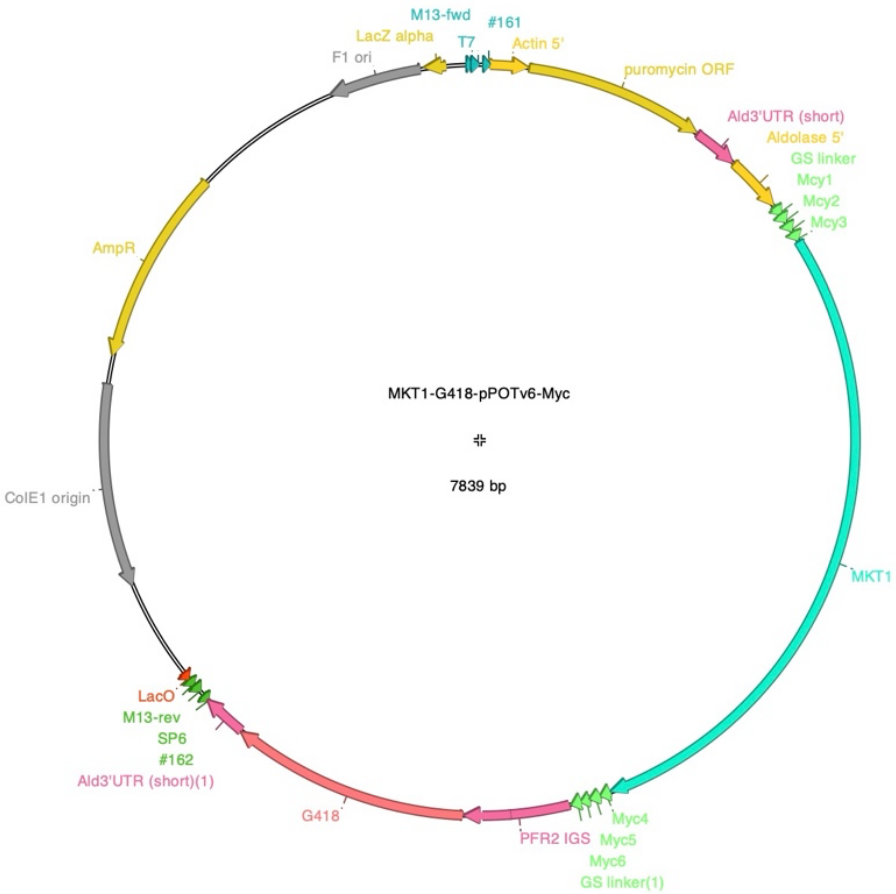

Figure 9.1: The final MKT1-G418-pPOTv6-Myc plasmid aimed to be produced within this study. This figure was generated using A plasmid editor (APE) (Davis and Jorgensen, 2022). Showing completion of an MKT1-tagged cell line upon the ligation of MKT1 into the G418-pPOTv6-Myc plasmid.